DISSERTATION

MOLECULAR REGULATION OF GLIAL INFLAMMATION IN PARKINSON'S DISEASE

Submitted by

Briana R. De Miranda

Department of Environmental and Radiological Health Sciences

In partial fulfillment of the requirements

For the Degree of Doctor of Philosophy

Colorado State University

Fort Collins, Colorado

Spring 2014

Doctoral Committee:

    Advisor: Ronald Tjalkens

    Takamitsu Kato
    Marie Legare
    Donald Mykles

ABSTRACT

MOLECULAR REGULATION OF GLIAL INFLAMMATION IN PARKINSON'S DISEASE

Parkinson's disease (PD) is the most prevalent movement disorder that affects adults, the primary pathology of which includes the loss of dopamine producing neurons from the substantia nigra (SN) and inflammatory activation of immune mediators in the brain. Reactive astrocytes and microglia have been implicated in driving the progressive phase of dopamine neuron loss in PD, the result of which leads to worsening neurodegeneration over time that no current therapy can inhibit. A significant need exists for small molecule therapeutics that reach the CNS, decrease glial activation, and confer neuroprotection over the progressive phase of PD. A novel class of anti-inflammatory compounds, originally shown to have anticancer properties, are examined here as potential therapeutic agents to decrease glial inflammation in a progressive mouse model of PD. Derived from indol-3-carbinol produced in cruciferous vegetables, *para*-phenyl substituted diindolylmethanes or C-DIMs have been shown to induce orphan nuclear receptor family NR4A in several different cancer lines, and have reduced inducible nitric oxide synthase (NOS2) expression in primary murine astrocytes. In order to examine the neuroprotective benefit selected C-DIM compounds have on the survival of dopamine neurons during the inflammatory progressive phase of PD, several experimental studies were conducted, and reported here. The initial development of a method using immunofluorescent sereological counts of TH-positive neurons in the SN, resulted in the ability to measure early neuronal degeneration with sensitivity to small changes in neuron loss through design-based 3D modeling of the SN. Additionally, a pharmacokinetic analysis of four C-DIM compounds determined that

structural variations changed the metabolism of these compounds in mice, however all C-DIMs tested were orally bioavailable, distributed to the brain, and displayed pharmacokinetic profiles equivalent to current PD therapies. Initial neuroprotective studies demonstrated that three of the selected C-DIMs are able to limit the progression of dopamine neuron loss from the SN after the onset of a lesion, in a progressive PD mouse model using 1-methyl-4-phenyl-1,2,3,6-tetrahydropyridine (MPTP, 80 mg/kg) and the drug clearance inhibitor probenecid (250 mg/kg, expressed as MPTPp). A post lesion model was utilized in transgenic NF-κB-EGFP adult mice, where MPTPp treatment was given for 7 days (MPTPp7d) and animals were given either corn oil (vehicle) or one C-DIM (DIM-C-pPhOCH$_3$, DIM-C-pPhOH, DIM-C-pPhCl) via daily oral gavage for the next 7 days (MPTPp14d). Further investigation into the mechanism by which C-DIMs reduced dopamine neuron loss revealed that activation of microglia and astrocytes was reduced in the SN from MTPPp7d to MPTP14d in animals given daily oral gavage of the compounds, compared to corn oil control. NF-κB-EGFP intrinsic reporter detection of NF-κB expression was reduced in C-DIM treated animals compared to animals that received no treatment from MPTPp7d to MPTPp14d. Reduction in NF-κB related cytokines (TNF, IL-1α, IFNγ) were also seen after C-DIM treatment. As a final investigation into C-DIM mechanism of action, DIM-C-pPhCl was examined in the BV-2 microglia cell line treated with LPS to stimulate cytokine production. DIM-C-pPhCl treatment reduced the expression of inflammatory proteins such NOS2, TNFα, and IFNγ after LPS treatment, and its effectiveness was dependent on the nuclear receptor transcription factor NR4A2 (Nurr1). In addition, DIM-C-pPhCl treatment increased the amount of Nurr1 present at the NOS2 promoter, suggesting that it enhances the Nurr1-dependent transrepression of NF-κB, recently described as a novel mechanism in glial cells to reduce inflammatory protein and protect against the progression of PD.

ACKNOWLEDGEMENTS

TABLE OF CONTENTS

V. CHAPTER 5
TRANSREPRESSION OF NF-κB IN BV-2 MICRGLIA BY NOVEL *PARA*-PHENYL
DIINDOLYLMETHANE DIM-C-pPhCl BY A NURR-1 DEPENDENT MECHANISM

VI. CHAPTER 6
DISCUSSION 118

LIST OF TABLES

LIST OF FIGURES

FIGURE

CHAPTER 1

LITERATURE REVIEW

1. Neuroinflammation

   1.1 Immune Mediation in the CNS

     The regulation of inflammatory processes in the brain is rigorously controlled by the cells that support neuronal function and survival. Much like peripheral inflammatory responses, the central nervous system (CNS) is maintained in homeostasis by activation of immune cells after the detection of pathogens or cellular injury, followed by self-sustaining inflammatory resolution (Maguire-Zeiss and Federoff, 2010). Distinct from other systems, the CNS is an immune-privileged organ, deriving protection and separation from the periphery via the blood-brain barrier (BBB; Glass et al., 2010). Because the BBB tight junctions restrict the passage of cells and many substances from crossing into the brain, specialized cells exist within the CNS to monitor and respond to cellular distress. Resident immune cells, microglia, are a type of glial cell that patrol local micro-environments, act as antigen presenting cells, and exhibit phagocytic activity to clear pathogens and cellular debris (Cho et al., 2003). Activated microglia release proinflammatory mediators to surrounding cells, leading to activation of another glial cell type, the astrocyte, which can proliferate to create a "glial scar" (Brambilla et al., 2005). Additionally, T-cells are signaled to infiltrate the CNS upon injury, although recent evidence suggests they may be present under healthy conditions as well (Hirsch and Hunot, 2009a). Together, these cells work to resolve cellular damage that may occur within populations of neurons that make up each distinct facet of the CNS.

While the neuroinflammatory process is designed to promote neuron survival, it is also the basis for chronic neurodegenerative diseases where uncontrolled inflammation drives the progressive loss of neurons. Clear evidence has linked excessive inflammation to multiple neurodegenerative diseases including Alzheimer's disease (AD), Parkinson's disease (PD), multiple sclerosis (MS), amylotrophic lateral sclerosis (ALS), Huntington's disease, and multiple system atrophy (Glass et al., 2010). Each of these progressive disorders is categorized by the loss of a distinct population of neurons accompanying clinical symptoms that worsen over time. Despite the common element of progression, it remains unclear whether inflammation plays an etiological role in these diseases or is an affect from some other type of neuronal injury (Tansey and Goldberg, 2010).

Several lines of evidence suggest that both genetic predisposition and environmental exposures throughout life cause neurological disease, in part through the accumulation of cellular damage to neurons, which have little regenerative capacity (Antosz and Osiak, 2013; Gao and Hong, 2008; Hauser and Cookson, 2011). Certain populations of neurons are also considered especially susceptible to damage based on the essential chemical reactions they preform. Exemplifying this, are the dopamine producing neurons of the substantia nigra (SN), responsible for synthesizing most of the dopamine within the CNS (Tripanichkul and Jaroensuppaperch, 2013). Dopamine synthesis is an oxidative process, where amino acid L-tyrosine is converted to the dopamine precursor dihydroxyphenylalanine (DOPA) via the enzyme tyrosine hydroxylase (TH) and O_2 (Phillipson, 2014). Dopamine production within these neurons also requires high levels of energy (ATP), and therefore preconditions dopamine neurons of the SN to sensitivities of metabolism dysfunction (Przedborski et al., 2000). Indeed, it is the byproduct from years of oxidative dopamine metabolism occurring in this area that produces neuromelanin, the dark

pigment lending the name to the substantia nigra (Gao and Hong, 2008). Additionally, the SN is located in the ventral midbrain of the CNS, a region rich in microglia population that produce high levels of inflammatory mediators upon injury (Ferris et al., 2013). Taken together, dopamine neurons are highly susceptible to death and dysfunction despite the lack of evidence for a clear inciting factor for dopamine neuron loss. Individuals who suffer from progressive damage of dopamine neurons have a reduction of dopamine input into their motor systems, exhibit an array of motor defects, and present clinically with Parkinson's disease.

1.2 Glial Cells

Perhaps the most highly specialized cell in the body, the neuron has unique requirements that allow it to function properly while maintaining its metabolic needs. Derived from neuronal stem cells, astrocytes are the most abundant cell in the CNS, and they provide trophic support to neurons in the form of lactate for energy production (Correa et al., 2011). Astrocytes also provide structural support and express potassium channels to maintain extracellular ion levels (Gao and Hong, 2008). In recent years, it was discovered that astrocytic end feet surround endothelial tight-junctions comprising the BBB and allow astrocytes to monitor and respond to changes in blood-oxygen demand (neurovascular coupling; Kacimi et al., 2011). Additionally, astrocytes in conjunction with neurons form the "tripartite" synapse, where astrocytes surround pre- and post-synaptic neuron terminals in order to clear excess neurotransmitters as well as transmit their own metabotrophic signals (Liu, 2006). Their role in immune modulation of the CNS is multi-factorial but glial cells express pattern recognition (PRR), cytokine, and chemokine receptors and become activated upon binding of misfolded proteins or components of infectious agents (Thompson and Van Eldik, 2009). Activated astrocytes respond primarily by upregulating the production of reactive oxygen species (ROS), cytokines, and chemokines; altered

metabotrophic signaling and neurovascular coupling has also been detected under inflammatory conditions (Kacimi et al., 2011; Thompson and Van Eldik, 2009).

Unlike astrocytes, microglia are derived from a myeloid lineage, and migrate to the brain during fetal development (Napoli et al., 2009). In their resting state, microglia extend ramified processes to monitor their environment, and express a host of pattern recognition receptors on their surface which bind to foreign proteins (McGeer and McGeer, 2011). One such receptor family, toll-like receptors (TLRs), identify bacterial and viral proteins and transduce pro-inflammatory cell signaling pathways within the microglia (Saijo et al., 2013). Activated microglia release cytokines and chemokines as well as undergo morphological changes, retracting ramified processes into an ameboid shape (Polazzi and Monti, 2010). When fully activated, ameboid microglia can phagocytose foreign particles or debris, clearing damage from neuronal injury. Like peripheral macrophages, the antimicrobial function of microglia involves oxidative-burst, which requires several reactive oxygens (O_2), nitrogens (NO), and free radicals (Hirsch and Hunot, 2009b). Enzyme systems within microglia and astrocytes increase the production of these oxidative elements via NADPH oxidase, inducible nitric oxide synthase (iNOS/NOS2), and myeloperoxidase (MPO;Niatsetskaya et al., 2012). Under normal conditions, the reactive gliosis phase of a CNS immune response is coupled with negative feedback mechanisms that inhibit inflammatory signals after resolution of the injury. The return of microglia to a resting state is vital to homeostatic control, and the basis for excessive inflammation in systems where glial cells continuously activate (Gao and Hong, 2008).

2. Inflammation and Parkinson's disease.

While ongoing research continues to identify new genetic factors that predispose to the development of Parkinson's disease, only 10% of cases of PD can be attributed to familial or

spontaneous allele mutation (Glass et al., 2010). In the remaining population of individuals with idiopathic PD, the etiology remains unknown, and the lack of disease biomarkers leaves clinical observation of motor symptoms as the primary diagnostic tool. Unfortunately, at the time an individual presents with the main motor deficits of PD- bradykinesia, postural instability, rigidity, and resting tremor- approximately 70% of the dopamine in their nigrostriatal system is already lost (Burke and O'Malley, 2013). Dopamine deficits in the motor cortex result from the death of dopamine neuron cell bodies in the substantia nigra pars compacta (SNpc) and their axonal projections to the striatum (ST). Together, these nuclei form the nigrostriatal tract that inputs dopamine into the motor system, responsible for coordinated control over movement. Under the pathological conditions associated with PD, dopamine neuron death is progressive and will worsen until almost complete cessation of dopamine production, resulting in ataxic conditions for individuals with PD (Gao and Hong, 2008).

2.1 Progressive Phase of Neurodegeneration

The mechanisms behind progressive loss of dopamine neurons in PD involve a complex interaction between cellular and molecular functions that promote inflammatory conditions within the SN. Genetic models mimicking types of familial PD have uncovered multiple ways in which a dopamine neuron may become primed for apoptosis. The most common genetic mutation, LRRK2, is associated with late-onset PD caused by dysfunctional protein degradation pathways (Alladi et al., 2010). Several PD-associated mutations including SNCA, and Parkin (PARK2) are involved in protein misfolding, particularly a-synuclein, which aggregates in dopamine neuron cytoplasm during PD pathology (Nolan et al., 2013). Additionally, genetic mutations in PARK7 (DJ-1) and PINK-1 cause mitochondrial dysfunction leading to increased cellular oxidative stress (Kahle et al., 2009). While these identified mutations cause specific

dysfunction in individuals with familial PD, protein misfolding, α-synuclein aggregation, and oxidative stress within dopamine neurons are common to all PD cases.

2.2 Inflammatory Signaling in Glia

Although the etiology of dopamine neuron death in the SN is not entirely understood, it is clear that the progression of neuronal injury is closely linked to neuroinflammatory activation of both microglia and astrocytes and the multitude of inflammatory factors that they produce (Gao and Hong, 2008). Dopamine neuron death may precede glial activation, though the temporal occurrence of events remains unclear, and microglia become activated by apoptotic proteins, allowing for phagocytosis of cellular debris (Cho et al., 2003). Activated microglia release many factors to aid in tissue repair; TNFα, IFNɣ, for proinflammatory cytokine production, chemokines CCL5 (RANTES) and CCL2 (MCP-1) for cell attraction to injury, and MPO and ROS in for lysosomal breakdown of phagocytosed debris (Saijo et al., 2013). Master-regulator genes such as NF-κB and AP-1 are upregulated to drive the production of these cytokines (Ghosh et al., 1998). Current understanding of glial activation indicates that astrocytes are stimulated by the initial release of inflammatory cytokines by microglial cells, though direct activation by neuron death is possible as well (Hirsch and Hunot, 2009a). Astrocytes are situated in close proximity to neuronal synapses and may be directly activated by excitotoxicity, when damaged neurons cannot uptake excitatory neurotransmitters such as glutamate (Rossi and Volterra, 2009). Additionally, astrocytes may become activated when mitochondrial breakdown of damaged dopamine neurons occurs, flooding the immediate area with ROS. In general however, astrocytes are recognized as "amplifiers" of microglial inflammatory signals, and upregulate the production of cytokines, chemokines, and ROS in response to neuron damage. When astrocytes and microglia produce toxic levels of these proinflammatory gene products,

sensitive dopamine neurons become vulnerable to self-induced injury, and thus a progressive lesion of neuron damage and glial activation is formed (Gao and Hong, 2008). At later stages of the disease, it has been confirmed that microglia can be directly activated by binding of α-synuclein to TLRs (Cao et al., 2010; Saijo et al., 2013). Subsequent to the early phases of PD, protein aggregation within the cytoplasm of presynaptic dopamine neurons is a hallmark of the disease. Misfolded α-synuclein aggregates into insoluble fibrils that form Lewy Bodies (LB), dark inclusions seen in surviving dopamine neurons in the SN (Alladi et al., 2010). While the primary function of α-synuclein is thought to involve synaptic vesicle formation, relatively little is known about the protein outside the pathological aggregation in PD (Alladi et al., 2010; Burke and O'Malley, 2013). Synucleopathies like PD however, occur when cell machinery fails to correctly fold α-synuclein tetramers, lysosomal breakdown mechanisms are inhibited, or when dysfunctional E3 ubiquitin ligase does not properly tag the protein for degradation (Phillipson, 2014). Aberrant protein sensors on microglia are activated when LB proteins are detected. In a system of uncontrolled inflammation, TLR detection of α-synuclein can exacerbate inflammatory initiation, leading to increased NF-κB signaling within the glia, and producing higher levels of inflammatory effector proteins that lead to neurotoxicity (Saijo et al., 2013).

3. Molecular Signaling

3.1 NF-κB Signaling in PD

Molecular regulation of inflammation is controlled by master regulators of gene transcription such as NF-κB, AP-1, and IRFs, where convergence of receptor signals transduce transcription factors to inflammatory gene promoters (Glass et al., 2010). NF-κB exists in the cytoplasm of all cell types where it is bound by inhibitory protein IκBα, which masks nuclear localization signals (NLS; Hunot et al., 1997). Multiple receptors converge on NF-κB such as

TNF receptors, TLRs, interleukin receptors (ILRs), or ROS, which stimulate kinase protein IκB kinase (IKK). IKK phosphorylates the sequestering protein IkBα, exposing the NLS site of transcription factors p50/p65 (Rel A), causing them to translocate into the cell nucleus (van Loo et al., 2006). The p50/p65 heterodimer of NF-κB binds to its specific promoter site on DNA (high mobility group I; HMGI) constitutively occupied by ATF/c-Jun, which are phosphorylated by p38 kinase and c-Jun-terminal kinase (JNK) respectively (Thompson and Van Eldik, 2009). Coactivator proteins CREB-binding protein (CBP) and p300 facilitate the transcription of inflammatory genes by both remodeling chromatin and facilitating protein-protein interactions with RNA polymerase II (Collingwood et al., 1999). The dynamic control over NF-κB activation is mirrored by the feedback inhibition that returns inflammatory signals to basal levels upon resolution of injury. These co-repressor proteins, such as histone deacetylases (HDAC), nuclear co-repressor/SMRT (NCoR2), and the CoREST complex of modifying enzymes are involved in a transrepressive mechanism that actively removes NF-κB-p50/p65 from the promoter (Saijo et al., 2009a). NF-κB signaling is the subject of extensive PD-related research, because of the hundreds of the genes that it controls, and the presence of NF-κB-regulated cytokine expression in both animal models and human cases of neurodegenerative disease.

3.2 Nuclear Receptors and Inflammation

NF-κB is widely expressed throughout the CNS, where it functions as a cell survival protein, and may play a role in synaptic plasticity and memory (Kaltschmidt et al., 2006). While necessary for cell function, dysregulation of NF-κB is implicated in all neurodegenerative diseases, making it an attractive target for therapeutic manipulation. Experiments which globally over-express IkBα or knockdown IKK have shown improvement in PD disease models, where a measured reduction in inflammatory proteins has been observed (Brambilla et al., 2005; van Loo

et al., 2006). Unfortunately, total knockout of IKK is limited due to off-target effects such as vulnerability to infection and cancer (Lee et al., 2005). Recent studies have provided new potential targets for inflammatory control, where corepressor modulation of NF-κB is controlled by nuclear receptors(Collingwood et al., 1999; Huang and Glass, 2010). The nuclear receptor family of transcription factors are a superfamily of 49 members, classified into three main families; steroid hormone receptors (glucocorticoid receptors; GRs), orphan receptors (NR4A), and adopted orphan receptors (peroxisome proliferator-activated receptor; PPARs, retinoid X receptors; RXRs, and liver X receptors; RXRs; Huang and Glass, 2010). While nuclear receptors can activate gene expression, the focus in PD is through their ability to suppress inflammatory signaling, with recent emphasis on the NR4A family.

The NR4A orphan nuclear receptor family has three members, Nur77 (NR4A1), Nurr1 (NR4A2) and Nor1 (NR4A3) with conserved zinc finger DNA binding domains (DBD) and a ligand binding domain (LBD; Maxwell and Muscat, 2006). During development, Nurr1 is expressed in the CNS maturation of dopaminergic systems, and it has been confirmed that Nurr1 is required for neurons to express tyrosine hydroxylase both *in vitro* and *in vivo* (Saucedo-Cardenas et al., 1998). Additionally, rare familial mutations in the Nurr1 allele are linked with late-onset PD (Kadkhodaei et al., 2009; Zhang et al., 2012). Perhaps of the most pressing interest, is the recent discovery by Saijo et al. (2009) that Nurr1 plays an anti-inflammatory role in astrocytes in the adult mouse brain, acting to protect dopamine neurons in the SN from bacterial lipopolysaccharide (LPS) treatment. Knockdown of Nurr1 (shNurr1) in the BV-2 microglial cell line revealed significant increases in the expression of NOS2, TNFa, and IL-1B when treated with LPS (Saijo et al., 2009b). In addition, it was found that recruitment of Nurr1 to the NOS2 promoter resulted in decreased association of NF-κB-p65 at this site. Saijo and

colleagues determined that under inflammatory conditions in microglia and astrocytes, Nurr1 binds to p65 bound at the NOS2 promoter, and actively recruits corepressor CoREST complexes. CoREST and associated HDAC proteins promote the clearance of p65 from the NOS2 promoter, and thus decrease the expression induced by LPS (Saijo et al., 2009b). This novel mechanism for inflammatory suppression in the glia creates a new possibility for therapeutic intervention aimed at reducing dopamine neuron loss in PD.

4. Therapies for PD

    4.1 Anti-inflammatory Therapeutics

The observation that PD progression is the result of sustained inflammation has driven the focus of drugs that may alleviate the disorder to small molecule, anti-inflammatory compounds. Neuroprotective benefit from animal model treatments with anti-inflammatories suggests that human PD cases could be improved using similar strategies. While symptomatic treatment regimens such as L-dopa and selegiline can delay the main motor deficits of the disease, the progressive nature of PD limits the success these treatments provide (Emborg, 2004; Tansey and Goldberg, 2010). Long term use of NSAIDs has proven to reduce the risk of developing PD, though their use after the onset of PD has not resulted slowed degeneration (Hartmann et al., 2003). Several compounds already on the market have been investigated in clinical trials of PD; one example is Coenzyme Q10 (CoQ10), a known antioxidant that protects the mitochondria from redox cycling (Matthews et al., 1998). In mice treated with neurotoxin MPTP (1-methyl-4-phenyl-1,2,3,6-tetrahydropyridine), the administration of CoQ10 resulted in the reduction of dopamine neuron loss and prevention of a-synuclein inclusions in neurons (Cleren et al., 2008). Given the knowledge that CoQ10 levels are low in patients with PD, clinical trials for CoQ10 with vitamin E initially showed promise (Shults et al., 2004), however Phase III trials were

terminated due to any lack of benefit (Clinicaltrials.gov, 2011). The nuclear receptor PPARɣ agonist Rosiglitazone, a thiazolidinedione (TZD), has been shown to decrease reactive glial cells in the SN of animals treated with MPTP, thus providing protection against dopamine neuron loss (Carta et al., 2011; Schintu et al., 2009). PPARɣ activation by the TZD class of agonists is a therapy aimed at type II diabetes, but is being explored as potential neurodegeneration drugs (Kung and Henry, 2012). Indeed, Rosiglitizone did show benefit for improved cognition in phase II Alzheimer's trials, but unfortunately has been under scrutiny for safety issues related to heart attack (Glass et al., 2010; Kung and Henry, 2012).

4.2 Failure of Therapies to Attenuate PD

Many additional potential therapeutics have similarly ended in Phase II and Phase III failure, evidence of which is the complete lack of small molecules effective for slowing or reversing the progression of PD (Glass et al., 2010). This lack of successful translation into the clinic has itself become an area of research aimed at discovering solutions to prevent costly failures in late-stage clinical trials. The difficulty to fully recapitulate Parkinson's disease (PD) in the research lab is a major factor in the lack of therapeutics translated to clinical success. Neurotoxin models remain the standard protocol by which a lesion in the SN can be easily reproduced in mice, the most common of which is use of MPTP (Emborg, 2004). As a specific and potent dopamine neuron toxin, the use of MPTP is an attractive option because it reproduces mitochondrial respiration inhibition (ATP depletion), the production of excess reactive oxygen species (ROS), excitotoxicity, DNA damage, and protein adducts (Przedborski et al., 2000). Additionally, MPTP can elicit an inflammatory response in microglia causing increased proinflammtory inducers (e.g. TNFα and IL-1β) in the SN, similar to the inflammation seen post-mortem in human PD (McGeer et al., 1988).

Critics of the MPTP model argue that massive acute neurotoxin doses to ablate the SN in mice does not accurately represent the progressive nature of human PD (Petroske et al., 2001). Similarly, both the rapid onset of neuron loss coupled with dopamine depletion from the ST after MPTP treatment, results in pronounced motor deficits occurring over a relatively short period of time (Meredith et al., 2008). Refinement of this model in recent years has led to the use of adjuvants in more chronic settings in order to both reduce the amount of MPTP required to produce a lesion in the SN, and to mimic the onset of neuron loss seen in PD more accurately. Chronic 6-month studies using MPTP plus clearance inhibitor probenecid (MPTP/P) have identified neuronal and motor deficits that do not reverse upon the cessation of treatment, unlike acute MPTP treatment alone (Petroske et al., 2001). Furthermore, chronic MPTP/P treatments have shown that mice continue to degenerate over time, even after the neurotoxin is removed, indicating a possible progressive component to this model (Petroske et al., 2001; Schintu et al., 2009). While these new chronic MPTP/P regiments benefit the modeling aspect of PD research, small molecule therapeutics still face unsuccessful translation to the clinic, with decreased approval rates and long development periods (Glass et al., 2010). In part, this is due to preclinical treatment with potential therapeutics prior to or concomitant with a SN lesion, which does not accurately reflect the timing in which PD therapies would be useful. Furthermore, low oral bioavailability, inability to cross the blood brain barrier (BBB), off-target effects, and lack of efficacy or benefit all limit the development for central nervous system (CNS) drugs. Targeted small molecule therapeutics able to cross the BBB and elicit an affect on the progression of neuroinflammatory PD are in great demand despite the lack of a single successful therapeutic with this indication.

5. Summary

As the most prevalent movement disorder in humans, an urgency exists to find realistic treatment options that address the underlying pathology of PD, particularly in our rapidly aging populations (Hirsch and Hunot, 2009a). PD is a progressive disorder, the hallmark of which is the loss of dopamine neurons and their axons from the SN, leading to a worsening of movement deficits as well as nonmotor symptoms. The underlying cause of dopamine neuron death is perpetuated by uncontrolled inflammation in the glia, which serve as neurotrophic support in the healthy brain, but can induce a pathological phenotype when continuously stimulated. Complex molecular regulation of inflammation in the glia controlled by master regulator genes such as NF-κB have been identified as targets for new therapies aimed at reducing glial inflammation and having neuroprotective benefit. To date, no therapies have successfully attenuated either glial inflammation or slowed the progression of PD, likely because of poor translational models in the research lab, the difficulty for compounds to cross the BBB, and the elusion of the precise cause of idiopathic PD.

CHAPTER 2

STEROLOGICAL ASSESSMENT OF DOPAMINE NEURONS USING

IMMUNOFLUORESCENCE IN A LOW DOSE MODEL OF 1-METHYL-4-PHENYL-1,2,3,6-

TETRAHYDROPYRDINE NEURODEGENERATION

INTRODUCTION

Efforts to more accurately reproduce neuron loss and physiological changes in the brain that occur in PD, have yielded new research models that better predict the translation from animal to human. While genetic models can reproduce varying types of familial PD, and are useful in many applications, neurotoxin models remain the most timely and cost-effective way to model PD in the research lab. Rotenone, a pesticide, can be delivered via intraperitoneal injection to rodents, and induces dopamine neuron death by inhibiting mitochondrial respiration (Cannon et al., 2009). Administration of exogenous 6-hydroxydopamine (6-OHDA), also leads to oxidative stress within dopamine neurons after injection. Systemic infusion of LPS can mildly decrease dopamine neuron levels, but is more commonly given by stereotaxic injection into the midbrain, which produces high levels neuron loss in the SN (Saijo et al., 2009b).

MPTP (1-methyl-4-phenyl-1,2,3,6-tetrahydropyridine) is a neurotoxin that was discovered in the 1980s after contaminated heroin injected by young individuals lead to instantaneous PD-like symptoms (Langston et al., 1983). Mechanistic studies of MPTP revealed that the compound is bioactivated in astrocytes via monamine oxidase (MAO-B) to MPP^+ (pyridinium ion) that has a specific affinity for the dopamine transporter (DAT) (Przedborski et al., 2000). Rapid uptake into dopamine neurons via DAT allows MPP^+ to accumulate in dopamine neurons, where it is

14

either bound to vesicular monoamine transporters (VMAT), stored in the cytoplasm, or actively concentrated into the mitochondria. MPP^+ binds to complex 1 of the mitochondrial electron transport chain (ETC) and stops the electron flow required for ATP production within the cell (Przedborski et al., 2000). Additionally, complex 1 inhibition causes the production of free radicals, such as superoxide (O_2^-), which itself can cause oxidative stress, or can be transformed into hydroxyl radical (OH.) via the Fenton reaction, or peroxynitrite (ONOO-) that binds phenolic tyrosine residues leading to protein dysfunction (Dehmer et al., 2003; Niatsetskaya et al., 2012). Because dopamine neurons require high amounts of ATP and are sensitive to oxidative stress, MPTP administration leads necrosis of dopamine neurons at high levels, and apoptosis under more mild concentrations (Przedborski et al., 2000). The combined effects of MPTP, ATP reduction and oxidative stress, in conjunction with the ease of subcutaneous administration, has made MPTP the most typical neurotoxin by which researchers create a PD-like lesion.

Many different types of MPTP treatment regimens exist, however the use of MPTP has not always accurately predicted the type of dopamine neuron loss seen in human PD (Jenner, 2009). Inflammatory changes are thought to occur prior to the loss of dopamine neurons, and large doses of MPTP given to rodents contradicts the type of conditions preceding neuron death that would occur in humans (Jenner, 2009). Additionally, in order to detect low amounts of dopamine neuron cell loss, a sensitive measure of analysis needs to be employed. Considering both of these parameters, we hypothesized that low levels of MPTP (15 mg/kg, 30 mg/kg, or 60 mg/kg) would induce a minimal amount of dopamine neuron death in the SN. We analyzed dopamine neuron death with stereology, the most sensitive method for counting cell loss throughout brain nuclei, and adapted this method for immunofluorescence.

MATERIALS AND METHODS

Animal Treatment with MPTP. Transgenic EGFP reporter mice containing three NF-κB cis elements (cis-NF-κBEGFP; Magness et al., 2004; kindly provided by Dr. Christian Jobin, University of North Carolina at Chapel Hill) were used in this study. Male mice were aged to 12 weeks before being randomly divided into four groups: saline, 15 mg/kg MPTP-HCl 30 mg/kg MPTP-HCl, and 60 mg/kg MPTP-HCl. Doses of MPTP were prepared in saline as free base (Sigma, St. Louis, MO) and were delivered by subcutaneous injection 12 hours apart over 67days. All animal procedures were performed in accordance with NIH guidelines for the care and use of laboratory animals and were approved by the Colorado State University Institutional Animal Care and Use Committee. Every effort was made to minimize pain and discomfort, and all terminal procedures were performed under deep isofluorane anesthesia.

Tissue Collection and Processing. Seven days post-treatment, animals were terminally anesthetized with isofluorane before transcardial perfusion with 20 mM sodium cacodylate in phosphate buffered saline (PBS) containing 10 units per ml (10 U/ml) of heparin. Upon liver clearance, animals were fixed with 4% paraformaldehyde in PBS-cacodylate solution. Mouse brains placed in 4% paraformaldehyde solution at 4℃ for 3 hours, then transferred to 15% sucrose-PBS-cacodylate solution at 4℃ overnight. After saturation with sucrose, brains were transferred into a 30% sucrose-PBS-cacodylate solution at 4℃ overnight. Brains were removed from sucrose and placed into optimal cutting temperature (OCT) for sectioning. Serial coronal sections were obtained using a cryostat microtome, 40 µm thickness throughout the midbrain. Free-floating sections were stored in a cryoprotectant solution (30% w/v sucrose, 30% v/v ethylene glycol, 0.5M phosphate buffer, pH 7.2) at -20℃ until staining.

Tyrosine Hydroxylase Immunofluorescence. Serial sections were selected using a systematic random sampling throughout the length of the substantia nigra pars compacta (SNpc). Every third section was chosen for a 1/3 sampling fraction, and placed in 0.05M Tris-buffered saline solution (TBS, pH 7.2) for 3 wash cycles. Placement onto glass slides preceded a 1-hour incubation with 1% donkey and 1% goat serum prepared in TBS for blocking purposes. After blocking, sections were incubated overnight at 4°C with 1:500 tyrosine hydroxylase primary antibody (rabbit anti-TH, AB152; Millipore, Temecula, CA) diluted in TBS + 0.5% Triton X-100 (Chemicon, Temecula, CA) with 1% goat and 1% donkey serum (Sigma). Tissue was washed with TBS before secondary antibody incubation for 3 hours at RT (1:500 in TBS, AlexaFuor 555 anti-rabbit; Life Technologies, Carlsbad, CA). Sections were placed under coverslip and mounted with 4',6-diamidino-2-phenylindole (DAPI, Vector Labs) for nuclei visualization and stored at 4°C.

Stereological Analysis. Stereological imaging and counts of TH-positive cells were performed using Slidebook software (version 5.0; Intelligent Imaging Innovations, Denver, CO) with use of the optical fractionator method (West and Gunderson, 1990). Images were captured using a Zeiss Axiovert 200M inverted fluorescence microscope equipped with a Hammatsu ORCA-ER-cooled charge-coupled device camera (Hammamatsu Photonics, Hamamatsu City, Japan). The boundary of the SNpc was determined using low-magnification (10x) montage imaging. Nigral boundaries were observed as in Banquet et al. (2009); rostral boundary near the subthalamic nucleus (STh), caudal boundary near the retrorubal field (RRF), and medial boundary separated at the ventral tegmental area (VTA). Total numbers of TH-positive cells were obtained through imaging (40x) uniform randomly placed counting frames (100 x 100 mm) with use of an optical dissector of 30

17

mm with 5 mm upper and lower guard zones. Anatomic landmarks were used to select striatal sections for TH intensity staining in an identical process as described above and in Miller et al. (2011), staining all treatment groups simultaneously. 3D design-based stereological estimates of the total number of neurons in both hemispheres of the brain were calculated using equation 1 (1) Where Σ units is the sum of the neurons counted in all sections, h is the section thickness (40 um), asf = area of counting frame ÷ area of the sampling grid (150 x 150 mm)/(100 x 100 mm), and ssf = the section sampling fraction (1/3). Montage images of the striatum (ST) were created using a 10x objective and a mask generated to outline the striatum with use of Slidebook software, and mean fluorescence intensity in relative florescence units was obtained. Representative images of TH expression in the SNpc and the ST were captured using an Olympus FluoView (FV-10i; Olympus Optical Co. Ltd., Tokyo, Japan) laser scanning confocal microscope equipped with water immersion lenses. Montage images were obtained using a 10x objective, and representative high-magnification images were obtained using a 60x objective.

(1) $$N = \Sigma \text{ units x } (1/h)(1/asf)(1/ssf)$$

RESULTS

Stereology Using Immunofluorescence

Immunofluorescent images in the SN used for stereology were generated both through the entire SNpc nuclei and in a Z-plane dissecting each tissue section as illustrated in Figure 1. Stereological assessment of dopamine neuron loss from mice treated with saline, 15 mg/kg MPTP, 30 mg/kg MPTP, or 60 mg/kg of MPTP resulted in minor changes between treatment groups, none of which were statistically significant ($P < 0.05$, ANOVA; Figure 2B). Representative confocal montage images of the SN (10x, 60x inset) comparing saline with 60

mg/kg MPTP treatment show a mild reduction in TH cell density, reflected in stereological counts that trend downward despite the lack of statistical significance (Figure 2A).

Striatal TH Fiber Density

The projections of dopamine neurons from the SN to the ST are especially sensitive to MPTP treatment because nerve terminals containing DAT uptake the MPP+ neurotoxin at this site. Additionally, the ST is the functional output of the dopamine motor system, and is integral in the control of fine motor movements which degrade in early phases of PD. Subtle losses within the ST are important markers for detecting neurological changes when modeling PD, therefore we employed the detection of TH fiber density in the ST using immunofluorescence. Mean TH intensity in the ST was decreased significantly after 60 mg/kg MPTP, though a clear downward trend was observed in each consecutive treatment group ($P < 0.05$, ANOVA; Figure 3B). Confocal 10x montage images displaying TH intensity in the ST show an apparent loss upon the highest MPTP treatment (Figure 3A).

Protein Dysfunction Precedes Neuron Loss

Considering the observation that the highest MPTP treatment (60 mg/kg) does not produce a significant loss of dopamine neuron cell bodies, but does produce TH-positive terminal loss, we investigated whether detectable protein dysfunction was occurring. An oxidative stress marker, 3-Nitrotyrosine (3-NTyR) represents tyrosine residues within cells that have been damaged by peroxynitrite (ONOO-) adducts. As tyrosine hydroxylase, the enzyme that synthesizes dopamine, is highly abundant in dopamine neurons, 3-NTyR damage is likely to precede dopamine neuron death in MPTP treated animals. Findings from immunofluorescent

19

staining of sections from the SN support the conclusion that 3-NTyR damage increases with MPTP treatment (Figure 4A,B). Quantitative data measuring the mean fluorescence intensity of 3-NTyR between saline and 60 mg/kg MPTP, show a significant increase in animals given MPTP over control (Figure 4C). Representative 40x images of the SN illustrate that TH positive neurons co-localize with 3-NTyR residues, and this oxidative damage is increased after 60 mg/kg MPTP treatment.

DISCUSSION

The objectives of this study were to generate a sensitive method to count dopamine neuron cell bodies within the SNpc using immunofluorescence, and identify inflammatory changes that occur prior to neuron loss. After treatment with increasing amounts of MPTP, dopaminergic neurons showed clear signs of damage, but cell body (soma) loss in the SNpc remained statistically insignificant. Loss of TH fibers (axons) in the ST were apparent after 60 mg/kg MPTP but not with 15 mg/kg or 30 mg/kg MPTP, indicating that these doses encompass the threshold for MPTP-induced damage in the ST. Even at the highest (60 mg/kg) dose of MPTP, these concentrations are considered a mild induction of a lesion in the SN (Jackson-Lewis and Przedborski, 2007), but these low doses confirm that nitrosative stress occurs prior to the loss of dopamine neurons.

When modeling PD, researchers use many methods to detect the loss of dopamine neurons within the SN, as well as their axonal projections to the ST (Jackson-Lewis and Przedborski, 2007; Jenner, 2009; Meredith et al., 2008). Immunoblotting is traditionally used to measure total TH protein in a brain sample, and can give helpful information as to global loss of TH based upon a given treatment (Jackson-Lewis and Przedborski, 2007). Cell counting of total neurons in

representative tissue sections preceded stereology methods for encompassing an entire nuclei, which as been labeled the "gold standard" for counting neurons in PD models (Baquet et al., 2009). Traditionally, stereological counts have been preformed using immunohistochemistry, where TH-ir neurons are detected against contrasting tissue (Baquet et al., 2009). Here, we present a stereological method where immunofluorescence is used with a DAPI counterstain, where TH-positive neurons are highly visible. Using this method, we were able to detect sub-threshold changes in dopamine neuron counts that would be difficult to distinguish using alternative methods of cell counting (Figure 2B). Sterological counts using our developed method correspond to the average number of TH-positive neurons in the nigra of C57/bl6 mice in similar published methods; approximately 12,000 (Baquet et al., 2009). In human PD, dopamine neurons are not lost in a randomly, rather they degenerate from the lateral portion of the SN nucleus first (near the caudal boundary of the RRF), followed by medial degeneration (near VTA) as the disease progresses (Damier et al., 1999). This pattern of neuron loss was observed during our assessment of the SN, increasing with MPTP concentration, indicating that this method of cell death detection considers the regional differences in neuron loss.

Additionally, we were able to visualize that TH fiber density in the ST occurred before dopamine cell loss in the SN; a result which concurs with the use of MPTP as an early PD model (Jenner, 2009). Nitrosative stress, as measured with the 3-NTyR antibody, is also increased in dopamine neurons before stereological counts detected significant cell loss (Figure 4). Additional inflammatory markers using this model have also been measured, showing that NF-κB and its downstream gene products are induced upon increasing concentrations of MPTP (Miller et al., 2011). Studies from our lab have also shown that behavioral locomotor deficits occur in mice after these low-dose MPTP treatments (Miller et al., 2011).

Taken together, we conclude that the stereological method developed here for counting dopamine neurons in the SN using immunofluorescence, is a sensitive marker for neuron loss in PD models using low doses of MPTP. The ability to measure inflammatory proteins during early pathological changes within the brain, is a useful tool for identifying both the mechanistic loss of neurons, as well as treatments that may attenuate this process. While proinflammatory changes are demonstrated here, this model does not recapitulate the etiology of a PD lesion in its entirety. Rather, this study indicates that higher doses of MPTP are required for generating neuronal cell body loss, and a more chronic disease model is necessary to properly mimic PD. Given these conclusions, the stereology method developed under these conditions will serve as an important base for future, more chronic PD studies.

FIGURES

FIGURE 1
STEREOLOGY
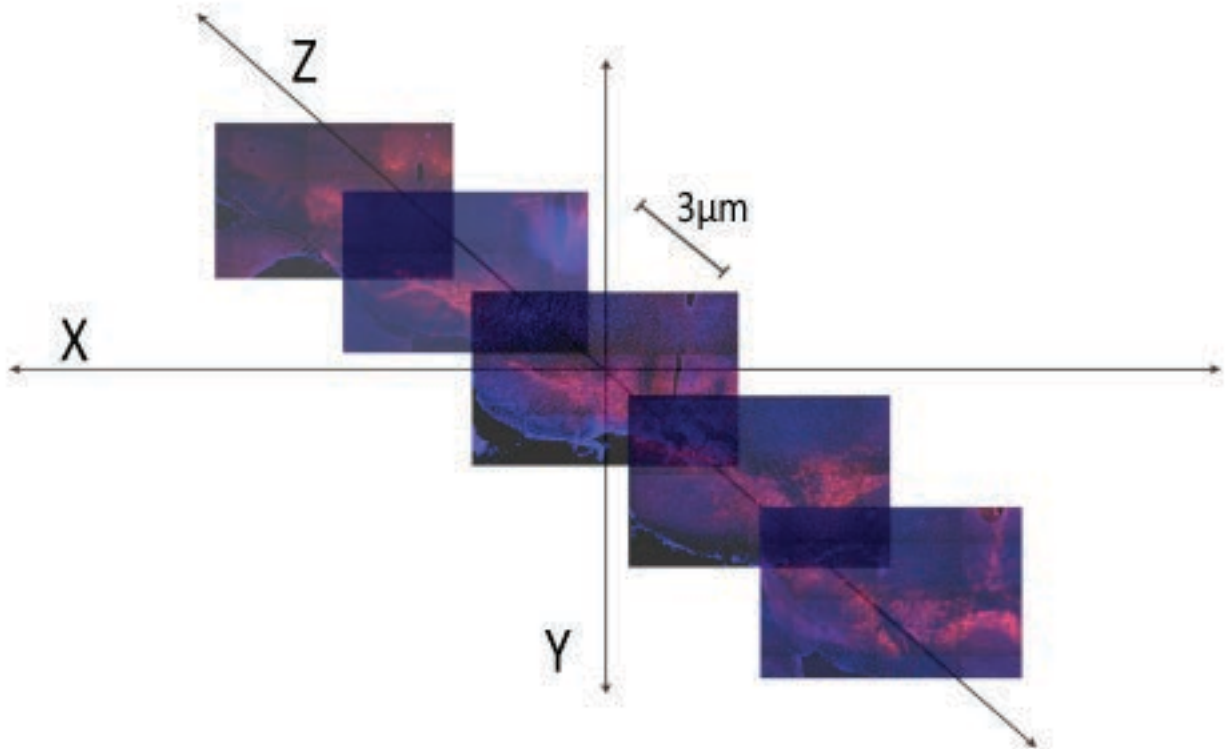
Figure 1. 3D design-based stereology method using immunofluorescence. A representation of the Z-stack plane of 40x images through each 40 μm tissue and the entire SN nucleus. Z-plane is dissected at 3 μm height.

FIGURE 2
DOPAMINE NEURON COUNTS IN SN
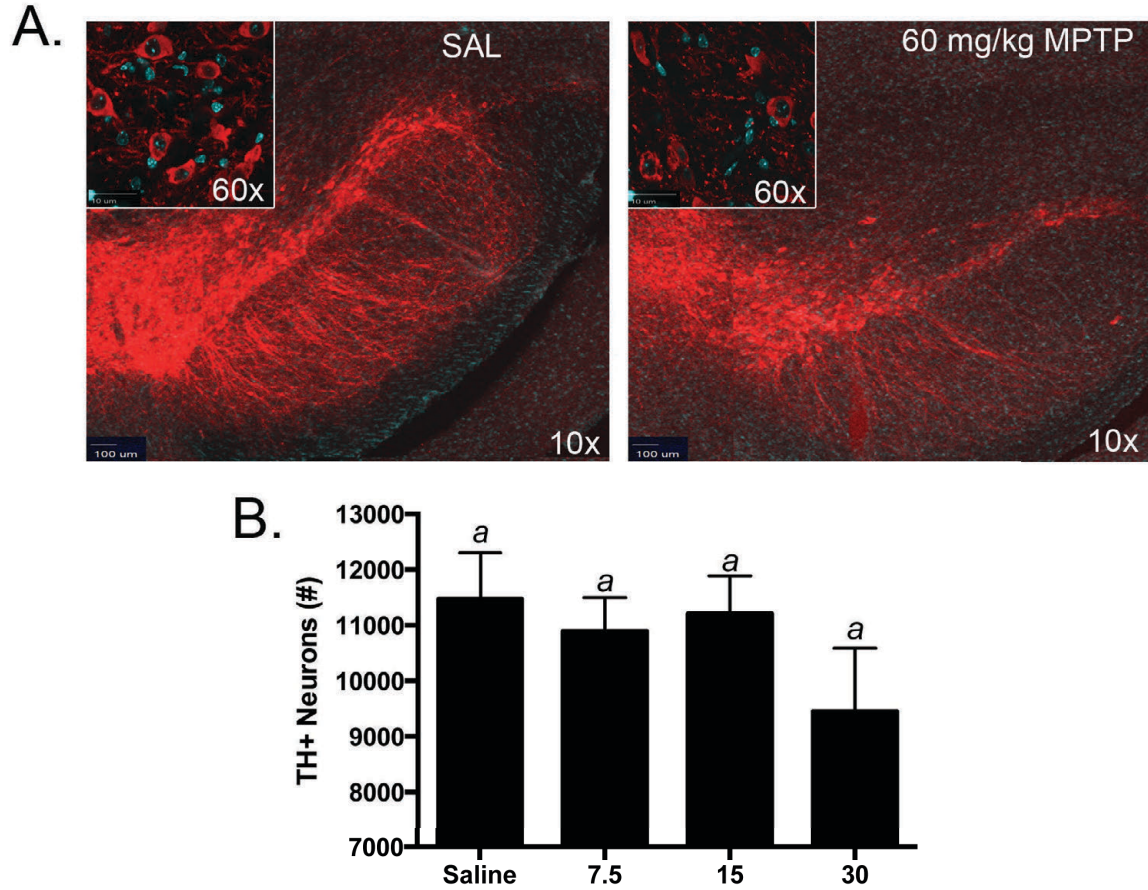
Figure 2. Dopamine neuron counts in the SN of animals given low doses of MPTP. A. Representative confocal 10x montage images of the SN from SAL and 30 mg/kg of MPTP with TH immunofluorescence (red) and DAPI (blue) counterstain. Inset: 60x confocal image of TH neurons. **B.** Sterological counts of TH-positive neurons after saline, 7.5 mg/kg MPTP, 15 mg/kg MPTP, or 30 mg/kg MPTP. Letters indicate statistical significance, one-way ANOVA with a Tukey post hoc test $P < 0.05$.

FIGURE 3
STRIATAL TH LEVELS
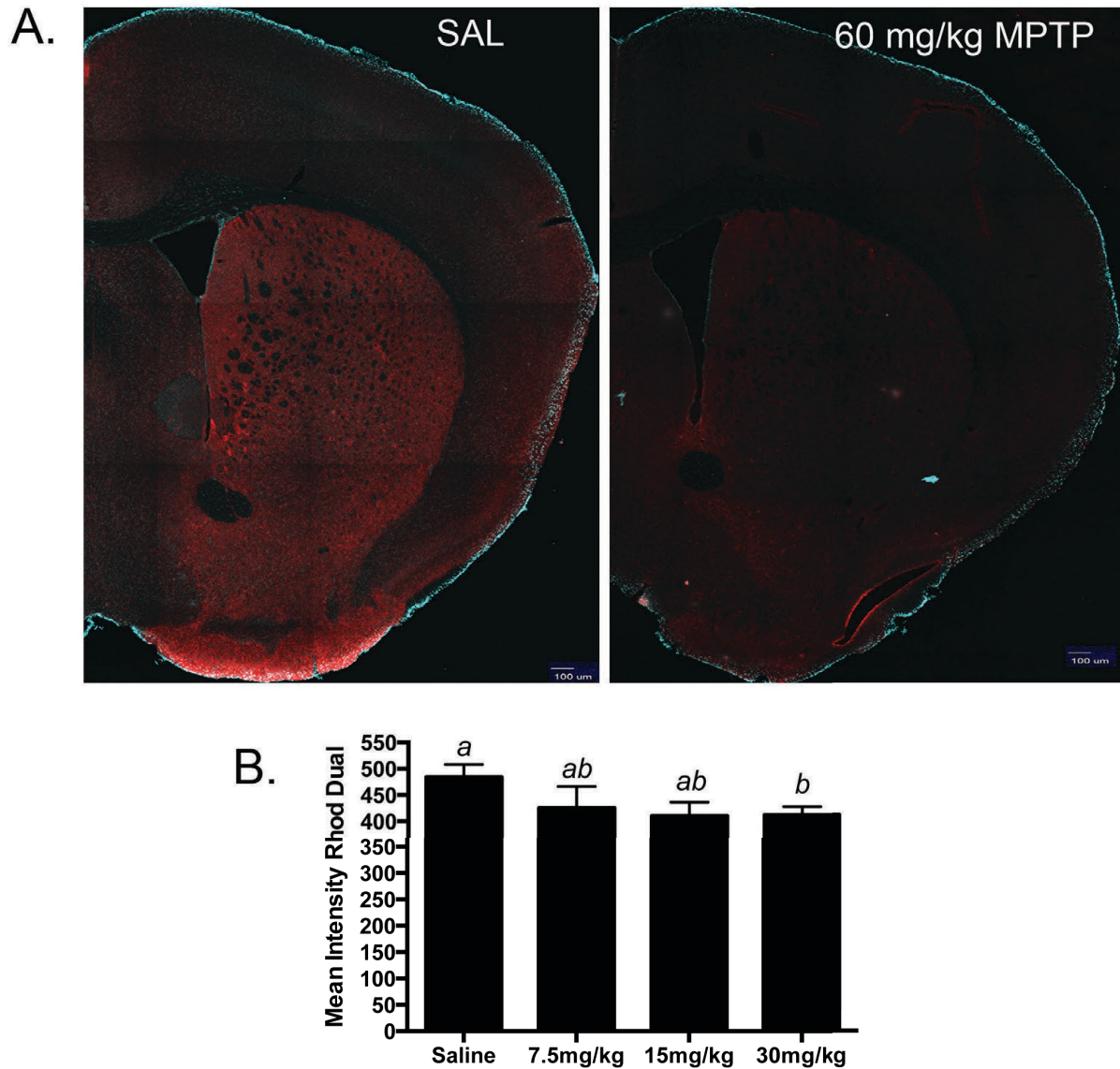
Figure 3. Dopamine terminal loss from the ST precedes neuron loss from the SN. A. Representative confocal 10x montage images of the ST from SAL and 30 mg/kg of MPTP with TH immunofluorescence (red) and DAPI (blue) counterstain. **B.** Mean intensity of TH (RhodDual) was determined using SlideBook software intensity measurement of MPTP treatment groups. Letters indicate statistical significance, one-way ANOVA with a Tukey post hoc test $P < 0.05$.

FIGURE 4
PROTEIN NITROSYLATION
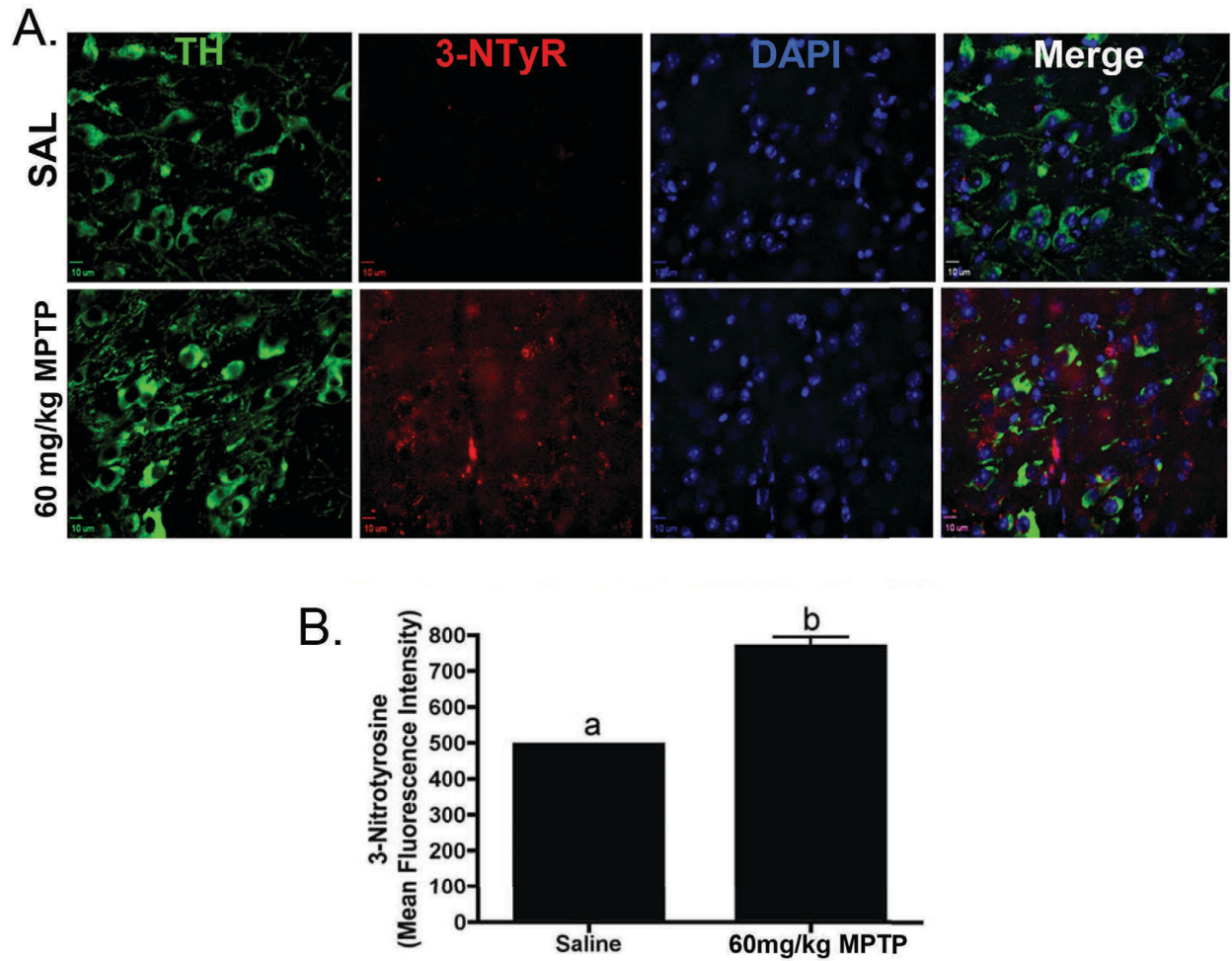
Figure 4. Protein dysfunction is visible prior to dopamine neuron loss. A. Representative 40x images of TH neurons (green), nitrotyrosine marker 3-NTyR (red) and DAPI (blue) show an increase in nitrosylation after MPTP treatment. **B.** Mean intensity of 3-NTyR in the SN indicates a significant increase in the animals receiving MPTP treatment over saline. Letters indicate statistical significance, student's t-test $P < 0.05$.

CHAPTER 3

NEUROPROTECTIVE EFFICACY AND PHARMACOKINETIC BEHAVIOR OF NOVEL

PARA-PHENYL SUBSTITUTED DIINDOLYLMETHANES IN A MOUSE MODEL OF

PARKINSON'S DISEASE[1]

INTRODUCTION

Efficient delivery of chemotherapeutics to the brain represents one of the main challenges in the development of effective treatments for neurodegenerative disorders. In addition to the difficulty of brain distribution, toxicity and lack of clinical efficacy limit the utility of many potential compounds that demonstrate efficacy in animal models. Small molecule therapeutics with a CNS indication have lower approval rates and longer development periods compared to compounds targeted to peripheral tissues (Glass et al., 2010), contributing to the current lack of neuroprotective modalities for treating neurodegenerative disorders. Furthermore, poor performance of translational animal models of neurodegeneration in predicting clinical outcomes has limited the progress of therapeutic development for CNS disorders (Carta et al., 2011; Schintu et al., 2009). Thus, a great need exists for orally-bioavailable drugs for treatment of diseases such as Alzheimer's (AD), Parkinson's disease (PD), amyotrophic lateral sclerosis (ALS) and multiple sclerosis (MS; Polazzi and Monti, 2010).

One class of compounds with potential neuroprotective efficacy is based on 3-3'-diindolylmethane, an acidic condensation product of indole-3-carbinol, a phytochemical found in

_____

cruciferous vegetables. 3-3'-Diindolylmethane has been extensively studied as a potential cancer chemotherapeutic compound (Safe et al., 2008) and several novel para-phenyl substituted diindolylmethanes (C-DIMs) demonstrate effective inhibition of tumor cell growth through activation or inactivation of nuclear receptors including Nur77/NR4A1 (Lee et al., 2010) and Nurr1/NR4A2 (Inamoto et al., 2008). In the CNS, Nurr1 is expressed during the development of dopamine neurons in the sustantia nigra (SN), the portion of the ventral midbrain affected in PD (Saucedo-Cardenas et al., 1998). Interestingly, Nurr1 also has important homeostatic effects in the adult brain, where it positively regulates expression of trophic genes in dopaminergic neurons and tonically suppresses inflammatory activation of microglia and astrocytes by inhibiting activation of NF-κB (Saijo et al., 2009).

Activation of microglia and astrocytes can result in persistent neuroinflammation that is associated with the progression of neuronal injury in neurodegenerative diseases (Rossi and Volterra, 2009; Polazzi and Monti, 2010). Signaling pathways responsible for initiating neuroinflammatory responses are dynamically suppressed in the absence of extracellular stimuli but are rapidly induced in response to stress, injury, or pathogens. Inflammatory mediators produced by activated glial cells, such as cytokines and reactive oxygen species (ROS), may progress to neurotoxic levels during states of chronic neuroinflammation (Lambertsen et al., 2009; Brown and Neher, 2010). It has been demonstrated that selected nuclear orphan receptors, such as the nerve growth factor responsive NR4A family (NR4A1/Nur77, NR4A2/Nurr1, and NR4A3/Nor1) can downregulate pro-inflammatory genes through transcriptional repression or 'transrepression' mechanisms by stabilizing binding of nuclear co-repressor proteins to regulatory elements in the promoters of inflammatory genes (Saijo et al., 2009). The discovery of this transrepressive property of nuclear receptors suggests that these proteins could be viable

---

targets for developing neuroprotective therapeutics involving ligand-induced blockade of neuroinflammatory signaling pathways in glial cells.

The anti-inflammatory and neuroprotective efficacy of C-DIM compounds in neural cells was demonstrated by the capacity of selected para-phenyl substituted analogs in this series to inhibit NF-κB-dependent expression of NOS2 in astrocytes and subsequent neuronal injury following inflammatory stimulation with cytokines and neurotoxins (Carbone et al., 2008; Tjalkens et al., 2008). Based on these in vitro findings, we generated pharmacokinetic data for each of the C-DIM compounds in order to determine their potential neuroprotective utility in vivo. To determine initial pharmacokinetic parameters for selected C-DIM compounds in adult male C57Bl/6 mice, intravenous (1 mg/Kg) and oral (10 mg/Kg) dosing were both used for 1,1-bis(3'-indolyl)-1-(p-methoxyphenyl)methane (C-DIM5), 1,1-bis(3'-indolyl)-1-(phenyl)methane (C-DIM7), 1,1-bis(3'-indolyl)-1-(p-hydroxyphenyl)methane (C-DIM8), and 1,1-bis(3'-indolyl)-1-(p-hydroxyphenyl)methane (C-DIM12). Levels of each compound were measured in plasma and brain tissue for both dosing routes; tissue levels of parent compound were quantified, and putative metabolites were analyzed in urine, liver and plasma. Based on the results of these pharmacokinetic studies, we then examined the effectiveness of selected C-DIM compounds in attenuating loss of dopaminergic neurons in C57Bl/6 mice following subacute dosing with MPTP and probenecid (MPTPp). Two of the three C-DIM compounds examined in efficacy studies significantly reduced additional loss of dopaminergic neurons in the substantia nigra of mice treated with MPTPp, with C-DIM12 displaying the highest activity. These results suggest that selected C-DIM compounds could be effective neuroprotective agents for attenuating progressive loss of neurons in neurodegenerative diseases.

MATERIALS AND METHODS

Chemicals and reagents. C-DIM 5, 7, 8, and 12 (Figure 5) were synthesized and characterized as described (Qin et al., 2004). All other reagents were of analytical grade and were purchased from Sigma (St. Louis, MO).

Compound administration for pharmacokinetic studies. C-DIMs were prepared for intravenous administration by dissolving in 25% solutol for a final dose of 1 mg/Kg, sterile filtered and administered through tail vein injection. Oral gavage preparations of C-DIMs were made as a suspension in corn oil for a final dose of 10 mg/Kg; controls were given saline or corn oil for I.V. or gavage dosing, respectively. Mice were randomly placed into groups for each C-DIM with n=3 each for I.V. and oral gavage. Each mouse was weighed and treated with a single dose of the appropriate volume of C-DIM (between 10 and 15 μL for I.V. and 90-130 μL for oral gavage). Following dosing, three mice per treatment group were sacrificed at 10, 30, 60, 120, 240, 360, 480, 720 minutes by cardiac exsanguination under deep isoflurane anesthesia, and plasma and brain samples were collected. Brain samples were quickly frozen in liquid nitrogen and stored at -80°C for analysis. For tissue distribution studies, mice (n=3 per C-DIM) were treated as described above using only oral gavage and housed in metabolic cages to collect urine over four hours. At four hours mice were sacrificed as described and plasma and brain were collected along with peripheral organs (heart, lung, liver, kidney, intestine, fat, brain) and rinsed in PBS before freezing in liquid nitrogen and stored at -80°C. All studies were conducted under an approved IACUC protocol at Colorado State University in accordance with the Guide for the Care and Use of Laboratory Animals as adopted by the National Institutes of Health.

MPTP treatment for C-DIM efficacy studies: Transgenic reporter mice (C57 background) expressing an EGFP reporter under control of an NF-κB reporter construct (cis-NF-jBEGFP; Magness et al., 2004; generously provided by Dr. Christian Jobin, University of North Carolina at Chapel Hill) were aged to 12 weeks and then randomly divided into treatment groups. A subacute dosing strategy with MPTP and probenecid (MPTPp) was used to create a progressive lesion in the substantia nigra, characterized by more gradual loss of dopamine neurons and a prominent neuroinflammatory response in glial cells (Schintu et al., 2009). Mice were injected every other day with MPTP (25 mg/Kg, subcutaneous) and probenecid (250 mg/Kg, i.p.) for 7 days (MPTP prepared in saline as free base (Sigma, St. Louis, MO). Control mice received saline and probenecid (250 mg/Kg, i.p.) only. After the final exposure to MPTPp, mice were either terminated at day 7 (MPTPp7d) or at day 14 (MPTPp14d). Mice terminated at day 14 were gavaged once daily with either corn oil (vehicle control) or 50 mg/Kg of each respective C-DIM compound dissolved in corn oil (MPTPp14d + C-DIM5, MPTPp14d + C-DIM8, MPTPp14d + C-DIM12). Treatment with MPTPp in this model causes initial loss of dopamine neurons and a sustained neuroinflammatory response that causes further loss of dopamine neurons even after treatment with MPTPp has ceased (Schintu et al., 2009; Carta et al., 2011). All animal procedures were performed in accordance with NIH guidelines for the care and use of laboratory animals and were approved by the Colorado State University Institutional Animal Care and Use Committee. Every effort was made to minimize pain and discomfort. Terminal procedures were performed under deep isofluorane anesthesia.

Stereological Assessment of Dopamine Neurons in the SN: Tissue processing and stereologic deterimination of dopamine neuron numbers in the SN were carried out as reported previously

---

[1]Copyright a 2013 by The American Society for Pharmacology and Experimental Therapeutics

(Miller et al., 2011). Briefly, 7 or 14 days after treatment, animals were terminally anesthetized with isoflurane and transcardially perfused. After perfusion fixation, the brains were carefully removed from the skull and immersion fixed in the same fixative at 4 °C for 3 hr. The brains were then cryoprotected in cacodylate-PBS containing 15% sucrose overnight, followed by 30% sucrose. The tissue was then embedded and sectioned on a cryostat microtome. Sections were stored at –20 °C, free floating, in cryoprotectant (30% w/v sucrose, 30% v/v ethylene glycol; 0.5 M phosphate buffer, pH 7.2) until staining.

Free-floating serial sections used for tyrosine hydroxylase (TH; Millipore) staining were obtained using systematic sampling from all sections encompassing the entire length of the SNpc. Slides were stored at 4 °C until imaged for stereological counting. Stereological counts of TH-positive cells were performed using Slidebook software (v5.0, Intelligent Imaging Innovations, Denver, CO) employing the optical fractionator method (West and Gunderson, 1990). Images were captured using a Zeiss Axiovert 200M inverted fluorescence microscope equipped with a Hammatsu ORCA-ER-cooled charge-coupled device camera (Hammamatsu Photonics, Hamamatsu City, Japan). The boundary of the SNpc was determined by low-magnification (10x) montage imaging. Total numbers of TH-positive cells were obtained through imaging (40x) uniform randomly placed counting frames (100 x 100 µm) using an optical dissector of 30 µm with 5 µm upper and lower guard zones. Representative montage images were generated for each treatment group using a 20x objective and displayed using inverted monochrome.

Liquid Chromatography/Tandem Mass Spectrometry Analysis of C-DIM Metabolites. Standard dilutions of C-DIMs were prepared in 1:1 acetonitrile (ACN)/10 mM ammonium

acetate pH 7.5. For the analysis of each C-DIM in plasma and tissue homogenate, C-DIMs standards (1 – 1,000 ng/mL) were added to control plasma, urine or tissue homogenate (100 mg/mL in water using a PowerGen 700 tissue homogenizer [Fisher Scientific]). Samples were prepared utilizing one hundred microliters (100 μL) of plasma, urine or homogenate. Each sample was spiked with 10 μL of 1:1 ACN/10 mM ammonium acetate pH 7.5 or 10 μL of the appropriate C-DIM standard, 10 μL of 250 ng/mL naringenin as an internal standard, vortex briefly, and then 600 μL of 1:1 ACN/methyl tert-butyl ether (MTBE) was added. Samples were vortex continuously for 10 min followed by centrifugation for 10 min at 20,800 x g at 4ºC. Then, 500 μL of each supernatant was collected and transferred to a fresh 2 mL microcentrifuge tube. The samples were then dried on a Savant Automatic Environmental SpeedVac AES 1000 (Farmingdale, NY) using medium heat for approximately 1.25 hr. The samples were then re-suspended in 200 μL of 1:1 ACN/10 mM ammonium acetate pH 7.5, vortex for 5 min followed by centrifugation for 5 min, then transferred to HPLC vials with inserts for analysis. The in vitro formation of the glucuronide metabolite for each C-DIM was assessed using the method previously described (Guo et al., 2007).

Negative ion electrospray ionization (ESI) mass spectra were obtained with a MDS Sciex 3200 Q-TRAP triple quadrupole mass spectrometer (Applied Biosystems, Inc., Foster City, CA) with a turbo ionspray source interfaced to a Shimadzu LC-20AD High Performance Liquid Chromatograph system (Shimadzu Corporation, Kyoto, Japan). Samples were chromatographed with a Waters Sunfire C8, 5 μm, 4.6 x 50 mm column (Waters Corporation, Milford, MA) protected by a C18 guard cartridge, 4.0 x 2.0 mm (Phenomenex, Torrance, CA). An LC gradient was employed with mobile phase A consisting of 10 mM ammonium acetate and mobile phase B consisting of acetonitrile. Chromatographic resolution was achieved by linearly holding the B

solvent at 40% for 1 min. The solvent mixture was then altered by increasing mobile phase B linearly from 40% to 98% between 1 to 2 min, maintaining at 98% between 2 to 4 min, and then decreasing linearly from 98% to 40% between 4 to 4.5 min, followed by re-equilibration of the column at 40% mobile phase B from 4.5 to 6 min. The LC flow rate was 750 µL/min, the sample injection volume was 60 µL, and the analysis run time was 6 min.

The mass spectrometer settings were optimized as follows: turbo ionspray temperature, 600°C; ion spray voltage, -4500 V; curtain gas, N2, (CUR), 30 units; collision gas, N2, (CAD), Medium; nebulizer gas, N2, 60 units; and auxiliary gas, N2, 60 units. The compound specific parameters for each C-DIM are shown in Supplemental Table 1. The product ion scans obtained upon infusion of 1 µg/mL each C-DIM (in beginning mobile phase, 10 µL/min) into a 0.750 mL/min flow of starting mobile phase and suggested formation of the precursor ion, product ion and neutral loss can be seen in Figure 6A. The predominant product ions were m/z 116.0, 220.0, and 335.0 amu for C-DIM5, m/z 116.0, 204.0, and 243.0 amu for C-DIM7, m/z 116.0, and 220.0 amu for C-DIM8 and m/z 116.0 and 243.1 amu for C-DIM12. Samples were quantified in the multiple reaction monitoring (MRM) mode monitoring the relevant ion transitions and then summing the counts for each C-DIM. Each ion transition was integrated for 50 ms. Q1 and Q3 were both operated in unit resolution mode. All C-DIMs eluted between 2.0 and 4.0 min. Peaks were detected by monitoring the appropriate ion transitions for each compound. No interfering peaks were detected at the monitored ion transitions in extracted matrix (Figure 6B(a)). Chromatographic conditions were optimized for peak shape. Representative chromatographs of each C-DIM is shown at 1 ng/mL in plasma are shown in Figure 6B(b). Quantitation of each C-DIM was based on linear standard curves in spiked matrix with 1/x2 weighting of linear regression.

Mouse microsomal metabolism assay. Incubation of C-DIM8 and C-DIM12 with microsomes were conducted as previously described (Fisher et al., 2000). Briefly, 0.25 mg of mouse liver microsomes, 0.1 M potassium phosphate buffer (pH 7.1), and 12.5 mg of alamethicin were mixed and placed on ice for 15 min. MgCl2 (3.3 mM in incubation) and C-DIMs (1 µM C-DIM8 or 300 nM C-DIM12 in incubation) were added, and the mixture was preincubated at 37°C for 3 min. To initiate the reaction, UDPGA (5 mM in incubation) was added to give a 100 µL final volume. Control incubations were performed with heat-inactivated microsomes and immediate quenching of reactions after addition of UDPGA by adding 200 µL of ice-cold acetonitrile. Following addition of acetonitrile, samples were centrifuged to pellet precipitated protein and supernatant was analyzed as indicated above for metabolites in tissue and plasma samples. Relative abundance of metabolites was determined measuring peak areas of theoretical MRMs and comparing to parent peak areas for each C-DIM compound.

Plasma and urine incubation with β-glucuronidase. Plasma and urine were collected from animals 4 hrs following a single dose of C-DIM5, C-DIM7, C-DIM8 or C-DIM12, delivered by oral gavage at 10 mg/Kg in corn oil. Plasma and urine samples were then incubated with 300 µM saccharic acid or 500 units β-glucuronidase (Karunairatnam and Levvy, 1949; Guo et al., 2007) and analyzed as described above using mass spectrometry for the quantitation of parent C-DIM compound in each sample.

Pharmacokinetic and Statistical Analysis. Pharmacokinetic parameters were calculated from plasma or brain homogenate concentration-time data with standard noncompartmental methods using Excel. Descriptive statistics were used for pharmacokinetic variables (including Cmax,

Tmax, AUC0-t, and t1/2). Statistical analyses were performed using GraphPad Prism software

(v5.0); data sets were analyzed using one-way ANOVA with a Tukey-Kramer post test

(significance is denoted at *p<0.05). Oral bioavailability was calculated using eq. 1:

$$(1) \text{ \% Oral Bioavailability}=((AUC (Oral)/Dose (Oral))/(AUC (IV)/Dose (IV)))$$

RESULTS

Analytical characterization of diindolylmethane compounds.

Structures and masses of the four para-phenyl substituted diindolymethane compounds

examined in this study are described in Figure 5. The relative abundance of the C-DIM parent

compounds and the respective product ions under the mass spectrometry conditions used for

analysis are presented in Figure 6A. Multiple reaction monitoring (MRM) analyses detecting the

most abundant product ions for each drug were measured to ensure accuracy and sensitivity for

detection of each compound. Representative chromatographs used for analytical determination of

each C-DIM compound is described in Figure 6B, which depicts chromatograms of either blank

spiked with internal standard (a), C-DIM spiked plasma (b) or unknown sample (c).

Chromatograms shown in Figure 6B for plasma are similar to the standards measured for each C-

DIM compound in the various tissues examined in this study. Using this analytical method, we

were able to detect all four C-DIM compounds in biologically relevant matrices with a high level

of sensitivity.

Plasma levels of C-DIM compounds following intravenous and oral administration.

The plasma concentration over time for each substituted diindolylmethane analog is shown

in Figure 7, with the corresponding calculated non-compartmental pharmacokinetic values in

---

Table 1. AUC values for each C-DIM compound varied based on route of administration and individual C-DIM structure. Half-life (t1/2) in plasma for I.V. administration ranged from 71 (C-DIM8) to 144 min (C-DIM5); oral gavage t1/2 values ranged from 55 (C-DIM5) to 131 min (C-DIM7). The time each C-DIM took to reach Cmax (Tmax) following oral gavage administration was 60 minutes for C-DIM8 and 120 minutes for all others. Clearance as a function of bioavailability (CL/F), extrapolated volume of distribution (Vss), and mean resonance time (MRT) were dependent on C-DIM structure and route of administration; C-DIM8 was rapidly cleared when given orally, displaying a low AUC via this route.

The percent of oral bioavailability of each C-DIM compound was calculated based on their total exposure (AUC; Table 1). C-DIM5 and C-DIM12 exhibited the highest bioavailability at 38 and 42% respectively. It is likely that C-DIM8 (6% oral bioavailability) undergoes rapid first-pass hepatic metabolism when dosed orally because of glucuronidation of the phenolic group; this was further examined following incubation of C-DIM8 and C-DIM12 with liver microsomes (Table 3) and treatment of plasma and urine collected from treated mice with β-glucuronidase (Figure 9).

Brain levels of C-DIM compounds following intravenous and oral administration.

Brain levels of each C-DIM were determined to investigate the suitability of these compounds for use as potential neuroprotective agents in the CNS. Concentration of each compound in brain over time for each C-DIM analog are shown in Figure 8, with the corresponding calculated non-compartmental pharmacokinetic values in Table 2. Values reported in Table 2 for brain: plasma AUC suggest very reasonable distribution to the brain for each C-DIM compound evaluated, with brain:plasma AUC ratios for oral delivery of 3.2 (C-DIM8), 4.1

(C-DIM7 and C-DIM12) and 6.0 (C-DIM5). Corresponding Cmax values in brain tissue ranged from 31.2 (C-DIM8) to 1,173 ng/ml (C-DIM12). Amongst the compounds evaluated, C-DIM12 had the highest values for AUC in brain tissue following oral administration. The t1/2 measurements in brain tissue are similar to t1/2 plasma values for each respective C-DIM compound with the exception of C-DIM8, which displayed a significantly shorter plasma t1/2 (71 minutes in the plasma versus 248 minutes in the brain following I.V. dosing). Tmax, CL, and Kel across all C-DIM compounds varied based on compound and route of administration but, in general, were similar to their respective plasma pharmacokinetic measurements. These data indicate that each C-DIM reaches the brain via both I.V. and oral gavage routes of administration, with selected compounds, such as C-DIM12, exhibiting increased partitioning to the brain.

Tissue distribution of C-DIM compounds and identification of glucuronide metabolites in plasma and urine.

The pharmacokinetic analysis profiled plasma and brain levels of each compound, based on CNS as the primary intended target tissue, but we also determined the initial tissue distribution for each C-DIM compound, as well as the major metabolites in plasma and urine (Figure 9). Because AUC and half-life values for orally dosed C-DIMs peaked approximately 4 hours for brain tissue, we investigated the tissue distribution of each C-DIM at 4 hours following oral gavage (10 mg/Kg). As illustrated in Figure 9A, C-DIM levels are highest in the intestine for oral dosing and displayed similar distribution profiles as suggested by pharmacokinetic data; C-DIM8 levels were lowest in the peripheral tissues and C-DIM12 were highest, with the exception of the liver, where C-DIM5 levels were increased. No significant differences were observed

_____

between C-DIM levels in most tissues, except for the lung and liver where C-DIM8 was significantly lower than C-DIM5 and 12 (*$p<0.05$).

The structure of C-DIM8 contains a phenolic *R*-group substituent, which suggested that is was very likely to undergo glucuronide conjugation. To investigate this possibility for each C-DIM compound examined, we obtained plasma samples from mice four hours after a single 10 mg/Kg oral dose of each compound and then measured metabolites by LC-MS-MS following incubation with β-glucuronidase (n=3 mice per group). The addition of β-glucuronidase resulted in significantly increased levels of C-DIM8 parent compound, consistent with glucuronidation of the phenolic substituent (***$p<0.0001$, Figure 9B). β-glucuronidase treatment of plasma from mice treated with other C-DIM compounds did not result in a significant increase in concentrations of parent compound. Plasma was also treated with saccharic acid, an inhibitor of β-glucuronidase, but the levels of parent compound for C-DIM5, C-DIM7 and C-DIM12 remained unchanged relative to the increase observed in C-DIM8; indicating a possible metabolite other than a glucuronide that is converted back to parent C-DIM8. Similar metabolite profiles were observed in urine samples collected over four hours from mice housed in metabolic cages a single oral dose of each C-DIM compound at 10 mg/Kg (Figure 9C). Excreted C-DIM parent compounds measured in the urine were not affected by the addition of β-glucuronidase inhibitors with the exception of C-DIM8, which was significantly increased in the presence of β-glucuronidase, suggesting that the glucuronidated form of C-DIM8 is abundant in the urine four hours after a single oral dose of this compound.

_____

Determination of oxidative metabolites of C-DIM compounds.

Extracts from plasma, urine and various peripheral tissues were analyzed for putative metabolites of each C-DIM following a 10 mg/Kg oral dose for each drug. Mice were housed in metabolic cages and samples from plasma, urine and liver were collected 4 hrs after a single 10 mg/Kg oral dose of each C-DIM compound, based upon the calculated Tmax values (Table 1). Without valid reference standards for each metabolite, it was not possible to establish a complete quantitative profile of oxidative metabolites for each compound but theoretical MRM for various metabolic reactions that resulted in an identifiable mass signature are shown in Table 3. Metabolites were detected in plasma and urine, muscle, heart, and kidney tissues, as well as in reactions containing murine hepatic microsomes incubated with C-DIM8 and C-DIM12 for comparison of possible glucuronide formation. Microsomal preparations treated with 1 µM of C-DIM8 and 300 nM C-DIM12 revealed minor levels of oxidation (max abundance of 15% at 40 min of the parent AUC at 0 min) and di-oxidation (max abundance of 3% at 70 min of the parent AUC at 0 min). Oxidation of the indole ring (R2) was observed in plasma and urine for all C-DIM compounds, with the exception of C-DIM5, for which oxidation was only detected in urine. These similarities in metabolism are not surprising given the 1,1-bis (3'-indolyl) moiety, common to all C-DIM compounds. Measurement of C-DIM12 in urine incubated with β-glucuronidase indicated that oxidative dehalogenation occurred, resulting in generation of C-DIM8 parent compound, which is then metabolized to a glucuronide conjugate. A summary of the metabolism of each C-DIM compound is presented in Figure 10, which demonstrates that dealkylation of C-DIM5 and oxidative dehalogenation of C-DIM12 each generate the C-DIM8 parent compound.

Upon analysis of liver and urine of C-DIM8-treated mice, we observe an extensive peak corresponding to parent MRMs with a retention time of 1.08 min, which suggests in-source decay of a C-DIM8-glucuronide.

Neuroprotective efficacy of C-DIM compounds.

Based on the oral bioavailability and brain concentrations of C-DIMs, in vivo efficacy studies were conducted to determine the capacity of each C-DIM compound to prevent loss of dopamine neurons in the SN subacute MPTPp model of PD (Figure 11 and Table 4). Stereologic counting of dopamine neurons numbers in the SN indicated that mice treated for 7 days with MPTPp (MPTPp7d) displayed modest but significant loss of tyrosine hydroxylase (TH) positive neurons compared to saline treated animals (Table 4). Numbers of TH-positive neurons continued to decrease from day 7 to day 14, even after cessation of MPTPp treatment on day 7, leading to approximately 50% loss of TH-positive neurons by day 14 day (MPTPp14d; †$p < 0.05$ compared to MPTPp7d, *$p < 0.05$ compared to saline control, n=4). The number and integrity of dopaminergic neurons was assessed by immunofluorescence staining for TH, presented as the negative grayscale image for each representative brain specimen (Figure 11). Based upon these data, the neuroprotective efficacy of each C-DIM compound was evaluated using a post-lesioning strategy for delivery, where C-DIMs were administered by oral gavage during the 7-day period after MPTPp treatment (50 mg/Kg in corn oil vehicle, once daily from day 7 – day 14. Thus, MPTPp14 + C-DIM groups represent animals that have sustained injury to the SN prior to treatment with each C-DIM compound. Loss of dopaminergic soma, axons and dendrites was evident at both day 7 and day 14 in mice exposed to MPTPp (Figure 11A-C). This loss was attenuated in mice treated orally with C-DIM5, 8, and 12 (Figure 11D-F), with C-DIM12

resulting in the most obvious preservation of dopamine neuron number and structure. Stereological assessment of TH-positive neurons in the SN (Table 4) revealed that the number of dopamine neurons in mice treated with MPTPp + C-DIM5 and C-DIM12 was the same as MPTPp-treated mice at day 7, indicating that there was no further loss of dopaminergic neurons in the SN from day to day 14 in these groups. Moreover, the number of TH-positive neurons in the SN in mice treated with MPTPp + C-DIM5 and C-DIM12 was also significantly greater than the MPTPp14d group. The numer of TH-positive neurons in C-DIM8-treated mice was not different from the MPTPp7d group but also not different than the MPTPp14d group, despite an obvious trend toward a greater number of neurons in the SN.

DISCUSSION

The objective of this study was to characterize the pharmacokinetic behavior of selected para-phenyl substituted diindolylmethane (C-DIM) compounds and to assess the comparative efficacy of each compound in vivo in attenuating the progressive loss of dopamine neurons in the subacute MPTPp model of PD. Determination of levels of each C-DIM compound and major metabolites by LC-MS-MS in plasma, urine and tissues indicated bioavailability and pharmacokinetic values following oral dosing that are acceptable for a potential small molecule therapeutic. The pharmacokinetics of the parent 3-3'-diindolylmethane molecule has been previously studied in mice following administration of a single dose by oral gavage, which revealed that levels of diindolylmethane (a diaryl methane) rapidly increased in tissues followed by a relatively long elimination phase (Anderton et al., 2004). A single oral dose of para-phenyl substituted C-DIM compounds (a triaryl methane) in the present study gave a similar result, with a rapid increase in the plasma concentration of each drug, as well as distribution into brain and

peripheral tissues. Each of the four C-DIM compounds tested displayed variable distribution in the plasma and brain based on structure and route of administration (Table 1, Table 2). Oral administration yielded increased accumulation in brain tissue for each C-DIM compound, except C-DIM8, and significantly increased the Cmax in brain for C-DIM12 from 272 ng/ml (I.V.) to 1,173 ng/ml (oral; Table 2). Calculated values for the brain/plasma AUC ratio further support oral dosing as an acceptable route of administration for C-DIM compounds targeted to the CNS, with markedly increased brain AUC/plasma AUC values over intravenous injection (Table 2). An orally bioavailable drug has obvious advantages as a therapeutic agent and verification of distribution to the brain via this route supports further study of C-DIM compounds for treatment of neurodegenerative diseases.

Based on plasma pharmacokinetics, we determined which C-DIM compound displayed the most biologically relevant kinetic properties for in vivo efficacy studies. C-DIM12 given orally has the largest AUC (115,891 ng/ml/min) and Cmax (606 ng/ml), and the slowest clearance rate (86.3 ml/min*Kg) in plasma. In contrast, orally dosed C-DIM8 has the smallest AUC (9,129 ng/ml/min) and Cmax (28.0 ng/ml) and the most rapid rate of clearance (1,941 ml/min^{-1} Kg; Table 1) in plasma. Because C-DIM8 administered by oral gavage was more rapidly metabolized than after I.V. dosing, we postulated that glucuronide conjugation likely took place during first-pass metabolism in the liver. Urine and plasma measurements showed a significant increase in C-DIM8 parent compound when treated with β-glucuronidase, an enzyme that degrades glucuronic acid conjugates (Figure 9B and C). No other C-DIM compounds were significantly affected following incubation with this enzyme, suggesting that only the C-DIM8 parent compound undergoes direct glucuronide conjugation, which is consistent with its phenolic R-group. Due to its rapid metabolism and clearance, C-DIM8 may be less effective as a

---

neuroprotective agent in chronic disease studies; however, initial in vitro screening studies conducted in our laboratory indicated that C-DIM8 displayed similar activity to C-DIM5 and 12 in suppressing cytokine-induced expression of inflammatory genes such as NOS2, TNFα family member 10 (TRAIL), and IL-1β mRNA in activated astrocytes (unpublished data). Thus, the presence of a small, relatively polar R- group on the aryl ring substituent may correlate with neuroprotective activity, although more extensive structure-activity studies will be needed to determine the precise structural components contributing to this activity.

The putative metabolites of C-DIMs were identified using theoretical MRM and indicated that the shared indole structure undergoes common oxidative metabolism for all compounds (Table 3; Figure 11). Despite the similar parent structure, differential metabolism of the substituent group for each C-DIM clearly plays a role in the pharmacokinetics of C-DIMs and this was particularly evident for glucuronide conjugation to the hydroxyl group of C-DIM8 (Figure 11). Although more detailed metabolic studies need to be performed for each C-DIM compound, identification of major metabolites is helpful in establishing an initial profile for further examination of therapeutic efficacy.

The failure of small molecule therapeutics to modulate neurodegenerative disease is largely blamed on unsuccessful translation of rodent studies to human trials (Glass et al., 2010). This may be due in part to poor CNS pharmacokinetic behavior following oral dosing and incongruities between routes of administration in rodent studies compared to human clinical trials. Oral bioavailability is a desirable property of any putative therapeutic agent and calculated oral bioavailability for the C-DIM compounds ranged from 6% (C-DIM8) to 42% (C-DIM12) (Figure 9), similar to Levodopa (41 ± 16%), the most widely used PD symptomatic treatment. In comparison, the monamine oxidase B inhibitor Selegiline indicated for idiopathic PD has an oral

bioavailability of less than 10% (Robertson et al., 1989; Heinonen et al., 1994; Azzaro et al., 2007). Based on these data, it is reasonable to postulate that orally delivered C-DIM compounds, particularly C-DIM12, would distribute adequately to the CNS and could therefore be suitable agents for translational efficacy studies.

To determine to the neuroprotective efficacy of C-DIM compounds in a relevant animal model of PD, we used a subacute dosing strategy with MPTP and probenecid in mice to induce modest loss of dopamine neurons over a 7-day period, after which neuronal loss continued for an additional 7 days in the absence of MPTPp exposure, indicating an ongoing neuroinflammatory lesion (Schintu et al., 2009; Carta et al., 2011; Hirsch and Hunot, 2009). Administration of either C-DIM5 or C-DIM12 attenuated the progressive loss of neurons in the SN after the initial neurotoxin-induced lesion (Figure 11 and Table 4). In contrast, C-DIM8 demonstrated less neuroprotective activity following MPTPp exposure, with neuronal counts in the SN remaining statistically unchanged from the MPTPp 14-day time point, although counts did trend toward those determined at the 7-day time point (Table 4). The relatively lower efficacy of C-DIM8 may be the result of its greater clearance due to high first-pass metabolic elimination through rapid formation of the glucuronide conjugate. Interestingly, oxidative metabolism of both C-DIM5 and C-DIM12 generates the phenolic metabolite corresponding to the C-DIM8 parent compound, which could extend the potential window of efficacy of these compounds by forming a metabolite that retains a degree of neuroprotective activity.

The dosing regimen used in these studies was established to mimic what is clinically relevant for individuals with early stages of PD, when dopamine neuron loss in the SN has already occurred at the time of diagnosis (Meredith et al., 2008). The selected C-DIM compounds examined in this model, particularly C-DIM5 and 12, displayed excellent

pharmacokinetic behavior following oral administration and were effective and inhibiting progressive loss of dopamine neurons in a post-lesioning model of PD. In previous in vitro studies with two other C-DIM analogs in this series, 1,1-bis(3'-indolyl)-1-(p-trifluoromethylphenyl)methane (C-DIM1) and 1,1-bis(3'-indolyl)-1-(p-t-butylphenyl)methane (C-DIM4), we reported that these compounds suppressed activation of NF-κB in mixed glial cultures exposed to inflammatory stimuli that prevented expression of inducible nitric oxide synthase (NOS2) and protected co-cultured neurons from apoptosis (Carbone et al., 2008, Tjalkens et al., 2008). The mechanism underlying this anti-inflammatory activity in glia involved stabilization of nuclear co-repressor proteins that prevented DNA binding of NF-κB at cis elements in the NOS2 promoter. Because C-DIM5 and C-DIM12 are activators in cancer cell lines of the NR4A family nuclear receptors Nur77 and Nurr1, respectively (Inamoto et al., 2008, Lee et al., 2011; 2012; Li et al., 2012) they may exert neuroprotective effects by broadly suppressing NF-κB-dependent expression of inflammatory genes in glia, as suggested in recent studies characterizing the neuroprotective role of Nurr1 in PD (Saijo et al., 2009). Examination of the three C-DIM compounds used in the present studies indicated that although these compounds may have similar neuroprotective activities in vitro, the differing substituents on the aryl ring yield distinct pharmacokinetic profiles, which may in part be responsible for the differences in efficacy observed in vivo. These data should be useful for designing additional pharmacodynamic efficacy studies to further characterize mechanisms underlying the neuroprotective efficacy of these and related C-DIM compounds and the role of NR4A receptors in mediating these effects.

FIGURE 5
C-DIM STRUCTURES

Compound Name	'R'	MW
C-DIM5: 1,1-bis(3'-indolyl)-1-(*p*-methoxyphenyl)methane	-OCH3	352.4
C-DIM7: 1,1-bis(3'-indolyl)-1-(phenyl)methane	-H	322.4
C-DIM8: 1,1-bis(3'-indolyl)-1-(*p*-hydroxyphenyl)methane	-OH	338.4
C-DIM12: 1,1-bis(3'-indolyl)-1-(*p*-chlorophenyl)methane	-Cl	356.9
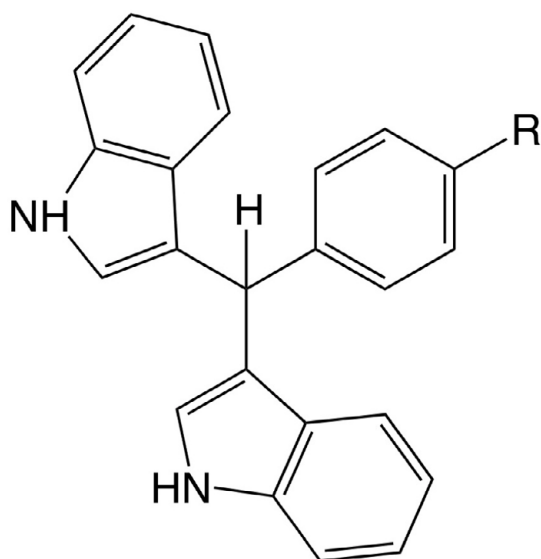
Figure 5. Structure and molecular weight of *para*-substituted diindolylmethane (C-DIM) compounds.

FIGURE 6
DETECTION OF C-DIMS

48
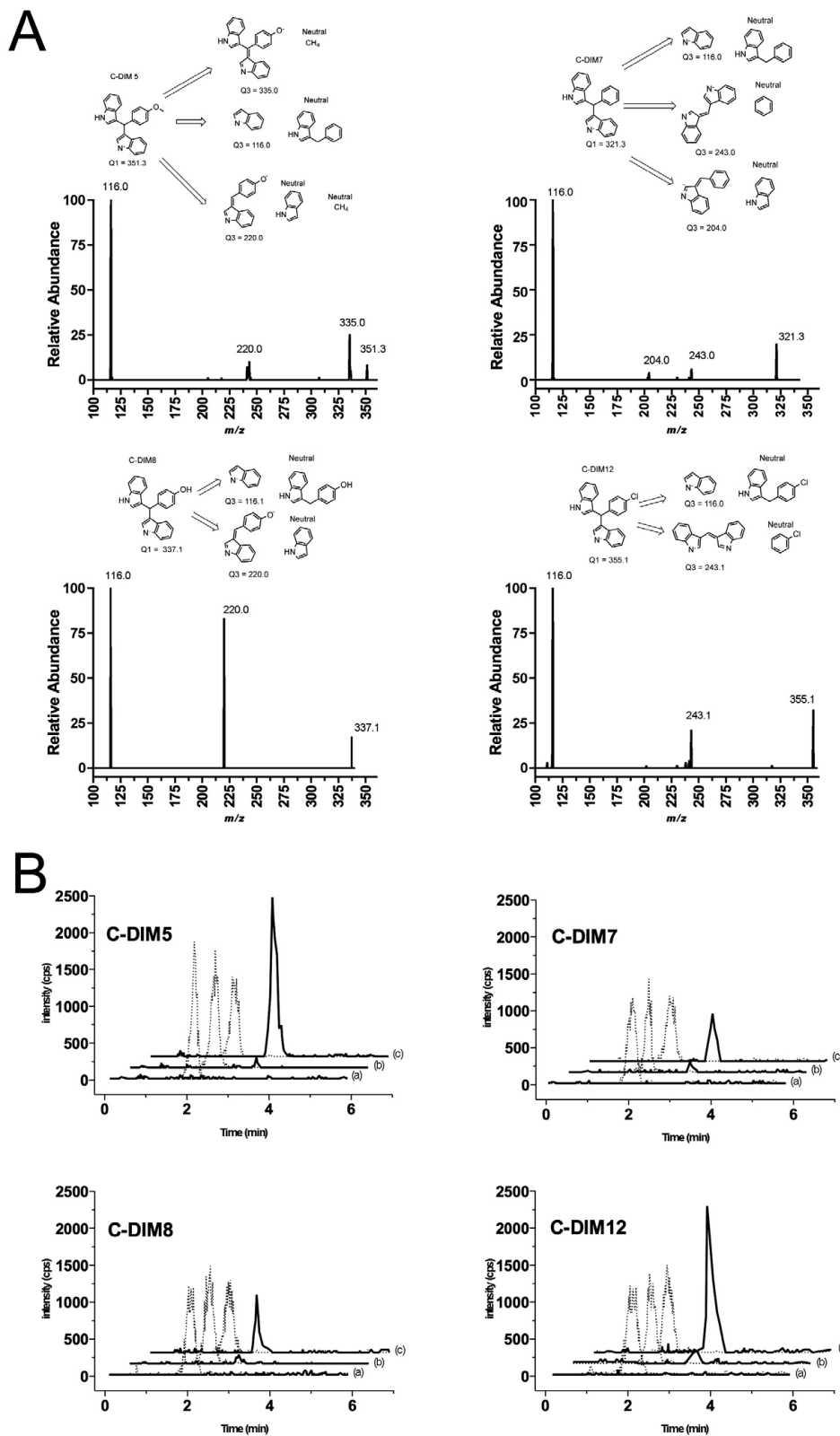
Figure 6. Analytical determination of C-DIM compounds in plasma by liquid chromatography tandem mass spectrometry (LC-MS-MS). (2A) Product ion spectra and proposed structures for each C-DIM compound identified by LC-MS-MS. (2B) Blank mouse plasma spiked with 25 ng/mL of naringenin, the internal standard (A). C-DIM 5, 7, 8, and 12 were spiked into blank plasma at 1 ng/mL with internal standard (B). A representative mouse plasma sample spiked with 25 ng/mL naringenin internal standard (C). The solid line represents the summed m/z transitions for each C-DIM compound. The retention times for C-DIM5, C-DIM7, C-DIM8 and C-DIM12 were 3.0 min, 3.0 min, 2.8 min and 3.0 min, respectively. The dashed line represents the internal standard for the m/z transition from $271.0 \rightarrow 119.0$ (R_t = 1.9 min).

FIGURE 7
PLASMA C-DIM CONCENTRATION
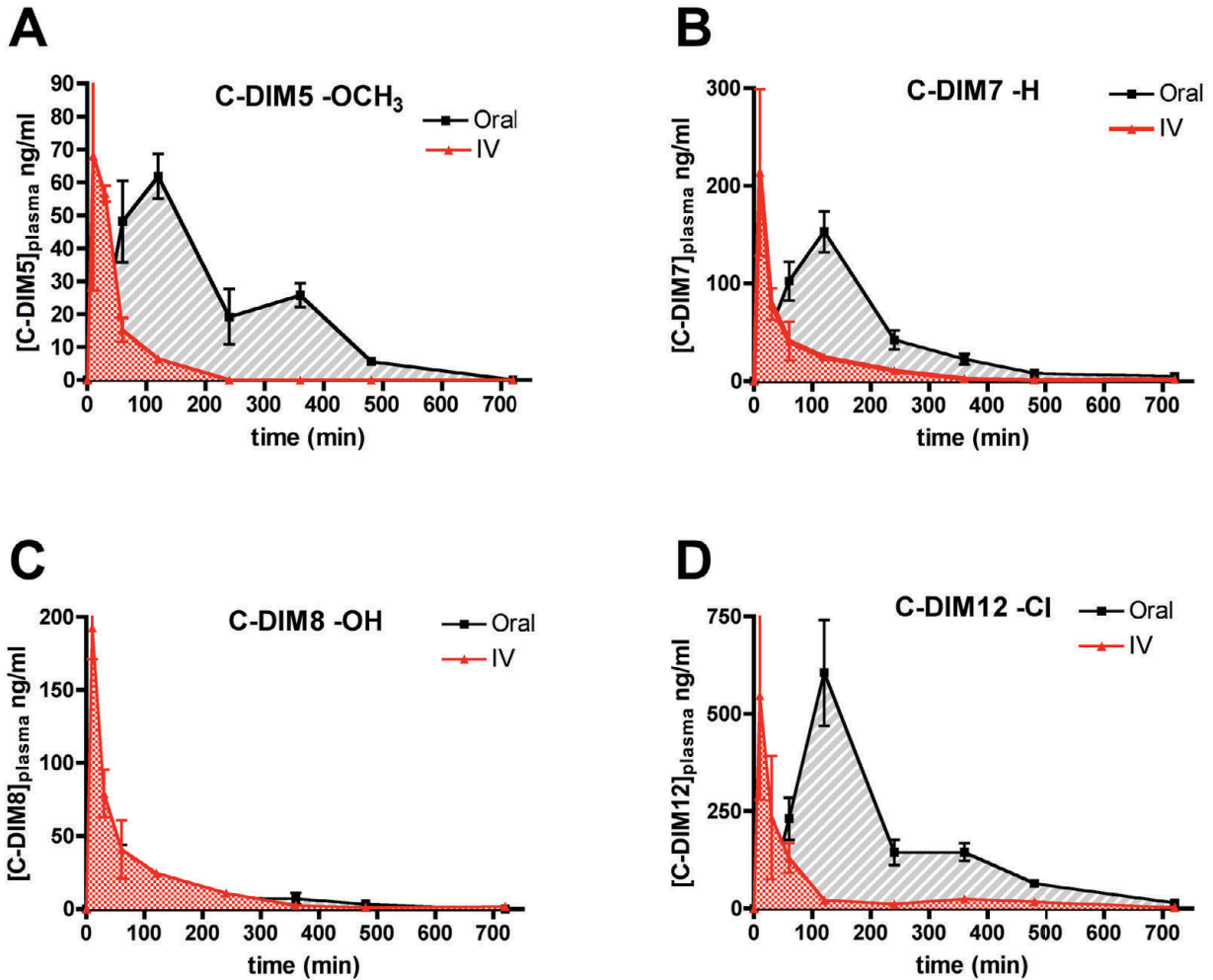
Figure 7. Plasma pharmacokinetic distribution of C-DIM compounds. Plasma concentrations for C-DIM compounds and relationship between the route of exposure and plasma concentration. Points represent average plasma level for either IV (red) or oral gavage (black) of C-DIM5 (A), C-DIM 7 (B), C-DIM8 (C) or C-DIM12 (D) over a period of 12 hours (n=3 animals per timepoint for each route of exposure).

FIGURE 8
BRAIN CONCENTRATION OF C-DIMS
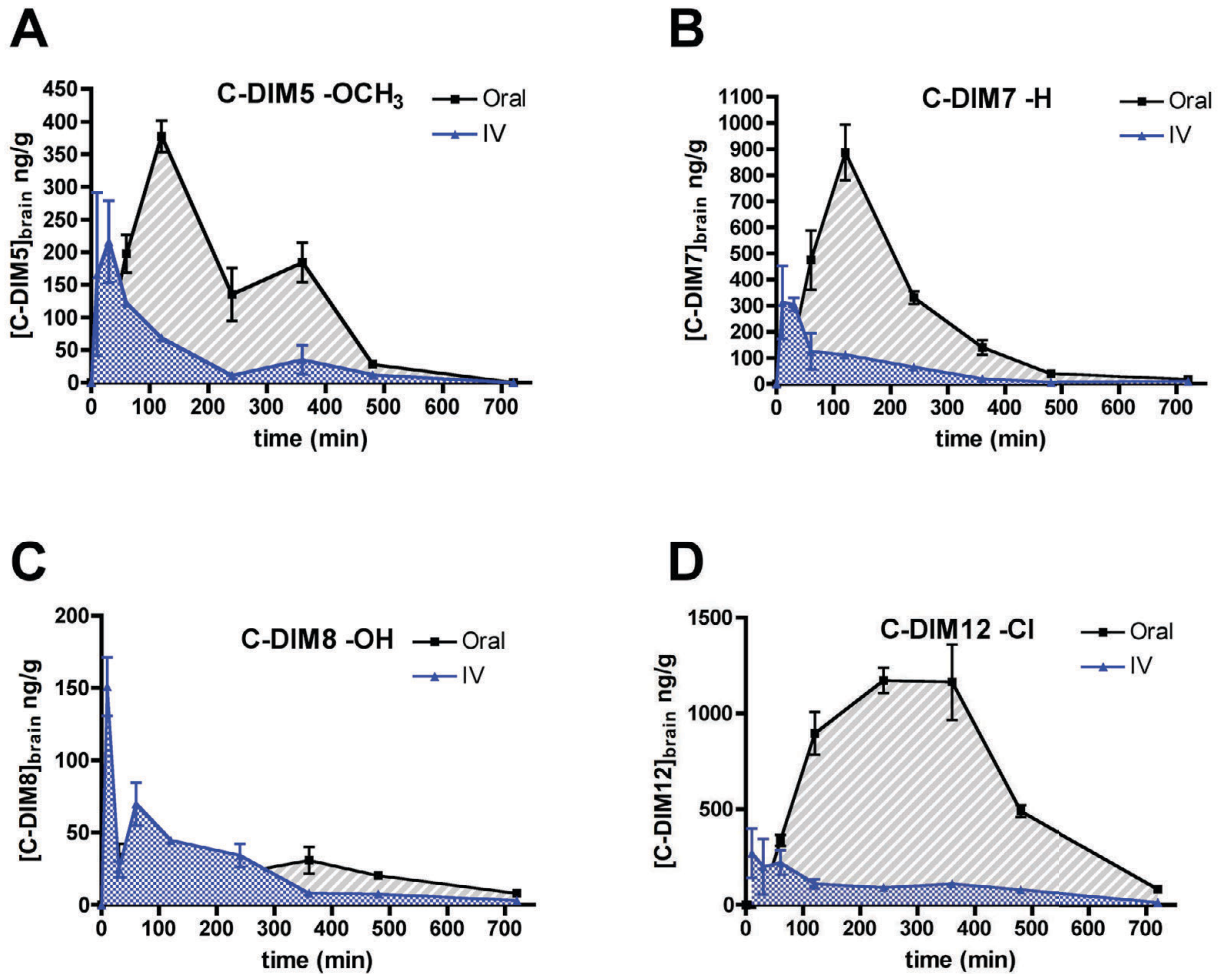
Figure 8. Brain pharmacokinetic distribution of C-DIM compounds. Brain tissue concentrations for C-DIM compounds and relationship between route of exposure and concentration in brain. Points represent average brain tissue level for either IV (blue) or oral gavage (black) of C-DIM5 (A), C-DIM7 (B), C-DIM8 (C), or C-DIM12 (D) over a period of 12 hours (*n*=3 animals per timepoint for each route of exposure).

FIGURE 9
TISSUE ACCUMULATION
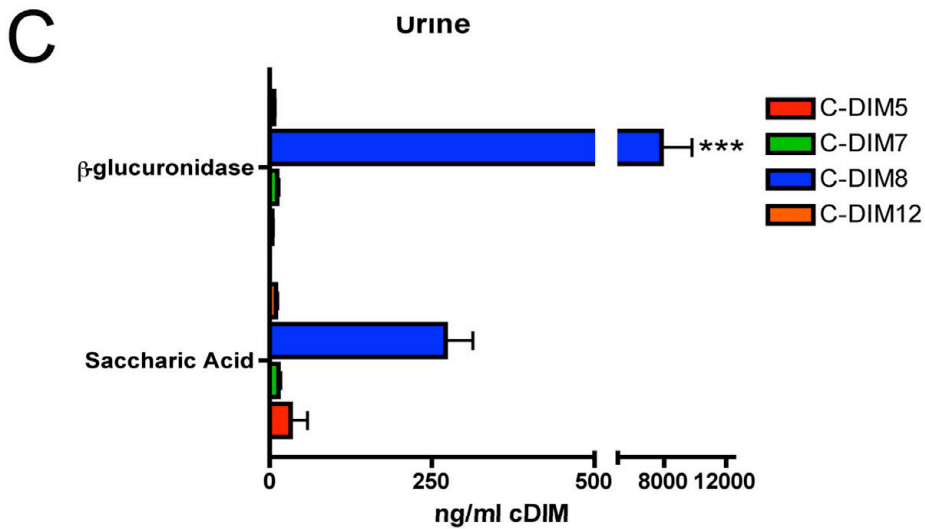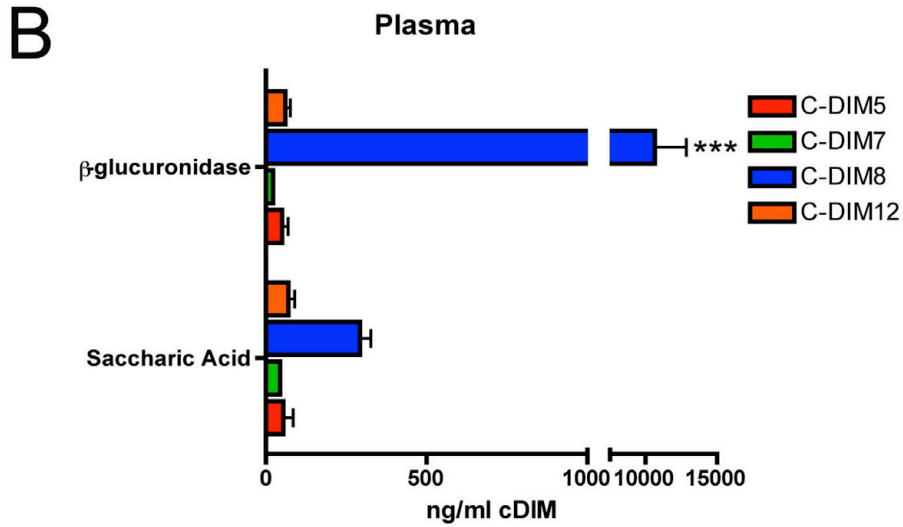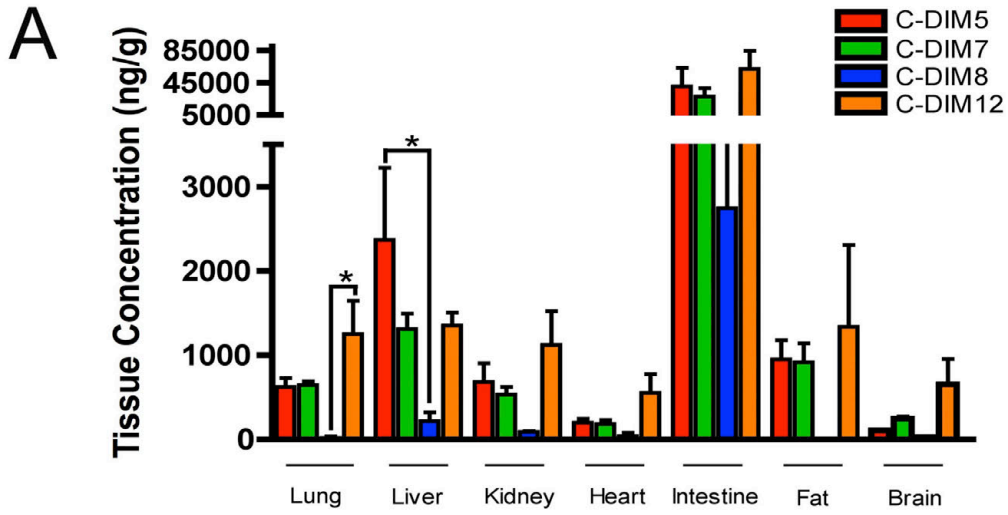
Figure 9. Tissue accumulation and metabolism of C-DIM compounds following oral dosing. (A) Mice were administered a single oral dose (10 mg/Kg) of C-DIM5, C-DIM7, C-DIM8 or C-DIM12 and examined for tissue distribution of each C-DIM compound 4 hours after dosing, the time at which peak plasma and brain concentrations of drug were measured in pharmacokinetic studies. Colors denote different C-DIM compounds, error bars represent standard deviation, and significance is indicated by * ($p<0.05$, $n=3$ animals per group). Plasma (B) and urine (C) were also collected and samples were treated with β-glucuronidase or saccharic acid (control) and the concentration of each C-DIM parent compound determined by LC-MS-MS. Mice were housed in metabolic cages for urine collection. Colors denote different C-DIM compounds, error bars represent standard deviation, and significance is indicated by *** ($p>0.001$, $n=3$ animals per group).

FIGURE 10
METABOLISM OF C-DIMS
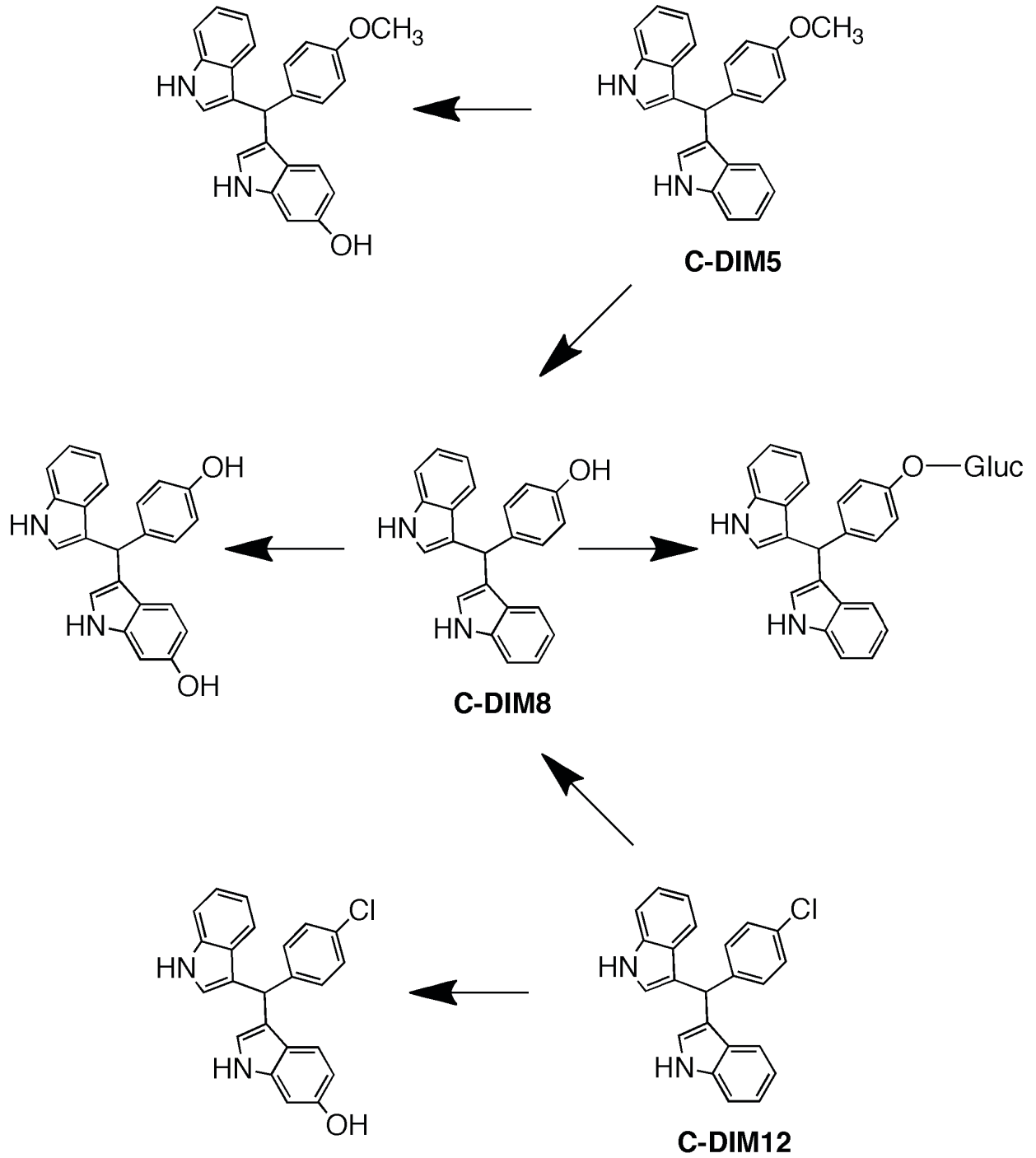
C-DIM5

C-DIM8

C-DIM12

Figure 10. Metabolic scheme for C-DIM compounds. Identified metabolites of parent C-DIMs reported in Table 3 are depicted here to illustrate the common oxidative metabolism observed for C-DIM5, C-DIM8 and C-DIM12.

FIGURE 11
C-DIM NEUROPROTECTION IN THE SN
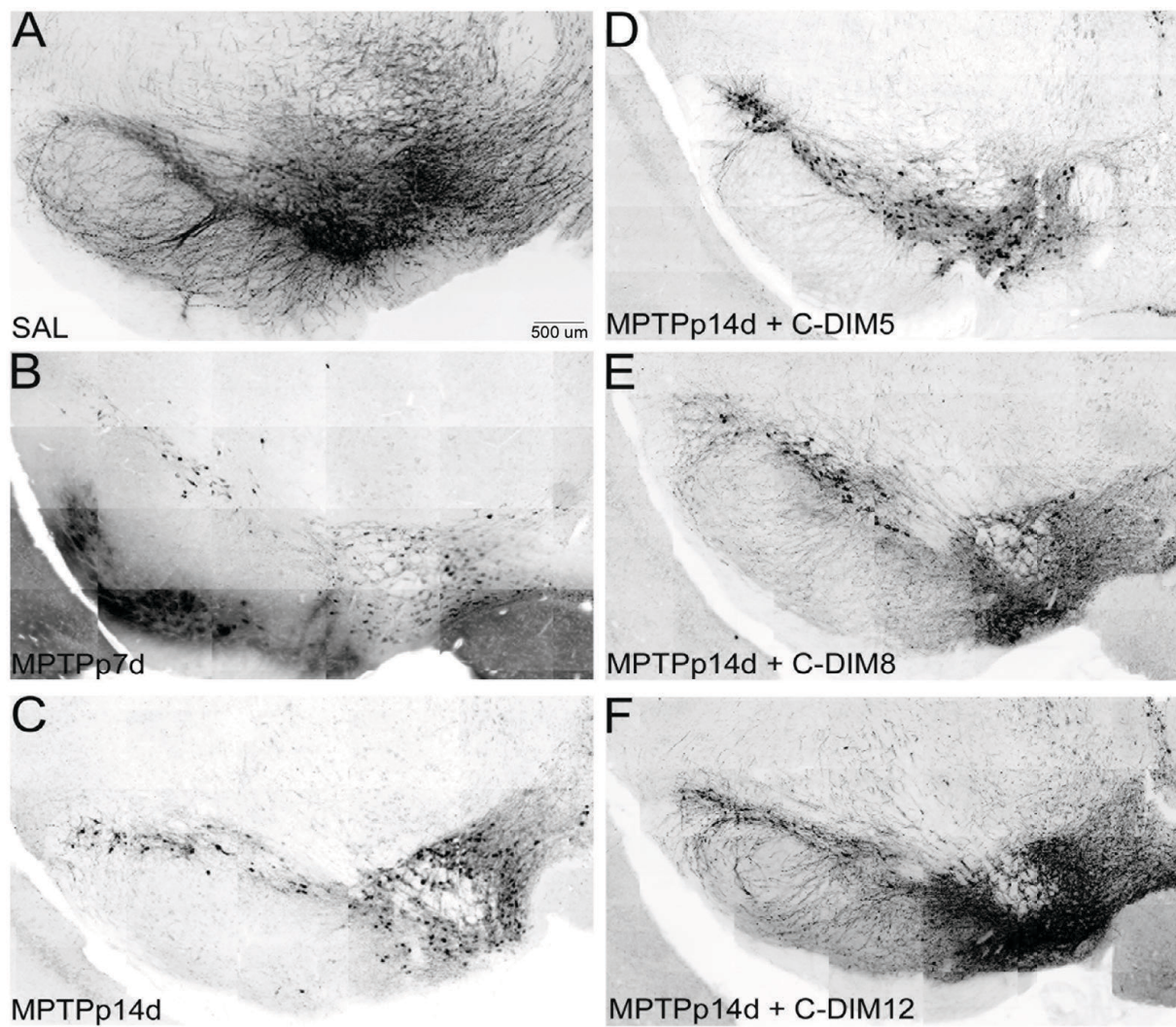
Figure 11. Neuroprotective effects of C-DIM compounds on tyrosine hydroxylase staining in the substantia nigra. Representative montage images of tyrosine hydroxylase-positive neurons in the substantia nigra pars compacta (SN) indicate that, compared to saline treated controls (A), MPTPp treatment causes loss of dopaminergic cell bodies and processes by 7 days (B) that progresses by 14 days (C), even after cessation of MPTPp treatment on day 7. Images in panels A-C depict the progressive loss of dopamine neurons expressing TH in the SN during MPTPp treatment regimen. Panels D-F represent the SN of C-DIM treated animals given daily oral gavage (50 mg/Kg) of C-DIM5, 8, or 12 from day 7 through day 14, after dosing with MPTPp. Dopamine neuronal cell bodies as well as axons are preserved in these animals at levels similar to MPTPp7d treatment, indicating protection against loss of TH-positive cells when C-DIMs are administered after the onset of neuronal injury. Montages were reconstructed from each series of 20X individual images. Tyrosine hydroxylase immunofluorescence images were converted to inverted monochrome for presentation. Scale bar = 500 μm.

FIGURE 12
C-DIM PROTECTION IN THE ST
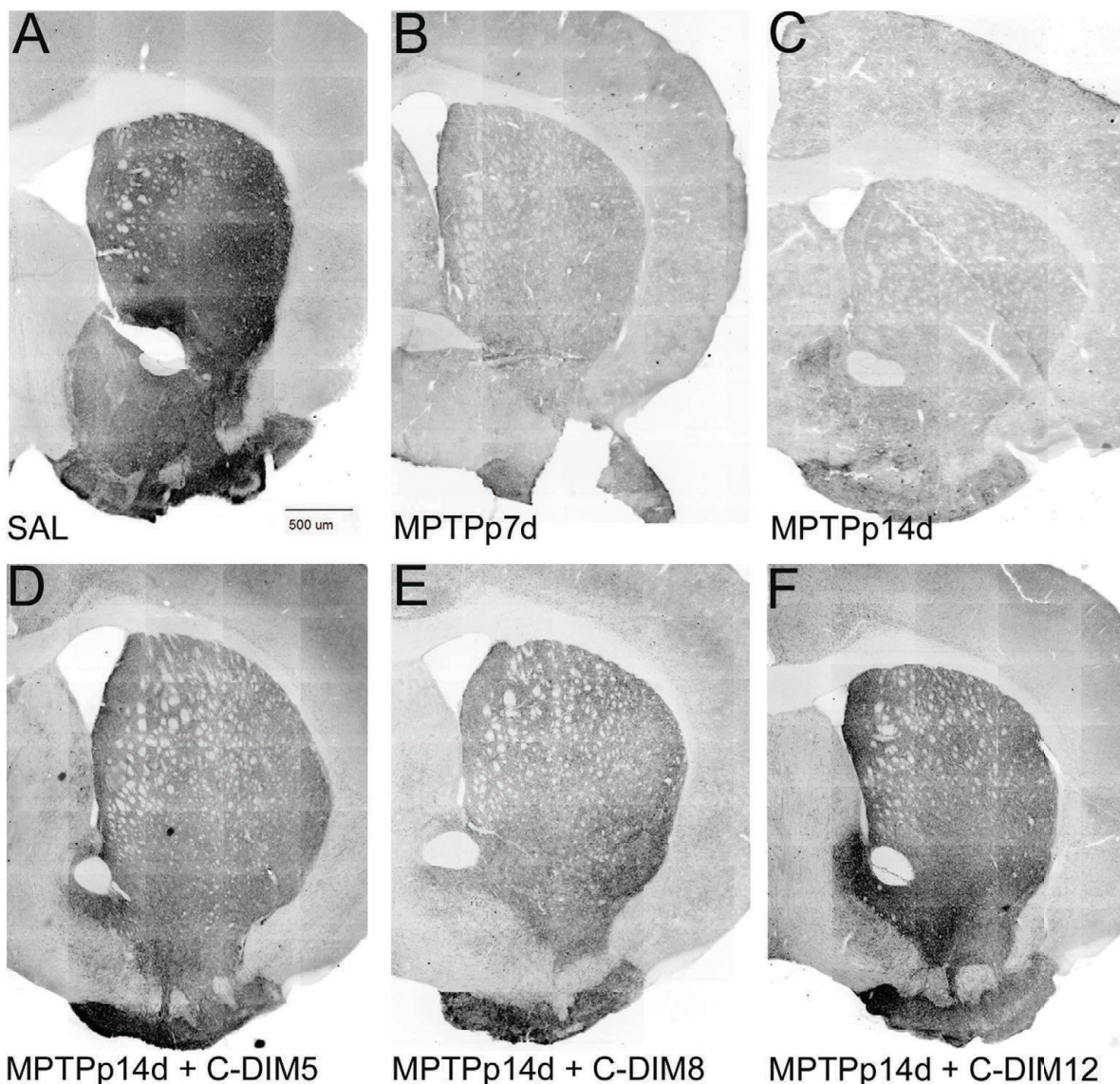
Figure 12. Neuroprotective effects of C-DIM compounds on TH expression in the ST.
Representative montage images of TH immunostaining in the striatum of mice treated with
saline (SAL) (A), MPTPp 7 days (B), MPTPp 14 days (C), MPTPp 14 days plua C-DIM5 (D),
MPTPp 14 days plus C-DIM8 (E), and MPTPp 14 days plus C-DIM12 (F). Loss of TH intensity
in the ST was evident 7 days after treatment with MPTPp and continued to decrease through 14
days after MPTPp treatment. All three C-DIM com- pounds prevented this progressive decrease
in striatal TH intensity on days 7–14. Representative montages were reconstructed from each
series of 10 individual images stained for TH immunofluoresence and converted to inverted
monochrome for presentation. Scale bar = 500 mm.

TABLES

TABLE 1
PLASMA PHARMACOKINETICS

Table 1. Plasma pharmacokinetic values of C-DIM compounds

Data representing the mean of three animals per time point per C-DIM compound were used for the construction of brain tissue concentration versus time curves (Fig. 3).

Noncompartmental modeling was used for the calculation of pharmacokinetic parameters based on the composite data.

C-DIM (Plasma)	$AUC_{0->720\ min}$	$t_{1/2}\lambda$	$CL_{(area)/kg}$	$AUMC_{0->t}$	V_{ss}	MRT	Oral Bioavailability
	$(ng/ml) \times min$	min	$ml/min \times kg$	$(\mu g/ml) \times min^2$	l/kg	min	$\%$
C-DIM5 I.V.	3,838	144	261	356	24.2	93	–
C-DIM5 Oral	14,828	55	–	2,971	–	200	39
C-DIM7 I.V.	9,727	139	103	993	10.5	102	–
C-DIM7 Oral	29,577	131	–	5,167	–	175	30
C-DIM8 I.V.	9,129	71	109	602	7.13	66	–
C-DIM8 Oral	5,151	114	–	1,012	–	196	6
C-DIM12 I.V.	27,391	133	36.5	4,184	5.58	153	–
C-DIM12 Oral	115,891	110	–	24,648	–	213	42

AUC, area under the curve; AUMC, area under the first-moment curve; C-DIM, *para*-phenyl subsitiuted diindolyl-methane; CL, clearance limit; K_{el}, elimination rate; MRT, mean residence time.

TABLE 2
BRAIN PHARMACOKINETICS

Table 2. Brain pharmacokinetic values of C-DIM compounds

Data representing the mean of three animals per time point per C-DIM compound were used for the construction of brain tissue concentration versus time curves (Fig. 4).

Noncompartmental modeling was used for the calculation of pharmacokinetic parameters based on the composite data.

C-DIM (brain)	$AUC_{0->720\ min}$	C_{max}	$t_{1/2}\lambda$	T_{max}	$CL_{(area)/kg}$	$K_{el}\lambda$	Brain AUC: Plasma AUC
	$(ng/ml) \times min$	ng/ml	min	min	$ml/min \times kg$	$(\mu g/ml) \times min^2$	
C-DIM5 I.V.	23,192	216	47	30	261	0.0146	6.0
C-DIM5 Oral	88,325	378	44	120	647	0.0157	6.0
C-DIM7 I.V.	39,397	313	147	10	103	0.0047	4.1
C-DIM7 Oral	171,596	887	112	120	338	0.0062	5.8
C-DIM8 I.V.	16,165	151	248	10	109	0.0028	1.8
C-DIM8 Oral	16,322	31.2	187	360	1,941	0.0037	3.2
C-DIM12 I.V.	68,042	272	117	10	36.5	0.0059	2.4
C-DIM12 Oral	465,845	1,173	95	240	86.3	0.0073	4.1

AUC, area under the curve; C-DIM, *para*-phenyl subsitiuted diindolylmethane; CL, clearance limit; K_{el}, elimination rate.

TABLE 3
C-DIM METABOLITES

Table 3. Identification of putative C-DIM metabolites using theoretical MRM(s)

Putative metabolites are listed for each C-DIM, indicating the structural position to which metabolism occurs. Metabolites were detected in several tissues, plasma and urine.
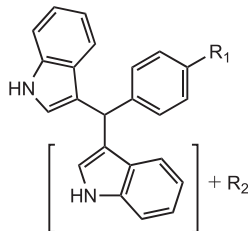
Compound	Theoretical Metabolism	Tissue/Microsome Observed in	R_1	R_2/Addition to Indole Ring	MRM(s) / Theoretical MRM(s) used to ID Putative Metabolite
C-DIM5			OCH_3	—	$351.3 \rightarrow 335, 116, 220$
	Oxidation	U ± β-gluc; L; B	OCH_3	O	$367.3 \rightarrow 132, 116$
	Demethylation	L; M; H; K; B	OH	—	$337.3 \rightarrow 116$
	Demethylation and addition of glucose	U	O-glucose	—	$513.4 \rightarrow 116$
C-DIM7			H	—	$321.3 \rightarrow 116, 243, 204$
	Oxidation	P ± β-gluc; U ± β-gluc; L; K; B	H	O	$337.3 \rightarrow 132, 116$
C-DIM8			OH	—	$337.1 \rightarrow 116, 220$
	Addition of glucose	P; U	O-glucose	—	$513.1 \rightarrow 116$
	Oxidation	P; U ± β-gluc; L; Micro	OH	O	$353.1 \rightarrow 132, 116$
	Glucuronidation	U; L	O-Gluc	—	In source decay to parent MRMs with RT=1.08 min
C-DIM12			Cl	—	$355.1 \rightarrow 116, 243$
	Oxidation	P ± β-gluc; U + β-gluc; L; Micro; K; B; Lung	Cl	O	$371.1 \rightarrow 132, 116$
	Dehalogenation oxidation and glucuronidation	U + β-gluc	O-Gluc	—	$337.1 \rightarrow 220$

β-gluc, β-glucuronidase treated; C-DIM, *para*-phenyl subsitiuted diindolylmethane; Gluc, glucuronic acid; H, heart; K, kidney; L, liver; M, muscle; Micro, liver microsome incubation; MRM, multiple reaction monitoring; P, plasma; U, urine.

TABLE 4
STEREOLOGICAL COUNTS

Table 4. Stereological assessment of dopamine neuron numbers in the SN and TH staining intensity in the ST.

Treatment	SAL	MPTPp 7 Days	MPTPp 14 Days	MPTPp 14 Days Plus C-DIM5	MPTPp 14 Days Plus C-DIM8	MPTPp 14 Days Plus C-DIM12
TH $^+$ Neurons (SN)	11,434 ± 566	8,061 ± 1010*	5,689 ± 406*,†	8,556 ± 699*,‡	7,408 ± 2,587*	9,572 ± 823*,‡
TH Intensity (%Control) (ST)	100.0 ± 5.3	81.6 ± 3.5*	65.4 ± 2.6*	88.5 ± 3.9*,‡	89.3 ± 1.9*,‡	88.4 ± 0.6*,‡

C-DIM, *para*-phenyl subsitiuted diindolylmethane; MPTP, 1-methyl-4-phenyl-1,2,3,6-tetrahydropyradine; MPTPp. 1-methyl-4-phenyl-1,2,3,6-tetrahydropyradine with probenecid; SN, substantia nigra; ST, striatum; TH, tyrosine hydroxylase.
*$P < 0.05$ compared with saline control.
$^\dagger P < 0.05$ compared with MPTPp 7 days.
$^\ddagger P < 0.05$ compared with MPTPp 14 days.

Mice were treated with saline or MPTPp (25 mg/kg MPTP subcutaneous, 250 mg/kg probenecid intraperitoneal) every other day for 7 days (total four injections). MPTPp 7 day mice were terminated at 7 days and assessed using stereology for TH-positive neurons in the SN. Remaining groups were either given corn oil (MPTPp 14 days), C-DIM5 (MPTPp 14 days plus C-DIM5), C-DIM8 (MPTPp 14 days plus C-DIM8), or C-DIM12 (MPTPp 14 days plus C-DIM12) via daily oral gavage (50 mg/kg) for the following 7 days. After a total of 14 days, mice were used for stereology studies in the SN. Mean fluorescence intensity of TH expression in the ST as a representation of dopamine neuron terminal survival is presented for each treatment group as a percentage of control (SAL). Data are expressed as mean 6 S.E.M. (n = 4 animals per group).

TABLE 5
NEUROCHEMISTRY

Table 5. Dopamine and DOPAC levels in the striatum.

Treatment	SAL	MPTPp 7 Days	MPTPp 14 Days	MPTPp 14 Days Plus C-DIM5	MPTPp 14 Days Plus C-DIM8	MPTPp 14 Days Plus C-DIM12
Dopamine, ng/mg	49.0 ± 6.7	20.3 ± 2.3*	7.0 ± 3.9*	6.4 ± 1.4*	8.4 ± 2.3*	11.9 ± 3.9*
DOPAC, ng/mg	3.9 ± .81	2.5 ± .32	0.9 ± .14*	0.8 ± .13*	1.1 ± .14*	1.4 ± .35*

DOPAC, 3,4-dihydroxyphenylacetic acid; HPLC, high performance liquid chromatography; MPTPp, 1-methyl-4-phenyl-1,2,3,6-tetrahydropyradine with probenecid; SAL, control; TH, tyrosine hydroxylase.
* $P < 0.05$ compared with saline control.

A separate set of mice from the same MPTPp study used in stereological and TH intensity assessment (Table 4) were also analyzed for striatal levels of dopamine and its primary metabolite DOPAC with use of HPLC. Data are expressed as mean 6 S.E.M. (n = 5 animals per group).

CHAPTER 4

NOVEL *PARA*-PHENYL SUBSITIUTED DIINDOLYLMETHANES PREVENT GLIAL

ACTIVATION OF NF-KAPPA-B-DEPENDENT SIGNALING IN A MOUSE MODEL OF

PARKINSON'S DISEASE

INTRODUCTION

A growing understanding of the mechanisms that underline dopamine neurotoxicity

in Parkinson's disease (PD), has greatly affected the view of potential therapies for this

neurodegenerative disorder. Once believed that the loss of dopamine producing neurons from the

substantia nigra pars compacta (SNpc) was the primary feature of the disease, it is now well

recognized that glial inflammation plays a central role (Glass et al., 2010; Hirsch and Hunot,

2009a; Nolan et al., 2013; Tansey and Goldberg, 2010). While it remains unclear whether the

inflammation produced by glial cells in the ventral midbrain is an inciting factor in PD, clear

evidence suggests that microglia and astrocytes are directly involved in the neurotoxicity that

drives the progressive phase of neuron cell death (Hirsch and Hunot, 2009a; Tansey and

Goldberg, 2010).

Immune modulation in the central nervous system (CNS) is regulated by resident

macrophage cells-microglia-which, under normal conditions, are in a deactivated state to survey

their microenvironment (Saijo et al., 2013). Microglia express pattern recognition receptors

(PRRs) on their cell surface to detect pathogens or tissue damage, and rapidly activate to initiate

tissue repair mechanisms when necessary (Lambertsen et al., 2009). Tight regulatory control

over the genes that upregulate inflammatory mediators in microglia (NF-κB, AP-1) are repressed

under healthy conditions by cytoplasm sequestering proteins (e.g., IkBa) and nuclear corepressors (e.g., NCoR2) on gene promoters (Carbone et al., 2008; Ghisletti et al., 2009). Production of antimicrobial factors such as reactive oxygen species (ROS), cytokines (e.g., TNFα, IL-1β), and chemokines to attract additional cells (e.g. CCL2, CCL5) are acutely toxic, but necessary to maintain homeostasis (Bianchi et al., 2010; Thompson and Van Eldik, 2009). After damage resolution, negative feedback mechanisms such as nuclear corepressors and anti-inflammatory proteins (e.g., IL-10) suppress inflammatory gene transducers (e.g., NF-κB) to return microglia to a resting state (Collingwood et al., 1999). This self-limiting system of glial activation is dysregulated in neurodegenerative disease, where sustained inflammation leads to a persistent activation of microglia and astrocytes, producing pathologic levels of neurotoxic factors (Gao and Hong, 2008).

A novel mechanism for inflammatory resolution in the glia was described by Saijo et al. (2009), where the orphan nuclear receptor Nurr1 (NR4A2) was shown to have transrepressive activity on NF-κB. The activation of Nurr1 was neuroprotective by inhibiting inflammatory protein expression in glia. Conversely, lentiviral knockdown of Nurr1 in glia exacerbated dopamine neuron loss from the SN after LPS treatment. Mechanistic data from these experiments revealed that Nurr1 bound to NF-κB-p65 on inflammatory gene promoters, and recruited corepressor complex proteins (CoREST), which actively removed the transcription factors from their target genes (Saijo et al., 2009a). The transrepression mechanism of Nurr1 in the glia is a previously unknown target for inflammatory regulation in PD, where transcriptional inhibition of NF-κB-regulated genes could be modulated to reduce sustained inflammation.

A novel group of *para*-phenyl substituted diindolylmethanes (C-DIMs), derived from indol-3-carbinol, are a group of structurally similar analogs studied as potential cancer

therapeutics. Extensive mechanistic studies discovered they have specific activity on the family of orphan nuclear receptors (NR4A) (Inamoto et al., 2008; Li et al., 2012; Yoon et al., 2011). *Para*-methoxy containing C-DIM (DIM-C-pPhOCH$_3$; C-DIM5), has been shown to activate nuclear Nur77 expression in pancreatic and colon cancer cell lines(Lee et al., 2010; Yoon et al., 2011). C-DIM5 was also shown to induce a Gal4-Nur77 construct that contained ligand binding domain of Nur77(Lee et al., 2011). In bladder cancer cells, *para*-chloro containing C-DIM (DIM-C-pPHCl; C-DIM12) was shown to be a novel transactivator of Nurr1, inducing Gal4-Nurr1 in a dose-dependent manner (Inamoto et al., 2008). Additionally, C-DIMs have shown to decrease the production of proinflammatory, inducible protein nitric oxide synthase (NOS2) in astrocytes following *in vitro* stimulation with cytokines (Carbone et al., 2008; Tjalkens et al., 2008).

Pilot efficacy studies involving selected C-DIM compounds showed neuroprotection of dopamine neurons in the SN during the progressive phase of a mouse model of PD (De Miranda et al., 2013). Given the recent discovery of Nurr1 as a transrepressor of NF-κB expression in astrocytes and microglia, and the reported ability for C-DIMs to modulate NR4A activity in cancer cells, we postulated that C-DIM compounds exert their neuroprotection by suppressing NF-κB-regulated glial inflammation. To this end, we reproduced an established MPTPp model of progressive neurodegeneration in mice, and examined the ability of C-DIMs to suppress both dopamine neuron loss and glial activation after the initial onset of a PD-like lesion. Pharmacokinetic studies involving C-DIM5, C-DIM8 (DIM-C-pPhOH), and C-DIM12 confirmed that these compounds cross the blood brain barrier (BBB) and are orally bioavailable (De Miranda et al., 2013). A lesion in the SN was created using transgenic NF-κB-EGFP mice over 7 days (MPTPp7d) with neurotoxin MPTP (1-methyl-4-phenyl-1,2,3,6-tetrahydropyridine)

and probenecid, after which daily oral gavage of one C-DIM compound (C-DIM5, C-DIM8, or C-DIM12) or corn oil (vehicle) was given. After an additional 7 days post lesion (MPTPp14d) animals were assessed to compare NF-κB-regulated glial inflammation. Here we report that C-DIM compounds, which slow dopamine neuron loss after an initial lesion in the SN, attenuated microglia and astrocyte activation in the ventral midbrain. In addition, we observed that C-DIM treatment reduced global NF-κB reporter expression, and modulated NF-κB-regulated genes in the brain. These results suggest that C-DIM compounds may exert their neuroprotective efficacy through transrepression of NF-κB-driven inflammatory gene expression in the glia, and could be a possible target for neurodegenerative therapeutic development.

MATERIALS AND METHODS

Chemicals and Reagents. C-DIM 5, 8, and 12 were synthesized by Dr. Stephen Safe and characterized as described in (Qin et al,). MPTP and probenecid and all other general reagents were purchased from Sigma-Aldrich (St. Louis, MO).

Progressive Lesion Treatment with MPTP and Probenecid. Transgenic male and female NFkB-EGFP reporter mice (C57 background) were obtained as generous gift from Dr. Christian Jobin (University of North Carolina, Chapel Hill) and described in (Magness et al., 2004). Dosing regimen of MPTP and probenecid was administered as described in De Miranda et al., 2013. Briefly, adult mice aged to 12 weeks were randomly divided into treatment groups and administed probenecid (250 mg/kg, ip.) followed four hours later by MPTP (20 mg/kg, subcutaneous) or saline every other day for 7 days (bid, 80 mg/kg MPTP, 4 doses; Miller et al., 2011). After day 7, mice were given daily oral gavage for 7 days of one C-DIM compound

66

suspended in corn oil, or corn oil (control). Mice were sacrificed on day 7 and day 14; behavior was assessed at these timepoints and prior to treatment (day 0). All animal procedures were performed in accordance with National Institutes of Health guidelines for the care and use of laboratory animals and were approved by the Colorado State University Institutional Animal Care and Use Committee. Every effort was made to minimize pain and discomfort. Terminal procedures were performed under deep isofluorane anesthesia.

Neurochemistry. Animals were sacrificed at the timepoints stated above, and brain tissue was removed quickly to minimize oxidation of brain chemicals. Midbrain dissections using a brain matrix block separated the striatum and substantia nigra, which were snap-frozen in liquid nitrogen before storage at -80°C. Catecholamine levels were determined in the striatum with use of high-performance liquid chromatography (HPLC) coupled with electro-chemical detection at the Neurochemistry Core Laboratory at Vanderbilt University's Center for Molecular Neuroscience Research (Nashville, TN). Samples were coded for unbiased results.

Immunohistochemistry. Tissue processing was performed as reported previously (Miller et al., 2011; De Miranda et al., 2013). In brief, at 7-day or 14-day timepoints, animals were terminally anesthetized with isoflurane and transcardially perfused with 4% paraformaldehyde. After perfusion, the brains removed and immersion fixed in 4% paraformaldehyde at 4°C for 3 hours. The brains were then transferred to cacodylate–phosphate-buffered saline containing 15% sucrose overnight, followed by 30% sucrose. The tissue was then frozen in OCT and sectioned at 40 μm thickness on a microtome. Sections were stored at –20°C, free floating, in cryoprotectant (30% w/v sucrose, 30% v/v ethylene glycol; 0.5 M phosphate buffer; pH 7.2) until staining.

Immunoflouresence tissue staning was completed as described in Miller et al., 2011. Antibodies were diluted in TBS and blocking buffer for a final concentration of 1:500; GFAP, Nitrotyrosine (Cell Signaling, Danvers, MA), IBA-1 (Wako Chemicals USA, Irvine, CA), γH2Ax, MAP2, Tyrosine Hydroxylase (Abcam, Cambridge, MA).

Stereological Counts of Dopmainergic Neurons. As reported in Miller et al., 2011, free-floating serial sections used for tyrosine hydroxylase (TH; Millipore) staining were obtained using systematic sampling from all sections encompassing the entire length of the SNpc, where every third tissue was selected and counted, for a total of 20 sections per animal. Stereological counts of TH-positive cells were performed using Slidebook software (version 5.0; Intelligent Imaging Innovations, Denver, CO) with use of the optical fractionator method (West and Gunderson, 1990). Images were captured using a Zeiss Axiovert 200M inverted fluorescence microscope equipped with a Hammatsu ORCA-ER-cooled charge-coupled device camera (Hammamatsu Pho- tonics, Hamamatsu City, Japan). The boundary of the SNpc was determined using low-magnification (10x) montage imaging. Total numbers of TH-positive cells were obtained through imaging (40x) uniform randomly placed counting frames (100x100 mm) with use of an optical dissector of 30 mm with 5 mm upper and lower guard zones. Representative montage images were generated for each treatment group with use of a 20x objective. Anatomic landmarks were used to select striatal sections for TH intensity staining in an identical process as described above and in Miller et al. (2011), staining all treatment groups simultaneously. Montage images of the ST were created using a 10x objective and a mask generated to outline the striatum with use of Slidebook software, and mean fluorescence intensity in relative florescence units was obtained. Representative montage images were generated for each

treatment group with use of a 20x objective.

Behavioral Analysis. Mice were evaluated at day 0, day 7, and day 14 for locomotor changes using VersaMax open-field behavior chambers (Accuscan Instruments, Inc., Columbus, OH). Mice were monitored over a 10-minute period, under lowered ambient light and white noise. VersaDat software (Accusan Instruments, Inc.) was used to analuyze open field behavior parameters. Hind-limb stride length measurements were conducted using an adapted methodology developed in Miller et al., 2011. Stride length was measured 1 day prior to treatment (day 0), on day 7 after MPTPp treatment, and day 14. Mice were trained using a catwalk system where paw placement could be tracked using a camera. The camera was set below a clear track, capturing the paw-prints as the mouse walked to the opening of its cage. Initial paw steps as well as those made immediately adjacent to the cage opening were omitted. A percentage change was calculated from the initial to final measurements from each mouse, and mean percentage change between dose groups was compared.

Real-time PCR Cytokine Expression Analysis. Frozen sections of SN were processed for RNA isolation using the QIAgen RNeasy kit (QIAGEN, Valencia, CA) with added DNAse steps on column and in-solution) following tissue homogenization. SA Biosciences (Frederick, MD) NF-κB Signaling Pathway PCR Array, 384-well plate (PAMM-025Z) was used for comparison of cytokines in the SN. cDNA was synthesized using BioRad iScript (CA), and real-time PCR Array analysis was completed using the PCR LightCycler489 PCR system (Roche Applied Sciences). Changes in gene expression were detected when Ct values were normalized to house-keeping genes b-actin, GAPDH, Beta-2 microglobulin and heat shock protein 90 (HSP90ab1) and considered significant when $P < 0.05$ (*) or $P < 0.01$ (#) using a paired t-test.

69

Statistical Analysis. Data are presented as mean ± SEM. Experimental group analyses were preformed using a one-way ANOVA with a Tukey post hoc test. Unrelated treatment groups of two were analyzed using a paired *t*-test with a two-sided P value and 95% confidence interval with a Bonferroni post test. Statistical significance was considered at $P < 0.05$ (*), $P < 0.001$ (**), $P < 0.001$(***), $P < 0.0001$ (****) unless described additionally in figures. All statistical analysis was completed using Prism (version 6.0; Graph Pad Software, San Diego, CA).

RESULTS

Dopamine neuron survival in a progressive MPTPp model

In order to mimic an early, progressive lesion in the SN, adult transgenic NF-κB-EGFP mice were treated with combined doses of MPTPp (20 mg/kg MPTP, 250 mg/kg probenecid), every other day for 7 days (bid 4 doses, 80 mg/kg MPTP) as previously described in De Miranda et al. (2013). Neuron loss was measured after the first 7 days using stereological counts of tyrosine hydroxylase (TH)-positive neurons in the SN, and confirmed a loss of approximately 50% of dopamine neurons (Figure 13A-B, H). Significant dopamine terminal loss was also observed after the 7-day MPTPp treatment (Figure 13A-B, I). After the onset of this SN lesion, animals were given a daily oral gavage of corn oil (control) or one of three C-DIM compounds (C-DIM5, C-DIM8, or C-DIM12) for 7 days. Mice that received only corn oil (MPTPp14d) exhibited approximately 25% further dopamine neuron loss at the 14-day timepoint, and a significant decrease in striatal TH intensity (Figure 13C, I). In contrast, the treatment groups receiving C-DIM5, C-DIM8, or C-DIM12 displayed no significant difference in dopamine neuron number or ST terminal intensity from the original lesion after an additional 7 days (Figure 13D-E, H-I).

These data indicate that efficacy of the C-DIM compounds as well as the MPTPp model as an early, progressive SN lesion are a robust and reproducible assessment for neuroprotection.

Nigrostriatal dopamine levels and functional behavior

Brain chemical analysis of mice receiving MPTPp treatment shows a significant decrease in dopamine, but in not its primary metabolite DOPAC, or HVA after the first 7 days, despite a clear downward trend (Figure 14A-D). Striatal dopamine levels do not reverse after cessation of treatment, with MPTPp14d and C-DIM treated animals showing significant decreases in dopamine, DOPAC and HVA. This is consistent with reports that MPTP/P treatment causes ST dopamine loss that remain depleted even up to 6 months after treatment (Petroske et al., 2001).

Immunoblotting of ST proteins involved in dopamine function, TH, DAT, and VMAT, reveal that significant reduction in TH and DAT appears at MPTPp7d treatment, with further reduction at MPTPp14d (Figure 14E-G). Animals that received daily oral gavage of C-DIM5, C-DIM8 or C-DIM12 had significantly increased TH and DAT levels over their counterparts that received corn oil alone (MPTPp14d). VMAT levels followed this same trend, however did not reveal significant changes across treatment groups at $P < 0.05$. As markers for dopamine cell survival and function in the striatum, TH, DAT, and VMAT levels indicate that C-DIM neuroprotection reduces further loss of these proteins after MPTPp treatment.

Locomotor behavior was evaluated at MPTPp14d, in order to determine differences between animals receiving C-DIMs or corn oil after onset of dopamine neuron loss. Striatal catecholamine levels indicate that dopamine is depleted at this timepoint, and using stride length analysis we observed significant locomotor reduction in mice receiving MPTPp14d treatment (Figure 14H). In contrast, MPTPp14d treatment groups receiving C-DIM8 and C-DIM12 showed

significant improvement in stride length, and C-DIM5 indicates a trend toward increase in stride length. Open field behavior parameters, such as rearing movement (Figure 14I) does not show detectable differences between treatment groups, perhaps not surprisingly due to the mild nature of this early-phase insult, as well as the test's less sensitive nature.

Neuronal death and dysfunction

Dopamine neuronal loss in the SN of rodents treated with MPTP is well established, though the typical measurement of cell death is loss of TH expression in the soma of neurons (Petroske et al., 2001; Przedborski et al., 2000). Nissl staining of total neurons is often conducted to counterstain TH and compare total neuron survival to TH expression in the SN of MPTP treated mice (Baiguera et al., 2012). In establishing this sub-chronic progressive model using MPTPp, immunofluorescence was utilized for the most accurate stereological count of TH positive neurons (Miller et al., 2011), however this prevented the use of Nissl as a counterstain for total neuron numbers. Some disparity has arisen in the total labeling of neurons in the SN pars compacta (SNpc) region via the use of fluorescent-tagged antibodies, therefore we adopted a method for counting total neurons in the SNpc using microtubule associated protein-2 (MAP2) (Cannon and Greenamyre, 2009). Using this method, we confirmed that there was a significant loss of neuronal cell bodies in the SN of animals treated with MPTPp at day 14 (Figure 15B). Representative montages of general neuron marker MAP2 and TH (Figure 15A) demonstrate the colocalization of both signals. The significant loss observed with MPTPp treatment does not translate in the groups of mice given C-DIM compounds, where MAP2 levels were insignificant from the 7-day starting point after neuron loss began (Figure 15B).

While dopamine neuron death is the primary hallmark of a SN lesion, dysfunctional neurons unable to synthesize dopamine are often seen prior to apoptosis (Crowe et al., 2011). Inflammatory transcription factor NF-κB binds to the inducible nitric oxide synthase (NOS2) promoter in astrocytes, resulting in high levels of NO in the SN after treatment of MPTPp (Brambilla et al., 2005). Using 3-nitrotyrosine as a marker for peroxynitrite damage, we found that mice exposed to MPTPp display increased nitrotyrosine adducts that colocalize with TH neurons when compared to their saline counterparts (Figure 15C-E). Even post-lesion, the mice given C-DIM5, C-DIM8, or C-DIM12 do not display as highly increased peroxynitrite adducts as animals given only corn oil (Figure 15F-H). Quantitative measurements of fluorescence in TH neurons of 3-nitrotyrosine indicate significant differences between saline and MPTPp treated animals, while C-DIM treated animals have significantly less nitrositive adducts (Figure 15I).

Additionally, apoptosis of TH neurons in the SN was identified via presence of phosphorylated histone H2A.X (anti-ɣH2AX) a marker of double-stranded DNA breaks (DSB). After 7 days of MPTPp treatment, ɣH2AX colocalization with TH neurons visibly increases, and is markedly elevated at MPTPp14d (Figure 15J-L). Animals receiving C-DIM treatment however, do not display ɣH2AX staining that is greater than MPTPp7d, the point at which C-DIM compounds were introduced (Figure 15M-O). The acute colocalization of ɣH2AX with TH neurons in MPTPp14d, is especially interesting, given that neurons undergoing apoptosis would likely contribute to continued degeneration within the SN, given additional time.

Global NF-κB expression is reduced by C-DIMs

Unresolved glial inflammation is believed to be the key factor driving progressive dopamine neuron death in PD. Microglial cells expressing TLRs are activated by apoptotic

dopamine neurons, ROS, and cytokines. In response to sensors of inflammation, activated microglia increase proinflammatory protein synthesis controlled by master gene regulators such as NF-κB. In order to evaluate whether the C-DIM compounds may reduce global inflammation during the progression of dopamine neuron loss, we used transgenic NF-κB-EGFP reporter mice containing three cis elements with high affinity for the NF-κB promoter (Magness et al., 2004). Coronal sections within the boundary of the SN from each treatment group were assessed for total intrinsic GFP expression (488 nm), and expressed in pseudocolor to show intensity (Figure 16). Basal expression of NF-κB-EGFP in saline (Figure 16A) is notably increased in MPTPp7d animals, and remains high at MPTPp14d (Figure 16B-C). C-DIM5, C-DIM8 and C-DIM12 treatments appear to decrease the global NF-κB production to levels below MPTPp7d threshold (Figure 16D-F). Inset 40x images of the SN indicate that neuronal bodies appear to be expressing the highest levels of intrinsic GFP, likely due to their large cell body size and high expression of NF-κB. In order to assess the glia for NF-κB-EGFP expression, SN sections were immunolabled for astrocytes (GFAP) and microglia (IBA-1). Co-expression of intrinsic GFP with either GFAP or IBA-1 in MPTPp14d tissue was compared with colocalization measurements (Figure 4I-J), which indicated that IBA-1 intensity more closely overlapped with intrinsic GFP intensity. Representative 40x images of astrocytes (Figure 16G) and microglia (Figure 16H) show that both cell types express visible NF-κB at MPTPp14d.

Glial activation increases during MPTPp progression

As the resident immune cells of the CNS, microglia survey their microenvironment with ramified processes expressing pattern recognition receptors (PRRs), and are able to rapidly activate upon aberrant protein binding (Polazzi and Monti, 2010). The dynamic response of

microglia involves an inflammatory cascade that results in the production of ROS, cytokines and chemokines. As the most abundant cell type, astrocytes have been labeled as amplifiers of microglial signaling, often exacerbating the production of inflammatory mediators when feedback inhibition signals fail (Glass et al., 2010; Hirsch and Hunot, 2009a). To explore the sequence of events in glial inflammation in our MPTPp model, we measured global microglia and astrocyte levels in the SN and the ST (Figure 17). Cell counting of GFAP and IBA-1 in the SN at MPTPp7d indicates a large increase over saline (Figure 17A-B, J-K). During the progressive phase of this model, MPTPp14d IBA-1 levels slightly increase within the SN, while GFAP levels remain approximately stable (Figure 17A-C, J-K). The SN of animals that received C-DIM5, C-DIM8 or C-DIM12 had significantly reduced glial inflammation at MPTPp14d (Figure 17D-E, J-K). In the striatum, the pattern of IBA-1 and GFAP increase of expression mirrors the SN (Figure 17L-M). Taken together, it appears that glial activation or gliosis during MPTPp treatment coincides with dopamine soma loss from the SN and axon loss from the ST, where MPTPp toxin is removed after 7 days, but gliosis remains amplified.

Gliosis in the midbrain does not only include increase in the number of reactive glial cells but also a marked changed in their morphology. Microglia become more amoeboid in their response to inflammatory activation, able to phagocytose debris from apoptotic neurons(Brown and Neher, 2010). To assess microglial morphology, we compared IBA-1 positive cells in saline, MPTPp14d, and MPTPp14d + C-DIM12 tissue from the SN (Figure 17G-1). In saline tissue, resting microglia express a ramified morphology (Figure 17G), and are activated in MPTPp14d tissue (Figure 17H) exhibiting a more amoeboid shape. The microglia in the SN of MPTPp14d + C-DIM12 appear to be less activated, with a morphology that appears more ramified than amoeboid, indicating that microglial activation may be partially suppressed (Figure 17I).

Cytokine gene expression is reduced with C-DIM treatment

The pathology observed in this MPTPp model suggests that glial inflammation increases even subsequently to the removal of neurotoxin treatment. Regulation of inflammatory pathways in the glia is a complex interplay between sensors of inflammation (TLRs, PRRs), their transducers (NF-κB, AP-1), and the promoter control of inflammatory gene transcription (NOS2, IL-1β, TNFα). To observe the genetic control over inflammatory transcription, we used RNA obtained from the SN of animals given saline, MPTPp14d, MPTPp14d + C-DIM5, and MPTPp14d + C-DIM12 treatments in real-time PCR analysis. The NF-κB Signaling Pathway qRT Array (SA Biosciences) revealed that gene expression controlled by NF-κB were significantly increased in animals at MPTPp14d over saline control (Figure 18A-H). Animals that received C-DIM12 daily oral gavage expressed significantly reduced levels of cytokines and chemokines (TNFα, IL-1α, CCL2) and mediators of inflammation (Caspase 1, TLR4). Interestingly, animals that received C-DIM5 did not display as significantly reduced levels of inflammatory gene expression at MPTPp14d, though decreasing trends do exist (Figure 18 A-H). The fold regulation if IL-10, IFNγ, and Nod1 (Figure 18J-L) also demonstrate that at MPTPp14d, proinflammatory gene expression is increased above control values. In contrast, C-DIM5 and C-DIM 12 treated animals display IFNγ and Nod1 levels below control. Considered an anti-inflammatory cytokine, IL-10 regulation of all groups assessed was below control levels (Figure 18J), but in C-DIM treated animals, the fold regulation of IL-10 seems to trend upward, a possible sign of anti-inflammatory control.

DISCUSSION

The cellular and molecular data presented here suggest that glial inflammation, driven by NF-κB-regulated genes, is responsible for the progressive loss of dopamine neurons in the SN after an initial lesion was created with MPTPp. The progression of dopamine neuron loss from the SN and their projections to the ST was protected by the addition of anti-inflammatory C-DIM compouds, via daily oral gavage (Figure 1). The neuroprotective efficacy of the C-DIMs and reproducibility of the MPTPp model are highlighted here, confirming initial efficacy studies conducted with C-DIM5, C-DIM8, and C-DIM12. Measurements of brain catecholamines indicated that the use of MPTPp did not result in reversal of dopamine levels and its metabolites after removal of the neurotoxin from the system (Figure 14A-D). While C-DIMs did not change acute dopamine levels, the survival of TH-positive neurons and their nerve terminals would suggest that over time dopamine production might recover. These results are consistent with chronic MPTP and probenecid studies, where even 6 months after treatment, striatal dopamine levels remained low. As a subacute study, this MPTPp model shows similar trends in neuron loss to more chronic MPTP studies, but allows for shorter time period in which to initially test these therapeutics.

The MPTPp treatment regimen analyzed here shows early deficits that may coincide with the first motor symptoms that present in human PD (Liepelt-Scarfone et al., 2013). Locomotor analysis revealed that at MPTPp14d, mice had reduced stride length, which was improved by C-DIM treatment (Figure 14I). As mice are refractory to MPTP treatment (Petroske et al., 2001), and open-field behavior is not as sensitive of a measure, rearing movements and other parameters of open-field analysis do not show any measurable difference between treatment groups (Figure 14J). Measurement of striatal proteins TH, DAT, and VMAT however, suggest

that at MPTPp14d there are clear deficits in functional dopamine proteins (Figure 14F-H). In humans, motor symptoms only occur when 70-80% of dopamine is lost from the ST, and approximately 50-60% of dopamine neuron loss from the SN (Fearnley and Lees, 1991). While complete ablation of the SN is similar to end-stage PD, the neuron loss observed in this MPTPp model may more accurately mimic early symptomatic motor deficits leading to initial clinical PD diagnosis. Addition of C-DIM5, C-DIM8, and C-DIM12 at this initial stage of neuron loss is successful at preventing the loss TH, DAT, and VMAT that occcurs from MPTPp7d to MPTPp14d, resulting in improved stride length.

As anti-inflammatory compounds, the C-DIMs have been shown to suppress the release of inflammatory cytokines in primary astrocytes *in vitro*, but have been most extensively studied as cancer therapeutics (Carbone et al., 2008; Inamoto et al., 2008). In these studies, C-DIM5, C-DIM8, and C-DIM12 were identified as potential modulators of orphan nuclear receptors, members of a superfamily of nuclear receptor (NR) transcription factors able to modify transcriptional gene regulation via recruitment of coactivator and corepressor proteins (Collingwood et al., 1999; Inamoto et al., 2008; Lei et al., 2008). The orphan nuclear receptor family (NR4A) consists of three members, Nur77 (NR4A1), Nurr1 (NR4A2), and Nor1 (NR4A3), of which no known endogenous ligand exists (Mohan et al., 2012). As a pharmacologic modulator of Nur77, C-DIM5 decreases the survival of cancer cells *in vitro*, but may have anti-inflammatory properties in the CNS, where Nur77 is translocated to the mitochondria under oxidative stress (García-Yagüe et al., 2013).

Nuclear receptor Nurr1 is expressed during neuronal development, and is required for the maturation of dopamine neurons in the brain (Kadkhodaei et al., 2009). Several lines of evidence, including the landmark study by Saijo et al. (2009) have indicated that Nurr1 plays a

role in adult brain homeostasis, where expression in astrocytes provides neuroprotection in the SN. Astrocyte-specific expression of Nurr1 indicated a transrepressive mechanism by which the nuclear receptor recruits corepressor complexes (CoREST) to NF-κB-p65 bound to inflammatory promoters in the nucleus (Saijo et al., 2009b). C-DIM8 and C-DIM12 have been shown to activate Nurr1 in several cancer cell lines, where GAL4-Nurr1 constructs show dose-dependent increases in Nurr1 expression (Inamoto et al., 2008; Li et al., 2012). Not surprisingly, this is an exciting target for neuroprotection in a PD model, where Nurr1 may play a role in both the developing dopamine neuron, and their survival under pathological conditions. It remains to be concluded if C-DIM8 or C-DIM12 alter Nurr1 expression in the adult mouse brain, however, both total glial activation in the SN, and global expression of NF-κB appear to be suppressed by treatment with C-DIM compounds (Figure 16, 17). This would suggest that C-DIM compounds are indeed modulating the expression of NF-κB in astrocytes and microglia, possibly through transrepressive mechanisms discovered to be activated in the SN during inflammation (Saijo et al., 2009b).

Gene expression of NF-κB pathway proteins measured here indicate that MPTPp14d treatment significantly increases the total amount of inflammatory proteins, which is also reported in human cases of PD, where increased cytokines have been measured in the blood. A comparison between C-DIM5 and C-DIM12 effect on cytokine expression was assayed because of the potential in differing molecular targets; Nur77 by C-DIM5, and Nurr1 by C-DIM12. While C-DIM12 treated animals displayed large reductions in NF-κB cytokines, C-DIM5 treated animals reported mild suppression in some genes (IL-1α, CCL2), and no suppression of others (TNF, Caspase 1, Card10; Figure 18). Pharmacokinetic data comparing C-DIM5 and C-DIM12 shows that C-DIM5 is more rapidly metabolized when dosed orally (Cmax$_{brain}$, 378 ng/ml) versus

C-DIM12 ($Cmax_{brain}$, 1,173 ng/ml) possibly reducing the effectiveness of C-DIM5. It is also possible that if Nur77 is targeted by C-DIM5 in glial cells, is a less potent inhibitor of glial inflammation than Nurr1. Of interest, animals given C-DIM12 during pharmacokinetic studies had detectable levels of C-DIM8, indicating that oxidative de-chlorination of C-DIM12 produces another compound with reported Nurr1 activity (De Miranda et al., 2013). C-DIM8 displays rapid metabolism from the brain and plasma, however it displays similar suppression of glial activation as C-DIM5 and C-DIM12, suggesting it may be a more potent pharmacological compound. This, in conjunction with the reduction of cytokines in animals treated with C-DIM12, may suggest dual pharmacological activation of Nurr1, leading to enhanced neuroprotection.

Neurodegenerative disorders with an inflammatory component remain extremely difficult to treat due to the complex nature of their onset, lack of biomarkers, pharmacological barriers, and unrealistic preclinical models (Glass et al., 2010; Maguire-Zeiss and Federoff, 2010). Despite the growing use of post-lesion models such as the one reported here, potential symptomatic therapies continue to fail in phase II and III clinical trials, either providing no efficacy or displaying off-target effects deemed unacceptable for use in their target population (Gao and Hong, 2008; Glass et al., 2010). Affirming this, a recent setback occurred when adenosine A2 receptor antagonist preladenant was pulled from phase III clinical trials when drug company Merck observed no improvement in motor function of PD patients despite reports phase II success (Hauser et al., 2011). Anti-inflammatory therapies such as the drug minocycline have had low success in translation to the clinic for PD treatment, even after reports of success in primary research and preclinical trials. Of note, adopted orphan nuclear receptor PPARɣ (peroxisome-proliferator activated-receptor-gamma) has been shown to be activated by the

diabetic drug rosiglitazone, resulting in inhibition of microglial activation in chronic MPTP and probenecid studies (Carta et al., 2011; Schintu et al., 2009). As PPARɣ functions in glucose metabolism, off-target effects from pharmacological manipulation have been a factor when targeting PPARɣ as a neuroprotective strategy, but an even greater risk of heart attack has currently cause rosiglitazone to be pulled from the European market (Kung and Henry, 2012). Although less studied, targeting the NR4A family of nuclear receptors may be an alternative target worth pursuing for development of therapeutics aimed at reducing inflammation in the brain. The ability of C-DIMs to attenuate glial inflammation in a progressive PD mouse model creates an appealing therapeutic prospect, though further mechanistic studies of C-DIM in glial cells will be necessary to understand their ability to modulate Nur77/Nurr1.
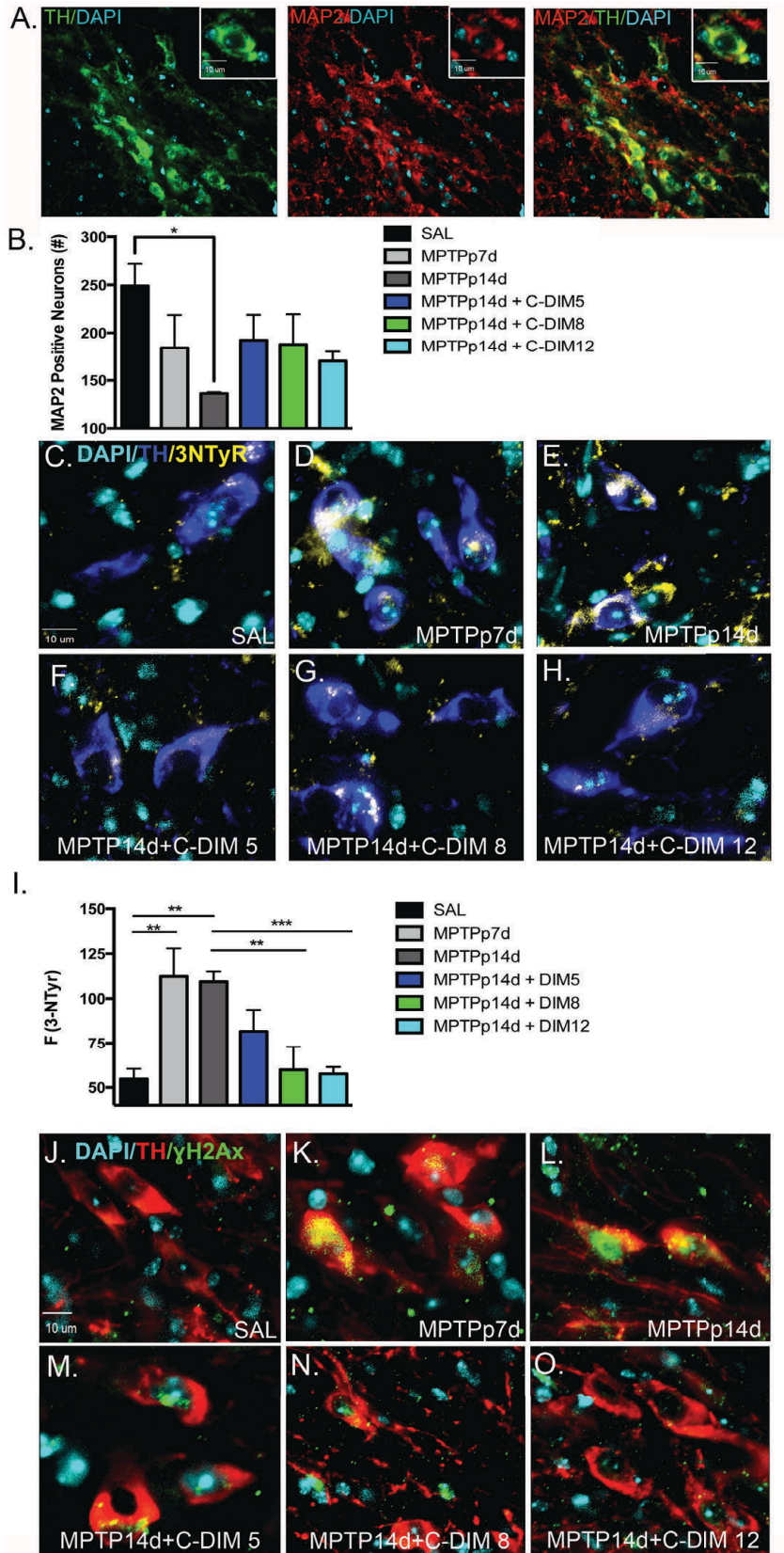
FIGURE 13
DOPAMINE NEURON PROTECTION
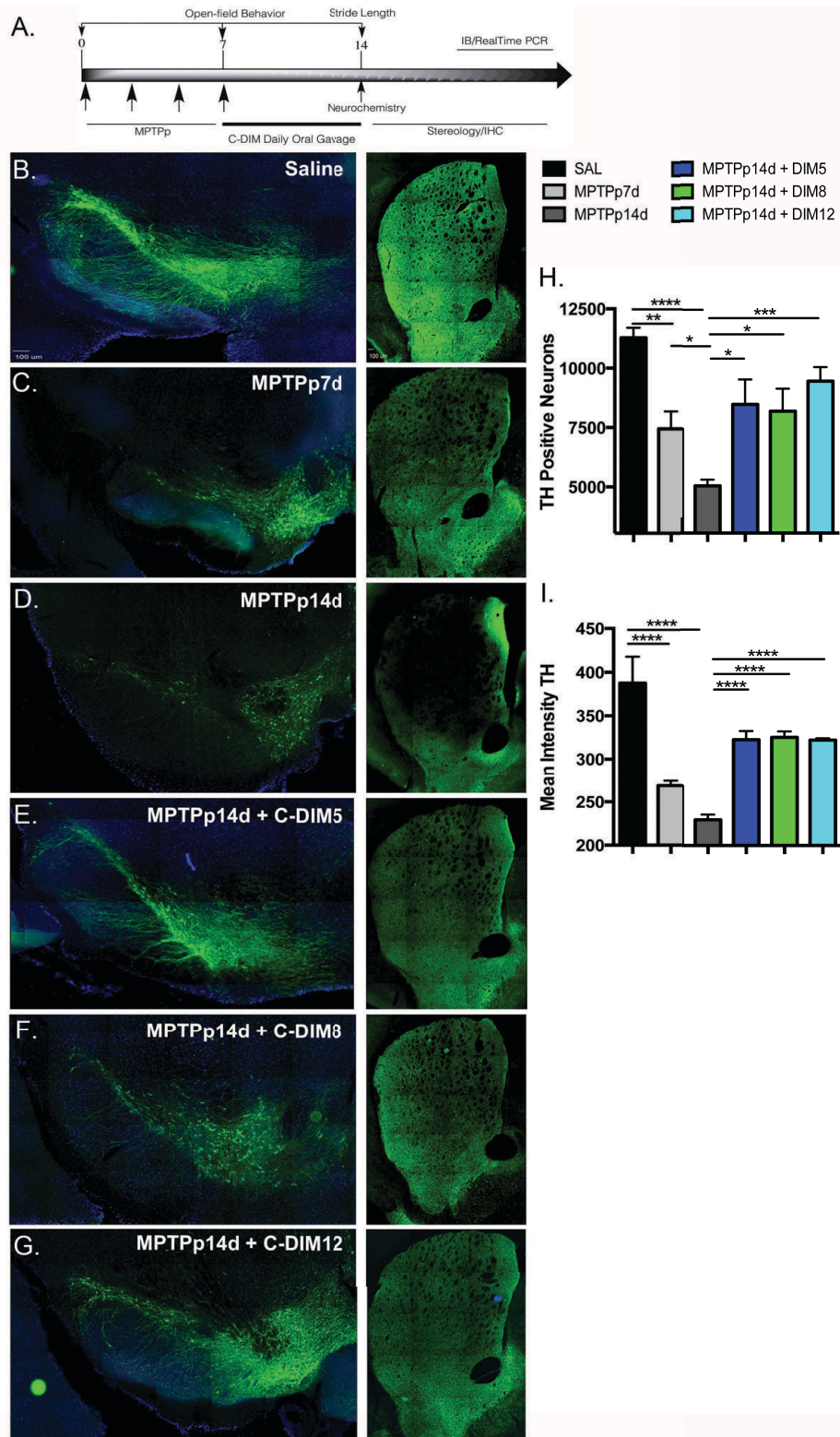
Figure 13. Progressive dopamine neuron death by MPTPp is attenuated by C-DIMs. A. Dosing regimen and timeline schematic for MPTP (80 mg/kg) and probenecid (250 mg/kg) treatment in adult NF-κB-EGFP reporter mice, followed by tissue analysis**. B-D.** Representative images of TH positive neuronal cell bodies in the SN and nerve terminals in the ST that are significantly reduced after 7 days of MPTPp treatment (MPTPp7d) and continue to degenerate 7 days after neurotoxin is removed (MPTPp14d; 20x montage images, scale bar 100 μm). **E-G.** Representative images of C-DIM5, C-DIM8, and C-DIM12 daily oral gavage (50 mg/kg) beginning at MPTPp7d attenuates dopamine neuron loss at MPTPp14d (corn oil daily gavage, vehicle control). **H.** Stereological counts of TH-positive neurons in the SNpc are significantly reduced at MPTPp7d worsening at MPTPp14d compared to saline. TH-positive neurons are significantly higher in C-DIM treated animals than their MPTPp14d counterparts. **I.** Mean fluorescent intensity of TH in the ST is significantly reduced in MPTPp7d, progressing to further loss at MPTPp14d, while C-DIM treatments prevented additional loss. Data are expressed as mean ± SEM (N=6); horizontal bars represent statistical significance between related groups.

FIGURE 14
NEUROCHEMISTRY, STRIATAL PROTEIN, AND BEHAVIOR
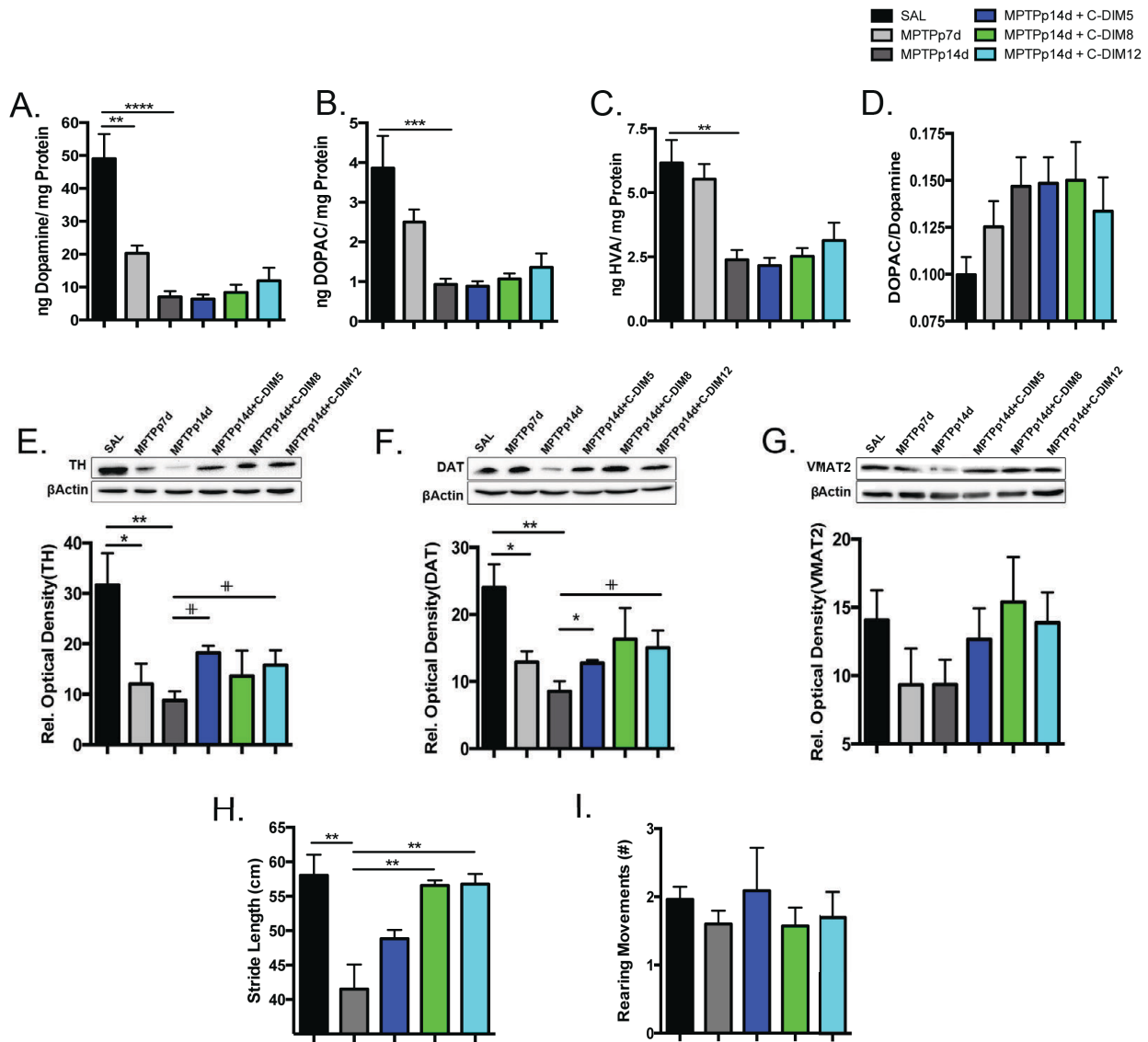
Figure 14. Striatal catecholamines, dopamine terminal proteins, and locomtor behavior after MPTPp and C-DIM treatment. A-C. Dopamine and metabolites DOPAC and HVA from the ST, measured by HPLC, are significantly reduced by MPTPp treatment, which was not immediately altered by C-DIMs (N=5). **D.** Dopamine turnover expressed as DOPAC/dopamine ratio. **E.** Western blots of TH, DAT and VMAT proteins from the striatum show lower expression at MPTPp7d, worsening at MPTPp14d, as compared to bactin; relative optical density compares quantitative blot measurements (N=4); *P* value <0.1[#], 90% confidence interval. **H.** Stride length measured in mice at MPTPp14d is significantly reduced from saline, and improved with C-DIM treatment. **I.** Open field behavior (rearing movement #) did not reveal changes between treatment groups. Data are expressed as mean ± SEM (N=6); horizontal bars represent statistical significance between related groups.
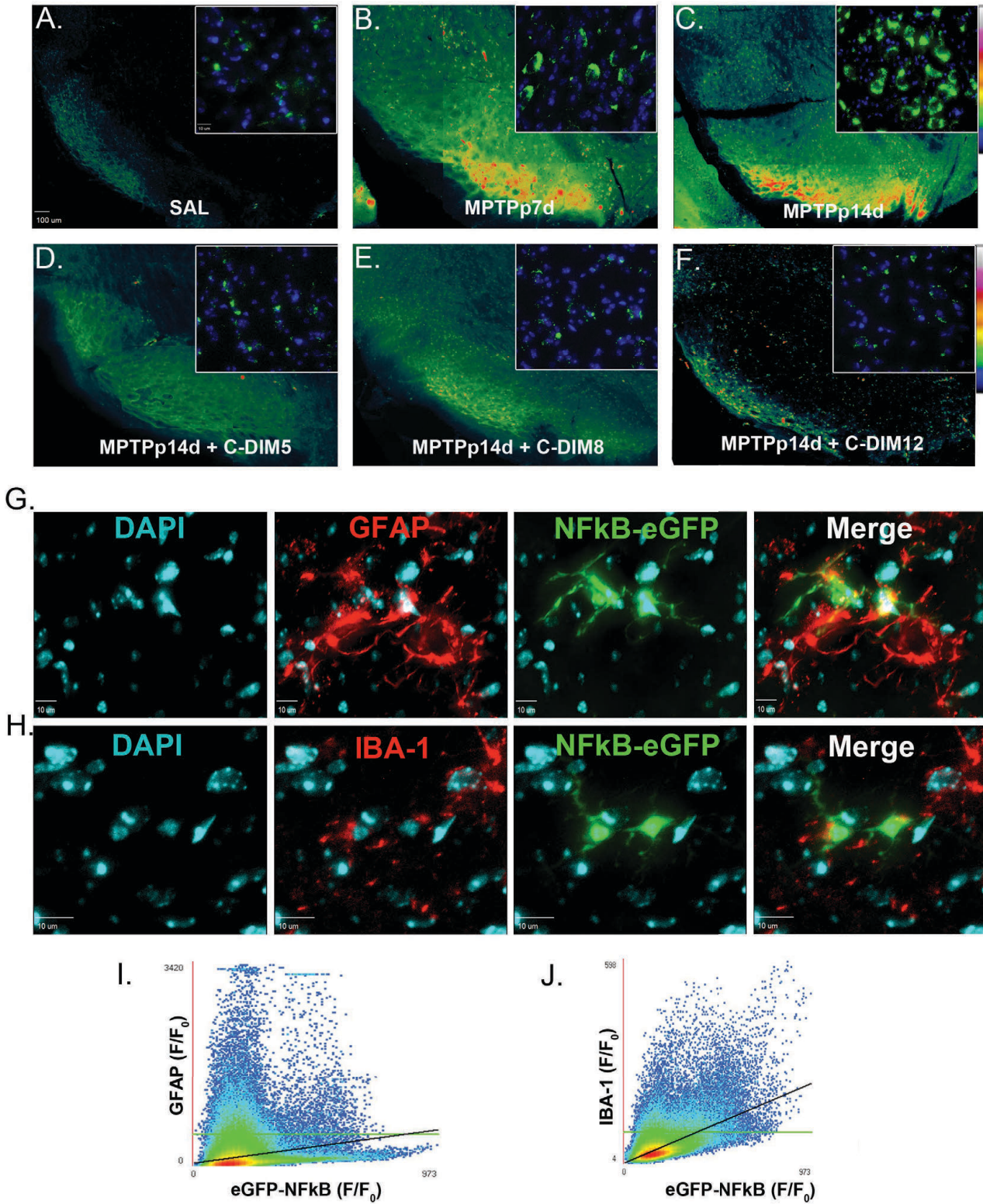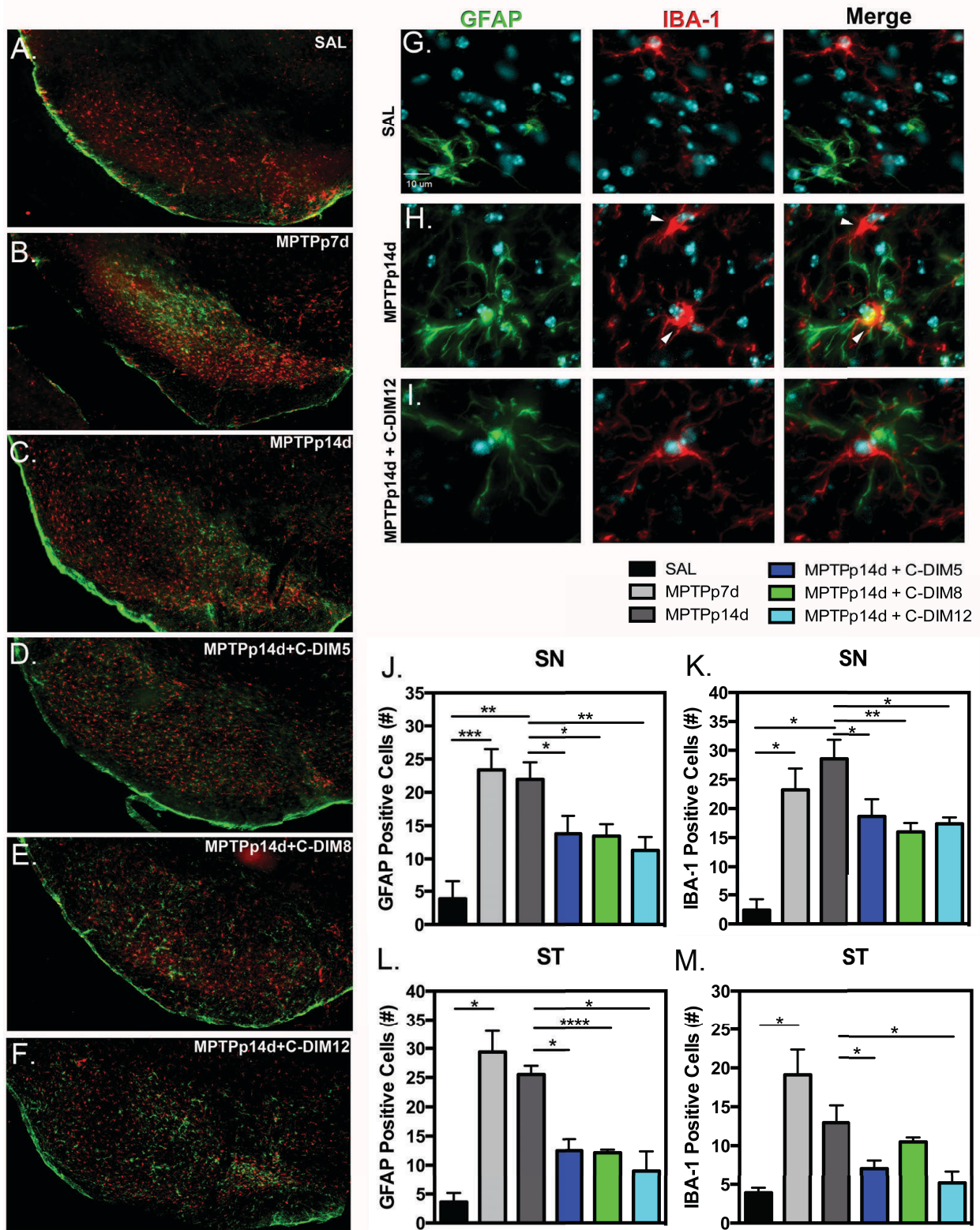
FIGURE 15
NEURONAL DEATH AND DYSFUNCTION

Figure 15. Neuronal death and dysfunction after MPTPp and C-DIM treatment. A. Representative 20x images of TH (green), MAP2 (red), and DAPI (cyan) show total neuron staining compared to TH-positive immunofluorescence, (63x inset). **B.** Quantitative MAP2 neuron counts of total neuron loss, significantly reduced at MPTPp14d, attenuated with C-DIM treatment (N=3;). **C-H.** Representative 40x images of nitrotyrosine adducts on TH neurons, identified by 3-Nitrotyrosine immunofluorescence (yellow), colocalizes with TH-positive neurons (blue), DAPI (cyan), increases with MPTPp treatment, but is reduced with C-DIMs. **I.** Quantitative measurement of nitrotyrosine fluorescence within TH-positive neurons shows significant increases at MPTPp7d and MPTPp14d, reduced by C-DIM treatment. (N=5); horizontal bars represent statistical significance between related groups. **J-M.** Representative 40x images of apoptosis marker yH2AX (green) increases in TH positive neurons (red), DAPI (cyan), at MPTPp7d. Greater yH2AX expression is visible in the nuclei of MPTPp14d neurons, but is reduced by C-DIM treatment. Data are expressed as mean ± SEM.

FIGURE 16
INTRINSIC NF-κB EXPRESSION

Figure 16. Intrinsic NF-*κ*B is expressed in the SN after MPTPp treatment. A-C. Representative tissue sections from the SN of transgenic NF-*κ*B-EGFP mice show global increases in intrinsic GFP expression after MPTPp7d and MPTPp14d treatments expressed in pseudocolor where red is most intense (20x montage, 40x inset, scale bar 100 μm). **D-F.** SN tissue sections from C-DIM treated animals show a decrease in total NF-*κ*B-EGFP expression at MPTPp14d. **G-H.** Astrocyte (GFAP) and microglia (IBA-1) representative 40x images from the SN of MPTPp14d animals show colocalization of NF-*κ*B-EGFP reporter (green), DAPI (blue). **I-J.** Scatter-plot analysis of GFAP (RhodDual) or IBA-1 (Cy5) and NF-*κ*B (FITC) channels, show a more intense overlap of NF-*κ*B-EGFP pixel intensity in microglia than astrocytes (SlideBook software colocalization analysis of F/F_0).

FIGURE 17
GLIOSIS IN THE SN AND ST

Figure 17. Microglia and astrocytes are activated in the SN during progressive dopamine neuron loss. A-C. Representative immunofluorescent 20x montages in the SN of astrocyte (GFAP, green) and microglia (IBA-1, red) activation at MPTPp7d and MPTPp14d compared to saline. **D-E.** Astrocyte and microglia expression in the SN of C-DIM5, C-DIM8, or C-DIM12 at MPTPp14d. **G.** Astrocyte (GFAP, green) and microglia (IBA-1, red) morphology in the SN of saline tissue show a resting phenotype. **H.** Activated astrocytes in MPTPp14d express increased GFAP; activated microglia undergo morphological changes retracting processes to amoeboid shape (arrows) capable of engulfing debris. **I.** Treatment with C-DIM12 at MPTPp7d reduces microglial activation at MPTPp14d; microglia express a less-activated phenotype. **J-M.** Quantitative counts of GFAP and IBA-1 positive cells in the SN and ST show increased gliosis at MPTPp7d and MPTPp14d, reduced by C-DIM treatment. Data are expressed as mean ± SEM (N=6); horizontal bars represent statistical significance between related groups.

FIGURE 18
NF-κB-REGULATED CYTOKINE EXPRESSION
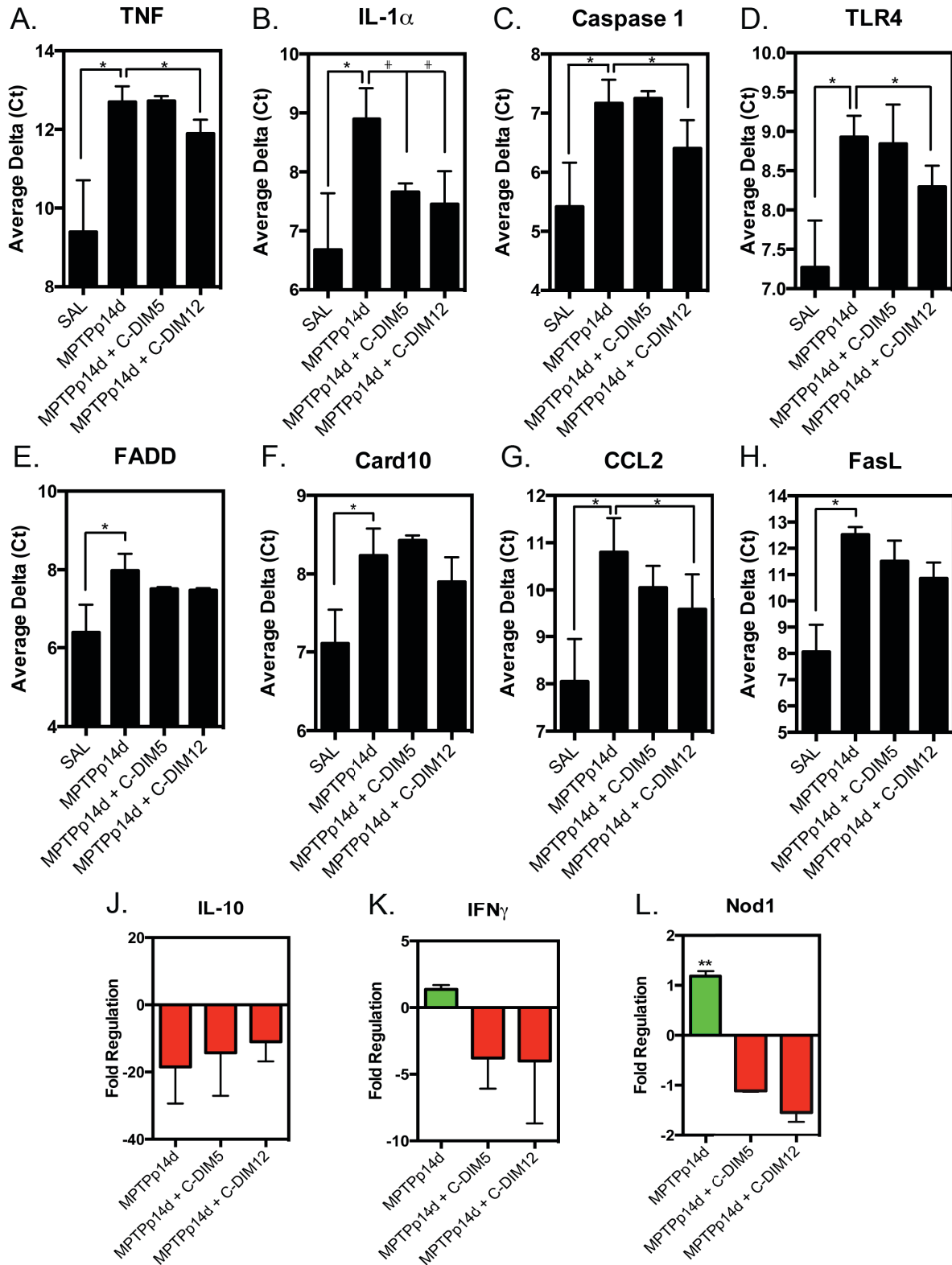
Figure 18. NF-κB-regulated cytokine gene expression in the SN. RNA isolated from the SN of Saline, MPTPp14d and C-DIM5 or C-DIM12 treated animals was analyzed using a real-time PCR array of NF-κB pathway genes (SA Biosciences). **A-H**. Average Delta Ct values from real-time analysis show global increases in NF-κB-regulated genes from saline to MPTPp14d (student's t-test, *P* value <0.1#, 90% confidence interval). **J-L.** Fold regulation over saline of IL-10 shows a trend for increased expression in C-DIM5 and C-DIM12 over MPTPp14d, while INFy and Nod1 are increased in MPTPp14d but reduced in C-DIM5 and C-DIM12 treatments. Data are expressed as mean ± SEM (N=4); horizontal bars represent statistical significance between related groups.

CHAPTER 5

DIM-C-pPHCl INHIBITS INFLAMMATORY ACTIVATION OF NF-KAPPA-B IN BV-2

MICRGLIA BY A NURR1-DEPENDENT MECHANISM

INTRODUCTION

Increasing focus on the abatement of inflammation in the brain of individuals with Parkinson's disease (PD), has lead to many recent discoveries of molecular signaling pathways targeted for therapeutic development. Among these is the nuclear factor-kappa b (NF-κB) family of transcription factors, which regulates hundreds of proinflammatory genes in the glia, as well as those responsible for homeostatic inflammatory resolution (Saijo et al., 2013; Maguire-Zeiss and Federoff, 2010). Despite the growing attention of NF-κB and its central role in glial inflammatory signaling, a molecular therapeutic has yet to be successfully approved for treatment of the progressive phase of neurodegenerative disease (Glass et al., 2011). Recent studies have demonstrated that cell-specific deletion of NF-κBfrom microglia or astrocytes results in neuroprotection in models of inflammatory neurodegeneration (Cho et al., 2008, Brambilla et al., 2009). These findings however, are difficult to repeat clinically, and total deletion of NF-κB has undesirable side effects unlikely to outweigh any neuroprotective benefit (Ghosh et al., 1998; Gilmore, 2006).

Microglial expression of pattern recognition receptors on their cell surface, such as toll like receptors (TLRs), provides immune surveillance of the central nervous system for foreign particles (Thompson and Van Eldik, 2009). Microglia are also stimulated by cellular debris, and when fully activated, have phagocytic activity in order to resolve neuronal injury (Polazzi and

93

Monti, 2010). During microglial activation, transcription factors including NF-κB, regulate the release of reactive oxygen species (ROS), cytokines, and chemokines that both activate nearby astrocyte cells and attract additional microglia to the region of damage (Saijo et al., 2013). Astrocytic amplification of these signals yields high levels of pro-inflammatory cytokines such as inducible nitric oxide synthase (NOS2), tumor necrosis factor alpha (TNFα), interleukin (IL)-1β and IL-6, and chemokines MCP-1 (CCL2; Thompson and Van Eldik, 2009). These proteins are found at elevated levels in the brain and cerebrospinal fluid (CSF) of both human and research cases of PD (Saijo et al., 2013).

One possible mechanism to alter NF-κB signaling in the glia without entirely knocking out its regulatory affects, is to target modulators of the p50/p65 transcription factors. This possibility was highlighted in a recent study by Saijo et al., (2009) who discovered the transcriptional regulation of NF-κB-related genes by orphan nuclear receptor NR4A2 (Nurr1) in astrocytes (Saijo et al., 2009). The NR4A family of nuclear receptors regulate gene expression via protein-protein interactions with transcription factors bound to inflammatory promoters via "transrepression" (Bensinger and undefined author, 2009). Nurr1 is established as a necessary protein involved in the development of dopaminergic neurons, and has been identified as a genetic mutation involved in familial, late-onset PD (Glass et al., 2010; Saucedo-Cardenas et al., 1998). A novel role of Nurr1 as a transrepressor of NF-κB signaling by the active removal of p50/p65 from proinflammatory promoters, could have far-reaching implications for therapeutic development, specifically for PD (Saijo et al., 2009b).

A series of novel molecular therapeutics, *para*-phenyl substituted diindolylmethanes (C-DIMs) are shown to have activity at nuclear receptors, including a high selectivity for the NR4A family (Inamoto et al., 2008; Lee et al., 2011; Yoon et al., 2011). One particular *para*-phenyl

diindolylmethane (1,1-Bis(3″-indolyl)-1-(p-chlorophenyl)methane; C-DIM12) has shown to activate Nurr1 in urothelial carcinoma cells, thereby inhibiting cancer cell growth (Inamoto et al., 2008). Additionally, 1,1-Bis(3″-indolyl)-1-(p-methoxyphenyl)methane (C-DIM4) had inhibitory action on induced inflammatory signaling in primary astrocytes in vitro, leading to a decrease of expressed NOS2 and TNFα (Carbone et al., 2008). Based on these observations, C-DIM12 was selected for *in vivo* efficacy studies in a mouse model of the progressive phase of PD (De Miranda et al., 2013). In this post-lesion model, C-DIM12 provided neuroprotection for dopamine neurons in the substantia nigra (SN) as well as dopamine terminals in the striatum (ST). In addition, pharmacokinetic data examined in this study determined that C-DIM12, delivered orally, is retained in the brain with a half-life and Cmax comparable to many PD symptomatic therapies currently on the market (De Miranda et al., 2013). Taken together, these data suggest that C-DIM12 may represent a novel compound able to enter the brain and limit inflammatory activation in the glia during the progressive phase of PD.

It remains unclear what specific role C-DIM12 plays in inflammatory gene transcription in glial cells, despite the evidence that it is able to reduce dopamine neuron loss in vivo. The action of C-DIM12 on Nurr1 discovered in a cancer model is especially intriguing given the implications of Nurr1 in both dopamine neuron development and its role in transrepression of NF-κB in primary astrocytes (Saijo et al., 2009b). To this end, we hypothesized that C-DIM12 inhibits inflammatory signaling in BV-2 microglia cells by modulating Nurr1 transrepression of NF-κB bound to proinflammatory gene promoters. We present here that C-DIM12 is able to suppress proinflammatory gene transcription in BV-2 microglia after stimulation with LPS.

Additionally, we investigated the relationship of C-DIM12 and Nurr1, and present evidence that C-DIM12 requires Nurr1 for its anti-inflammatory effects, recruiting corepressors that actively remove p65 from the NOS2 promoter.

MATERIALS AND METHODS

Reagents. C-DIM compounds were synthesized by Dr. Stephen Safe and characterized as described in (Qin et al., 2004). Lipopolysaccharide from Escherichia coli 0111:b4 (LPS) and all other chemical reagents were purchased from Sigma-Aldrich (St. Louis, MO) unless stated elsewhere. Antibodies used in immunofluorescent experiments were purchased from Cell Signaling (p65) and Santa Cruz (Nurr1).

Cell Culture Experiments. BV-2 microglia were obtained as a generous gift from Dr. Alan Schenkel, Professor of Microbiology, Immunology and Pathology, Colorado State University, Fort Collins, CO. BV-2 cells were maintained at or below passage 10, cultured in DMEM (supplemented with L-glutamine; Gibco) containing 10% FBS (heat-inactivated fetal bovine serum, Atlanta Biologicals) and a cocktail of 0.001 m/ml penicillin, 0.002 mg/ml streptomycin, 0.001 mg/ml neomycin; (1x PSN; Hyclone). BV-2 cells were grown until 60-70% confluent before treatments. Primary mixed glia were obtained through cortical isolations from C57/Bl6 of P0 mouse pups. Mixed glial cultures were maintained in MEM (supplemented with L-glutamine; Hyclone), 10% FBS, and 1x PSN as described above. Primary glial cultures were grown until 80% confluent before treatments. Glial purification by our lab was preformed as described in Carbone et al., 2008. All cell cultures were maintained at 37°C and 5% CO_2. All procedures involving animals were approved by the Colorado State University Institutional Animal Care and Use Committee (IACUC), and were conducted in accordance with current NIH guidelines.

Gene Expression Assays. Quantitative reverse transcriptase PCR (qRT-PCR) primers were synthesized by IDT Integrated DNA Technologies. BV-2 cells were pre-treated with 10 µM C-DIM12 (0.1 µM, 1.0 µM, or 10 µM in dose-response assays) for one hour in serum and antibiotic free OptiMEM (Gibco) prior to treatment with 1 µg/mL LPS. RNA was isolated using an RNEasy Mini kit (Qiagen, Valencia, CA) and purity and concentration was determined using a Nanovue spectrophotometer (Location). After purification, 1 µg of RNA was used as a template for reverse transcriptase (RT) reactions using iScript (BioRad, Hercules, CA). cDNA produced from this reaction was measured for gene expression levels of proinflammatory genes using an Eco Real-Time PCR System (Illumina, Inc. San Diego, CA). Target gene expression was normalized to β-actin, which was confirmed consistent between sample groups.

Chromatin Immunoprecipitations (ChIP). BV2 cells were grown to confluence in 10-cm tissue culture plates (approximately $2x10^7$ cells) and treated for the indicated time with LPS (1µg/ml), with or without C-DIM12 (10µM) or a DMSO vehicle control before cross-linking with 1% formaldehyde (Thermo Scientific) for 10 min. The remaining steps were adapted from the Chromatrap ChIP protocol, which accompanies the Chromatrap Pro-A Premium ChIP Kit (Porvair 100-200, UK). DNA was sheared into ~500 base pair fragments before removing 10% (200ng) for input controls. 2µg of chromatin were then loaded into IP reaction with 2µg precipitating antibody (as suggested by Chromatrap), Anti-CoREST (abcam 32631), anti-NCOR2 (abcam 5802), anti-HDAC3 (abcam 7030), anti-Nurr1 (Santa Cruz 991), and anti-p65 (Santa Cruz 372). Immunopurified DNA was isolated via the QIAquick™ PCR Purification Kit (28104) (suggested by Chromatrap). A 149 bp region of the NOS2 promoter proximal to the NF-κB site of transcription was amplified via quantitative-PCR and performed with SYBR-Green Supermix (Bio-Rad 170-8882) and analyzed using the % input method (Life Technologies™).

Immunofluorescence Protein Expression and Translocation. BV-2 microglia were plated on cover glass coated with FBS and pre-treated for one hour with 10 µM of C-DIM12 followed by 1 µg/ml LPS. After 30 minutes the cells were rinsed with PBS buffer and then paraformaldehyde fixed for 15 min at 4°C. Cells were blocked using bovine serum albumin (BSA; Sigma-Alderich) for one hour until incubation with primary antibodies overnight at 4°C. Secondary antibody incubation was at room temperature for 3 hours; Alexa-fluor 555, Alexa-fluor 647 (Life Technologies), DAPI counterstain (Vector Labs). Slides were imaged using a Zeiss Axiovert 200M inverted fluorescence microscope equipped with a Hammamatsu ORCA-ER-cooled charge-coupled device camera (Hammamatsu Photonics, Hamamatsu City, Japan).

RESULTS

Structure-activity of C-DIMs in suppression of proinflammatory cytokines.

Initial analysis of a series of C-DIM analogs (C-DIM1 through CDIM14) was preformed to determine their ability to suppress inflammatory gene expression in glia. In order to assess both the efficacy of cytokine suppression and structure-activity based on the molecular structure of each compound, mouse primary mixed glia were treated with 1 µg/ml LPS and either 1 µM or 10 µM of each C-DIM compound (Table 6). Compared to LPS treatment alone, several of the C-DIM compounds significantly decreased NOS2 and IL-1β expression at a concentration of 10 µM. The substituted *R* position of the *para*-phenyl substituted diindolylmethane structure changes the anti-inflammatory activity of a specific C-DIM, therefore resulting in a structure-dependent relationship of altered cytokine expression in the glia. This is more clearly demonstrated with C-DIM5, C-DIM9, and C-DIM12, where methoxy and chloro-substituted C-DIM5 and C-DIM12 respectively, are able to suppress NOS2 and TNFα but in comparison phenyl-substituted C-DIM9 does not provide any decrease in these inflammatory genes (Figure

98

19). Based on these results, and the initial pharmacokinetic and efficacy screening of C-DIMs in mice, we selected C-DIM12 for further *in vitro* analysis of its mechanism to suppress inflammatory cytokine expression in microglia.

C-DIM12 decreases inflammatory gene expression in BV-2 microglia in a dose-dependent manner.

Cytokine expression in glia is well documented both *in vivo* and *in vitro* following stimulation of microglial TLR receptors (Saijo et al., 2013). In this study, BV-2 microglia were challenged with 1 µg/ml LPS over a 24 hour time period in order to establish cytokine expression patterns specific to our treatment conditions (Figure 19A-D). Targeted for its potential to decrease inflammatory signaling in mixed glia cultures, and its ability to induce Nurr1 in a urothelial cancer model (Inamoto et al., 2008), C-DIM12 was examined in a dose-response assay in BV-2 cells treated with 10 µg/ml LPS for 24 hours (Figure 20E-H). In all inflammatory genes examined, except IL-1β, C-DIM12 is able to significantly suppress activation at 10 µM, and at 1 µM in NOS2 and IL-6 genes. A clear trend toward suppression of IL-1β is visible, though a higher concentration of C-DIM12 may be required to elicit a significant response (Figure 20H).

Nurr1 is involved in suppression of cytokines by C-DIM12.

Mechanistic data indicates that lentiviral knockdown of Nurr1 leads to higher cytokine expression levels and increased dopamine neuron death in the substantia nigra (SN) after LPS treatment *in vivo* (Saijo et al., 2009). Treatment of BV-2 microglia with double-stranded RNAi (dsiRNA) designed against Nurr1 results in higher expression of NOS2 and TNFα following LPS stimulation, indicating that Nurr1 is involved in BV-2 regulation of NF-κB-driven cytokines (Figure 21A-C). Following the knockdown of Nurr1 via dsiRNA, BV-2 cells were treated with

10 µM of C-DIM12 for 24 hours and then assayed for cytokine gene expression (Figure 21C-F). In treatment groups receiving Nurr1 dsiRNA, C-DIM12 is unable to fully suppress NOS2, TNFα and IL-6 (Figure 21C-D, F). C-DIM12 suppression of IL-1β remains unaltered, likely related to its inability to alter IL-1β expression in BV-2 microglia, though an upward trend of IL-1β levels in dsRNAi-Nurr1 treatments were detected (Figure 21F). These data indicate that C-DIM12 requires functional Nurr1 in order to fully suppress proinflammatory gene expression in BV-2 cells stimulated by LPS.

Nurr1 expression correlates with C-DIM12 anti-inflammatory efficacy

A longer treatment period (24 hours) of BV-2 cells with C-DIM12 and LPS was selected because timecourse evaluation of cytokines suggested they are most upregulated at this point (Figure 20). For comparison, we evaluated the outcome of C-DIM12 treatment at a shorter, 8-hour timepoint (Figure 22A-C). Interestingly, BV-2 cells treated with LPS in conjunction with C-DIM12 showed no significant decrease in NOS2 or IL-6 induction compared to LPS alone when assayed after 8 hours (Figure 22A-B). In comparison, BV-2 cells treated with LPS and C-DIM12 for 24 hours show almost complete reduction of NOS2 and IL-6 when compared to LPS-treated cells alone (Figure 22A-B). To explore the cause of discrepancy in C-DIM12 suppression of neurotoxic factors in BV-2 cells, we examined the gene expression levels of Nurr1 at these two timepoints. After 8 hours, no significant difference was detected in Nurr1 levels from saline control in either LPS or LPS + CDIM12 treatment groups (Figure 22C). After 24 hours however, Nurr1 levels are highly induced over saline control levels in both LPS and LPS + CDIM12. The induction of Nurr1 correlating with reduction in fold change of NOS2 and IL-6 in the C-DIM12 treatment groups suggests that the activation of Nurr1 is required for C-DIM12 to elicit an anti-inflammatory response.

It was recently discovered by Saijo et al. (2009) that GSK3β is required for docking of Nurr1 at p65 on inflammatory gene promoters. Their group established that phosphorylation of Serine-486 provides the docking site necessary to recruit Nurr1 to p65 (Saijo et al., 2009). In an effort to confirm that C-DIM12 and Nurr1 interaction occurs at inflammatory promoters, we treated BV-2 cells with SB216763 (SB21) an inhibitor of GSK3β, and challenged them with 10 µM LPS for 24 hours with and without the co-treatment of C-DIM12. When GSK3β is inhibited, NOS2 and TNFa are both significantly induced in LPS treatment alone, as well as LPS + C-DIM12 (Figure 22E-F). These data indicate that docking of Nurr1 to p65, recruited by GSK3β is a necessary mechanism involved in the suppression of microglial cytokines by C-DIM12.

C-DIM12 does not prevent p65 translocation.

Upon TLR binding in microglia, inflammatory gene cascades converge on NF-κB, where p50/p65 heterodimers translocate into the nucleus for activation of downstream inflammatory promoters (He et al., 2002; Saijo et al., 2013). A possible mechanism by which C-DIM12 may function, is the inhibition of p65 translocation, a common target for several anti-inflammatory small molecules. In order to evaluate this possibility, we treated BV-2 microglia with 1 µg/ml LPS and measured the rapid induction of p65 using immunofluorescence (α-p65, Abcam). After 30 minutes, p65 levels in BV-2 cells are markedly increased over saline (Figure 22D), and the nuclear void visible in saline disappears as p65 translocates in LPS treated cells. Additionally, the cytoskeletal marker isolection (Isolectin GS-IB$_4$, Alexa Fluor 488 Conjugate, Life Technologies) revealed a distinct change in cellular morphology, from a resting microglial cytoskeleton to more amoeboid, activated microglia. BV-2 microglia treated with 1 µg/ml LPS + C-DIM12 did not inhibit nuclear translocation of 65, however a reduction in overall p65 levels were visible, and the cellular morphology of the microglia appear less activated. These data

suggest that the measured suppression of inflammatory cytokines in BV-2 microglia by C-DIM12 is via a mechanism downstream of p65 nuclear translocation.

Transcriptional repression by Nurr1 is increased by C-DIM12

Recruitment of Nurr1 monomers to p65 involves several proteins with kinase action (GSK3β, NLK), as well as proteins that modify Nurr1 in order to recruit corepressors such as histone deactylases (HDAC2/3), and nuclear receptor co-repressor 2 (NCOR2; Saijo et al., 2009). Chromatin immunoprecipitation (ChIP) timecourse data indicate that BV-2 microglia treated with 10 µg/ml LPS over 24 hours have slight increases in Nurr1 recruitment to the NOS2 promoter, which steadily decrease by 24 hours (Figure 23A). In contrast, cells treated with 1 µg/ml LPS + C-DIM12 have a significantly increased amount Nurr1 bound to NOS2 promoters at 24 hours. ChIP experiments targeting p65 relative to the NOS2 promoter show that a significant increase in p65 occurs 2 hours post LPS treatment in BV-2 microglia, and p65 interaction stays elevated, trending slightly downward by 24 hours (Figure 23B). BV-2 cells treated with LPS + C-DIM12 have a significantly lower amount of p65 bound to the NOS2 promoter throughout the 24 hour timecourse, indicating that C-DIM12 affects the interaction of p65 at the NOS2 promoter.

Corepressor complex proteins NCoR2 and CoREST were examined under these conditions, and cells treated with LPS + C-DIM12 show a slight increase in NCoR2 bound to NOS2 after 24 hours post LPS treatment when compared to LPS alone (Figure 23C). Cells receiving only LPS show an initial increase in CoREST levels bound to the NOS2 promoter, which drop significantly by 8 hours (Figure 23D). In contrast, cells treated with C-DIM12 express sustained levels of CoREST bound to the NOS2 promoter at 24 hours, possibly

indicating that C-DIM12 stabilizes the CoREST complex bound to this site.

After ChIP experiments revealed that bound co-repressors to the NOS2 promoter were altered by C-DIM12 treatment, total protein levels of HDAC3 and NCoR2 were measured in BV-2 cells over a 24 hour timecourse with 10 µg/ml LPS and LPS + C-DIM12. Immunoblot data from these experiments indicates that HDAC3 protein levels drop slightly after LPS treatment (4 hours) but remains stable in LPS + C-DIM12 treated cells (Figure 23F). A similar result is observed in NCoR2 protein expression, where the addition of C-DIM12 to BV-2 cells treated with LPS seems to minimize the initial drop in total corepressor expression, and stabilizes it over the remainder of the LPS timecourse (Figure 23E).

C-DIM12 appears to be able to suppress inflammatory genes only when Nurr1 is active and bound to NF-κB transcription factors at a specific promoter. ChIP data suggest that Nurr1 levels bound to the NOS2 promoter are increased by C-DIM12, and co-repressor proteins known to be involved in transrepressive mechanisms are stabilized by treatment with C-DIM12. A possible mechanism for C-DIM12 anti-inflammatory action is illustrated in Figure 23G, where NOS2 promoter transcription activated by NF-κB-p50/p65 is reduced by co-repressor complex proteins recruited to the NOS2 promoter by Nurr1. Pharmacologic modulation of Nurr1 by C-DIM12 increases the nuclear receptor interaction with co-repressor proteins, actively removing p65 from the NOS2 promoter, and reducing inflammatory gene transcription.

DISCUSSION

The molecular data presented here suggests a strong correlation between C-DIM12 and the action of nuclear receptor Nurr1. C-DIM12 was initially selected for its ability to suppress NOS2 in astrocyte and microglial cells *in vitro*, but also because it displays a large distribution to the

brain and is orally bioavailable. Pilot neuroprotection studies with C-DIM12 indicate that it is able to prevent the progression of dopamine neuron loss in a subacute MPTP mouse model of PD, likely through the inhibition of NF-κB-regulated inflammation in glial cells (De Miranda et al., 2013).

Several indicators of C-DIM12 interaction with Nurr1 are established here, presenting a novel compound that affects nuclear receptor NR4A regulation of inflammation in glia. First, the structure-dependent inhibition of NOS2 and IL-1B shows that C-DIM12 has more potent anti-inflammatory action in primary mouse mixed glia than several other C-DIM analogs (Figure 19). As cancer therapeutics, the C-DIM analogs have been explored as inducers of proapoptotic proteins, increasing the activation of CHOP and PARP cleavage in colon cancer cell lines (RKO, SW480) in a structure-dependent manner (Lei et al., 2008). C-DIM12 has been shown to inhibit growth of urothelial carcinoma cells (KU7, 253J cell lines) by activating caspases, TRAIL, and PARP cleavage, and reduces *in vivo* bladder cancer growth (Inamoto et al., 2008). The anticancer properties of C-DIM12 were determined Nurr1-dependent, where C-DIM12 increases the expression of Gal4-Nurr1 luciferase reporter assay in a dose-dependent manner (Inamoto et al., 2008). We first demonstrated the regulation of glial inflammatory proteins by DIM-C-pPhtBu (C-DIM4), concluding that reduction of NOS2 in primary astrocytes treated with C-DIM4 was through a PPARɣ-dependent mechanism, stabilizing corepressor NCoR2 levels (Carbone et al., 2008).

The dose-dependent inhibition of inflammatory gene expression in BV-2 microglia displays that C-DIM12 suppresses NF-κB-regulated cytokines (Figure 20). C-DIM12 did not suppress the nuclear translocation of p65 in BV-2 cells (Figure 22D), indicating that it acts downstream of NF-κB-p50/65 translocation. Knockdown of Nurr1 protein however, decreases

104

the ability of C-DIM12 to suppress these inflammatory proteins (Figure 21D-G), as does the inhibition of Nurr1 docking to p65 by GSK3β (Figure 22E-F). Nurr1-mediated transrepression of NOS2 in BV-2 microglia involves the recruitment of the CoREST corepressor complex, which removes p65 from the NOS2 promoter (Saijo et al., 2009a). The loss of C-DIM12 suppression of cytokines by dsRNAi-Nurr1 demonstrates that C-DIM12 action is a Nurr1-dependent mechanism. Phosphorylation of Serine-468 on p65 was shown to be required for the recruitment of Nurr1 to p65 bound to target promoters, the inhibition of which increases the transcription of NF-κB-dependent TNFα and NOS2 (Buss et al., 2002; Saijo et al., 2009). Similarly, we demonstrated that GSK3β inhibition in BV-2 cultures challenged with LPS increases the expression of both NOS2 and IL-1β (Figure 22E-F). The reduced efficacy of C-DIM12 to suppress LPS-induced NOS2 and IL-1β expression by GSK3β inhibitor SB21 indicates that C-DIM12 function also requires phosphorylation of p65, an event necessary for the recruitment of Nurr1.

The NR4A family of nuclear receptors are described as immediate, early-response genes involved in cellular maintenance and development as well as inflammation (Zhao and Bruemmer, 2010). BV-2 microglia rapidly respond to LPS stimulation through TLR4 induction of inflammatory pathways that converge on NF-κB. Indeed, 2 hours post LPS (1 µg/ml) treatment all inflammatory proteins that we assayed were greatly increased (Figure 20A-F). After 24 hours with LPS treatment however, further induction of these cytokines were observed, except for IL-1β that decreases over time, but still remains activated over control levels. Interestingly, C-DIM12 suppression of these cytokines appears to be time-dependent, primarily effective after 24 hours of treatment (Figure 22A-B). While p65 translocation was observed after 30 minutes of LPS treatment (Figure 22D), Nurr1 mRNA levels remained low at 8 hours post

LPS, but increased after 24 hours. One explanation for this could be the nuclear export of Nurr1 in response to LPS treatment of BV-2 cells. Oxidative stress in neuronal cell lines (SH-SY5Y, MN9D) caused the nuclear export of Nurr1 60 minutes after treatment with sodium aresenite by a nuclear export signals (NES) located on the protein (García-Yagüe et al., 2013). Nuclear exportation of Nurr1 in response to oxidative stress may lead to the decrease in transcriptional activity of Nurr1 immediately following induction of cytokines such as NOS2, which produces nitric oxide (NO). It is unclear whether the nuclear export of Nurr1 in glial cells may occur in response to TLR4 activation, but time-dependent protection by C-DIM12 corresponds with the increase of Nurr1 mRNA after 24 hours. Of note, NR4A family member Nur77 (NR4A1) is exported to the mitochondria upon activation in a cell-specific manner, a process that has been modified by C-DIM analogs in a cancer model (Lee et al., 2011). Export of Nurr1 and Nur77 in astrocytes and microglial cells has yet to be identified, however Nurr1 has not been shown to translocate to the mitochondria in other cell types (García-Yagüe et al., 2013).

The interaction of p65 with the NOS2 promoter in BV-2 microglia following LPS treatment shows that initial increases in bound p65 do not decrease after 24 hours, an interaction confirmed with cytokine gene expression (Figures 20A, 23A). C-DIM12 decreased the p65 interaction at the NOS2 promoter over time, with greatest reduction at 24 hours. The interaction of Nurr1 with the NOS2 promoter is increased in cells treated with C-DIM12, with a marked increase at the 24-hour timepoint (Figure 23B). Early response of Nurr1 bound to the NOS2 promoter with LPS treatment alone decreases by 24 hours, when inflammatory gene expression is highest in the microglia. These data support the possibility that immediate export of Nurr1 decreases its transcriptional activity following TLR stimulation, though confirmation of this activity in microglia is necessary. A clear increase of Nurr1 bound to the NOS2 promoter in

microglia however, is induced by C-DIM12, leading to suppression of p65-driven cytokine expression through transrepression. The stabilization of CoREST bound to the NOS2 promoter by C-DIM12 supports this idea, where Nurr1-dependent recruitment of this complex is results in inflammatory reduction in microglia. Total levels of corepressor proteins HDAC3 and NCoR2 appear stabilized as well, though specific promoter binding is a more strong reflection of the transrepressive mechanism of Nurr1 (Figure 23E-F).

The discovery of Nurr1 as a transrepressor of NF-κB-regulated genes in glia is a novel development in the function of NR4A nuclear receptors, providing a new target for therapeutics in neuroinflammatory disease. Here, we present a compound from the class of *para*-phenyl substituted diindolylmethanes that activate Nurr1 in cancer models, has anti-inflammatory activity in glial cells through a Nurr1-dependent mechanism. This pharmacological manipulation of Nurr1 transrepression by C-DIM12 represents a novel mechanism to decrease NF-κB-driven genes in glial cells, and a new therapeutic agent for consideration in neurodegnerative disease.

FIGURE 19
STRUCTURE-DEPENDENT CYTOKINE SUPPRESSION BY C-DIM12
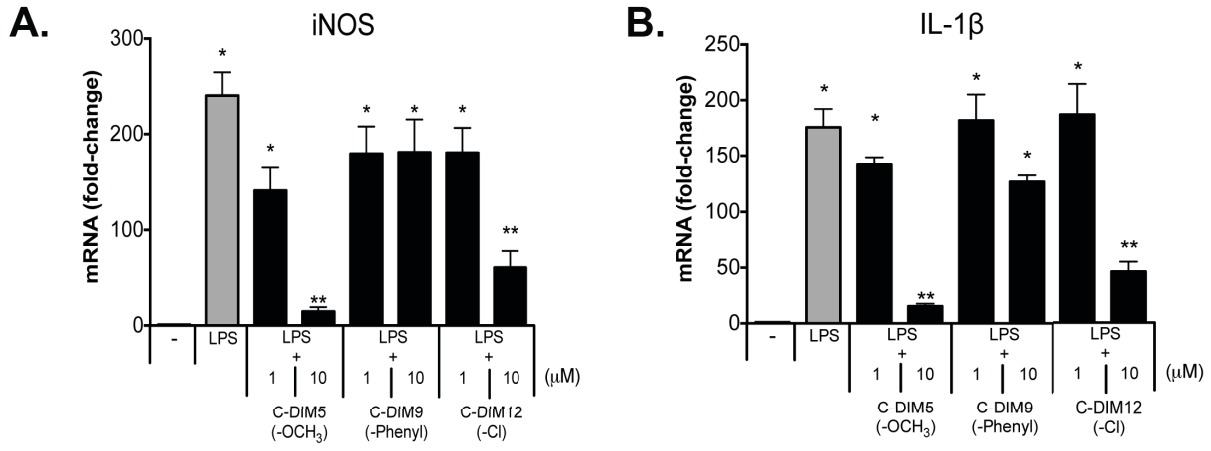
Figure 19. C-DIM inflammatory gene suppression in glia is structure-dependent. Primary murine mixed glial cultures were treated with saline or 1 µg/ml LPS and 1 µM or 10 µM of DIM-C-pPhOCH3 (C-DIM5), DIM-C-pPhPh (C-DIM9), of DIM-C-pPhCl (C-DIM12) for 8 hours, and assessed for **A.** NOS2 or **B.** IL-1β expression with real-time PCR. Data are expressed as mean ± SEM; mRNA fold change; internal control (β-actin); * $p < 0.05$, ** $p < 0.01$.
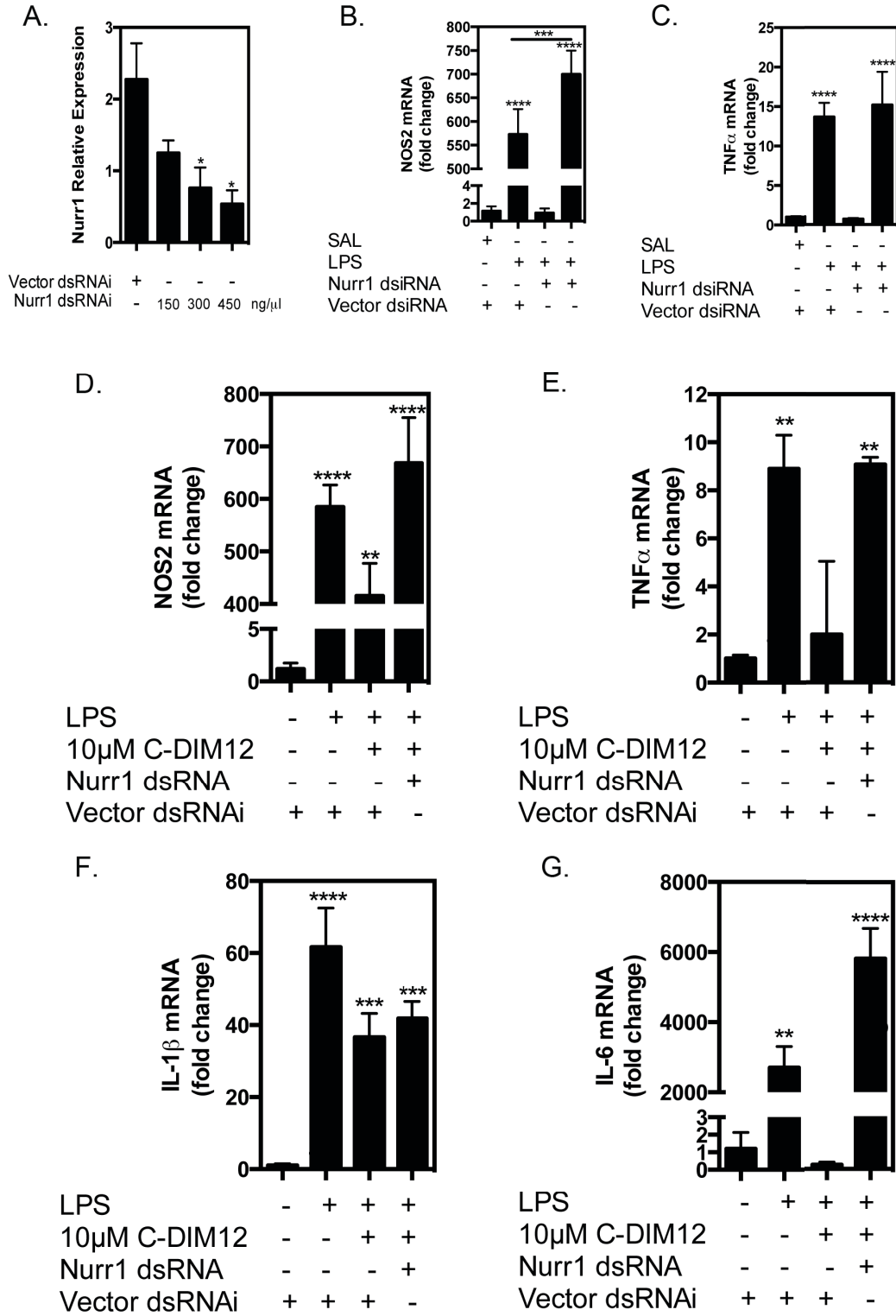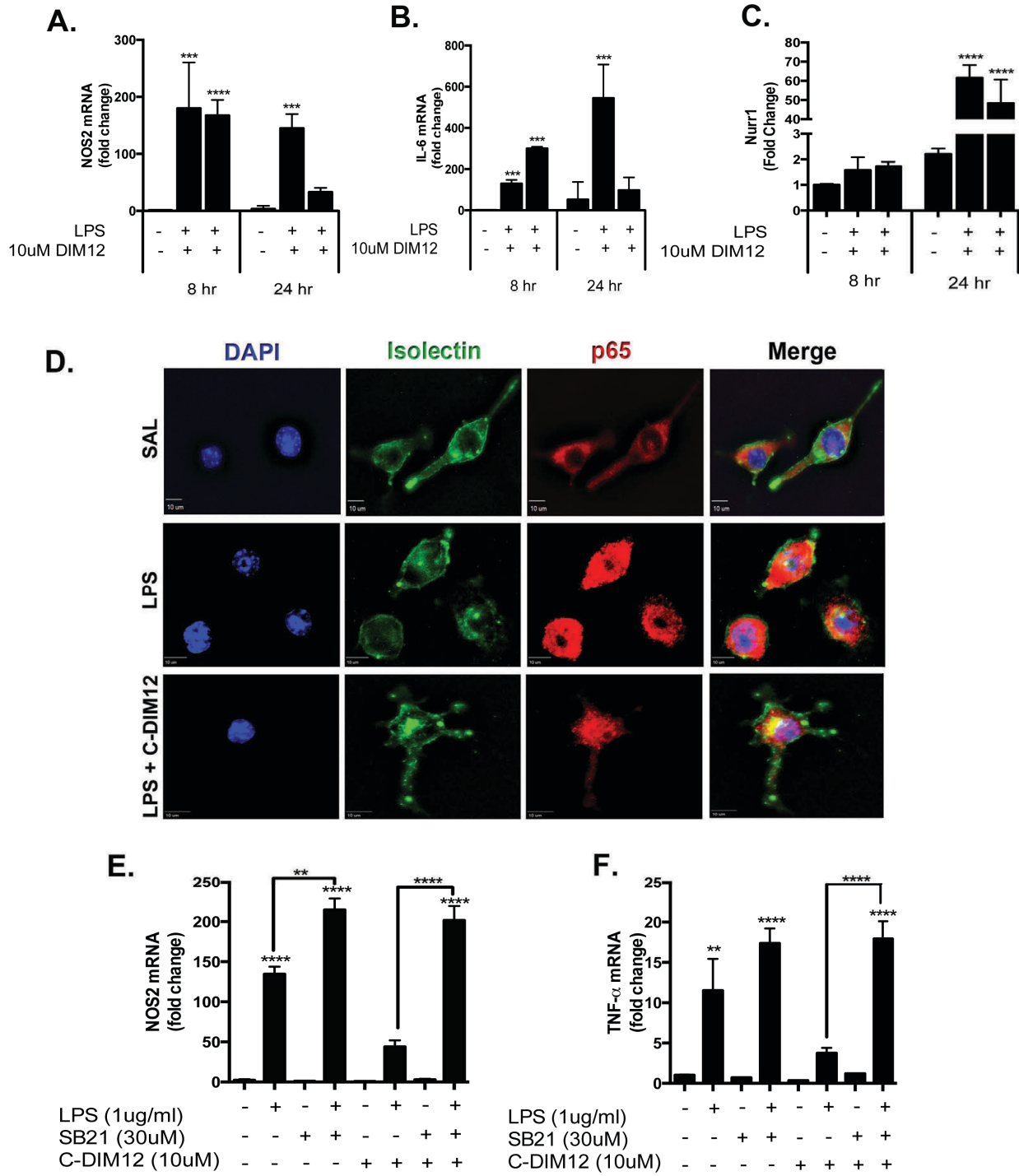
FIGURE 20
BV-2 TIMECOURSE AND C-DIM12 DOSE-RESPONSE
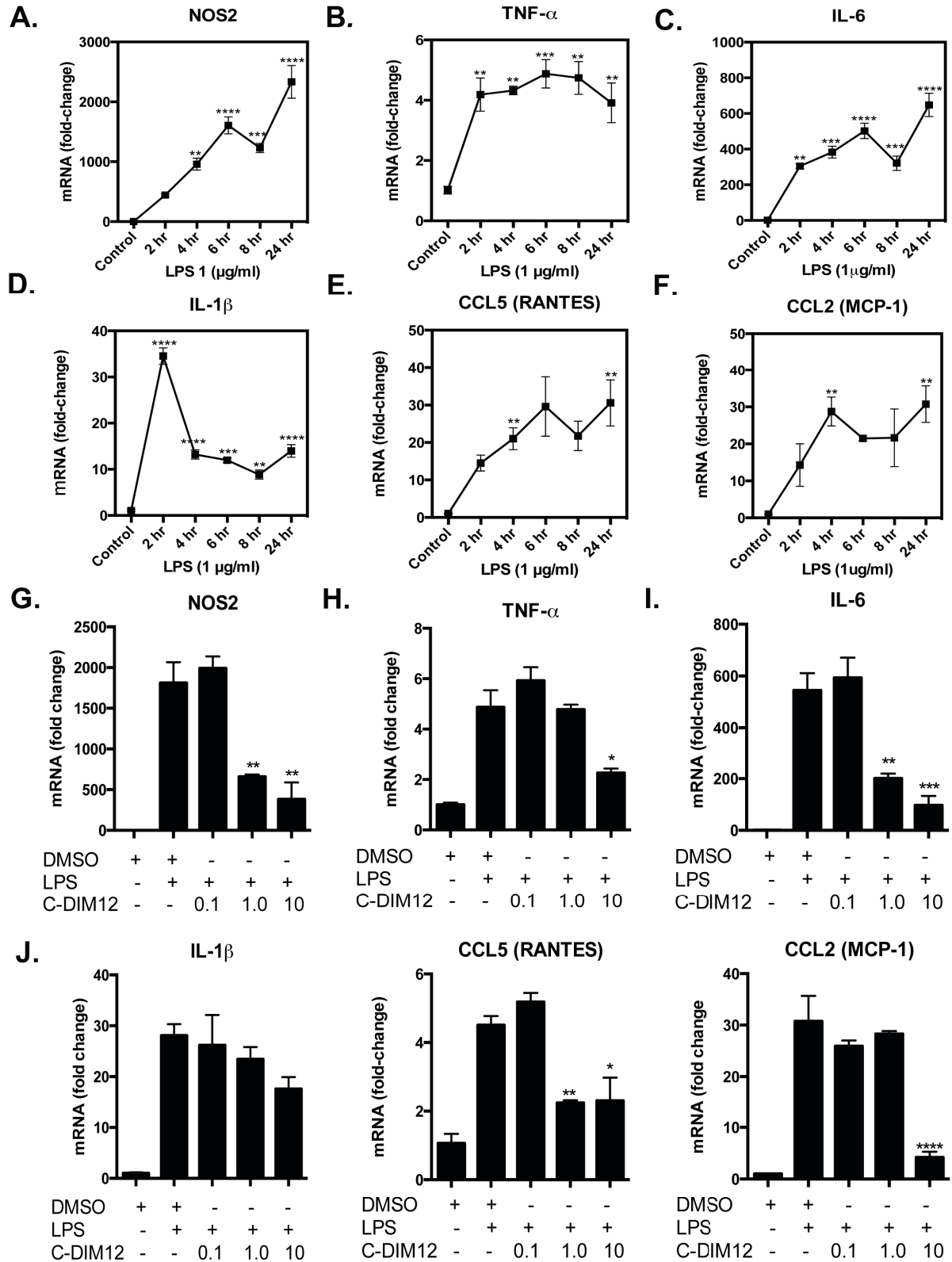
Figure 20. LPS-induced timecourse expression of cytokines in BV-2 microglia and dose-dependent suppression by C-DIM12. A-F. BV-2 microglia were treated with saline or 1 µg/ml LPS over a 24 hour time-point, and RNA was collected for real-time PCR analysis of cytokine mRNA expression. **G-L.** BV-2 microglia were pre-treated for 1 hour with 0.1 µM, 1.0 µM or 10 µM C-DIM12 followed by 24 hour LPS (1 µg/ml). mRNA expression was assessed for fold change of cytokine expression (β-actin internal control). Data are expressed as mean ± SEM; mRNA fold change; * $p < 0.05$, ** $p < 0.01$, *** $p < 0.001$, **** $p < 0.0001$.

FIGURE 21
NURR-1 DEPENDENT CYTOKINE SUPPRESSION OF C-DIM12

Figure 21. C-DIM12 suppression of cytokines is Nurr-1 dependent. A. BV-2 microglia were treated with dsRNAi-Nurr1 or scrambled dsRNAi (vector control), Nurr1 mRNA was measured using real-time PCR (HPRT internal control). **B-C.** BV-2 microglia were treated with dsRNAi-Nurr1 or dsRNAi-vector for 24 hours followed by saline or 1 µg/ml LPS for 24 hours and assessed for mRNA expression of NOS2 and TNFa. **D-G.** BV-2 cells were treated with dsRNAi-Nurr1 or dsRNAi-vector for 24 hours followed by 10 µM C-DIM12 (1 hour pretreatment) and 1 µg/ml LPS treatment and assessed for mRNA expression of NOS2, TNFα, IL-1β and IL-6. Data are expressed as mean ± SEM; mRNA fold change; * $p < 0.05$, ** $p < 0.01$, *** $p < 0.001$, **** $p < 0.0001$.
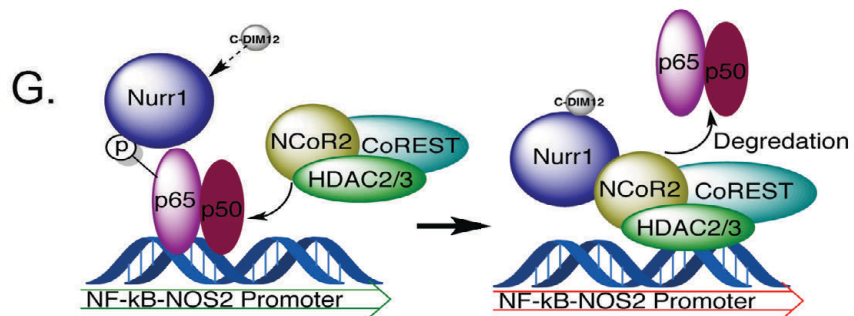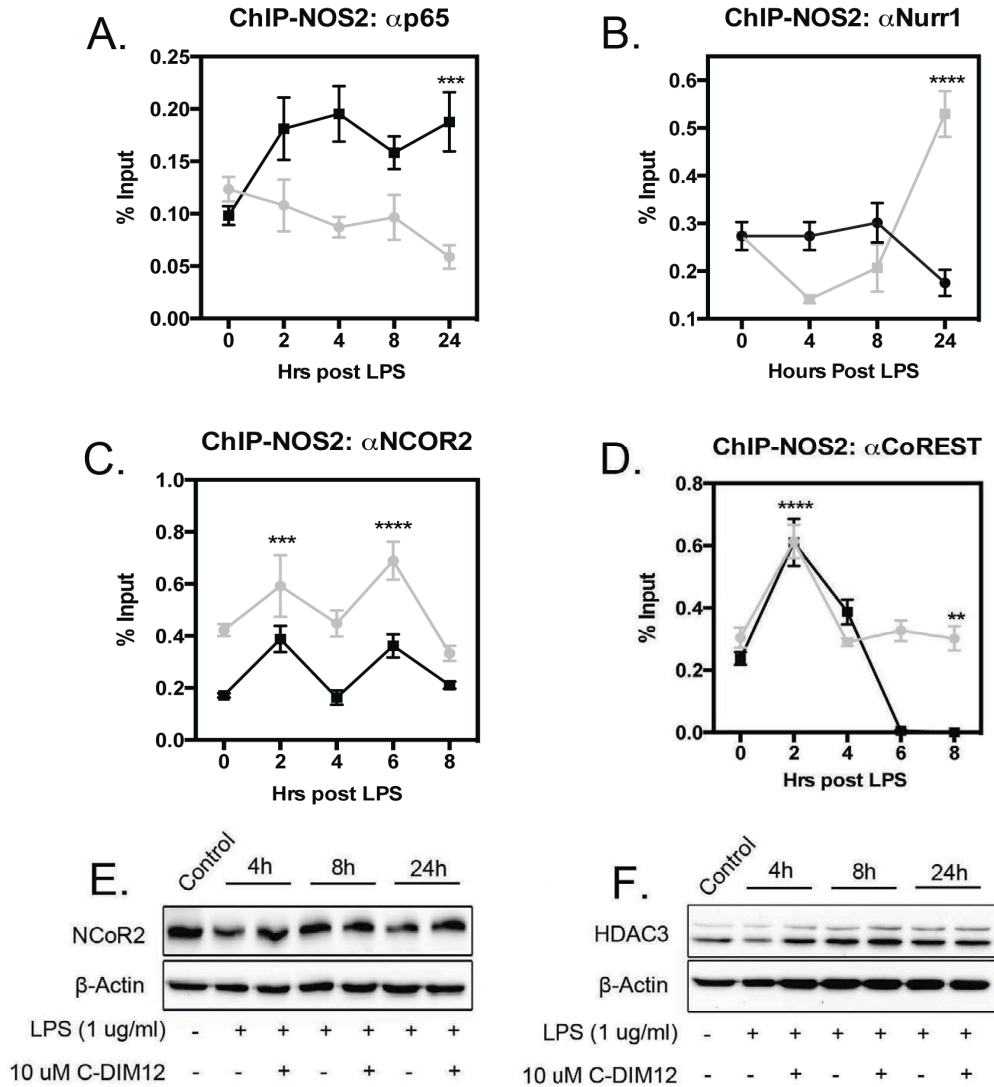
FIGURE 22
NURR1 FUNCTION IN C-DIM12 EFFICAY

113

Figure 22. C-DIM12 does not prevent p65 translocation, is dependent on Nurr1 recruitment. A-B. BV-2 cells were treated with 10 μM C-DIM12 for one hour followed by saline or 1 μg/ml LPS for 8hr or 24 hr, and assessed for NOS2 and IL-6 mRNA. **C.** Nurr1 mRNA levels were assessed for 8hr and 24 hr time-points. **D.** BV-2 cells were treated with 10 μM C-DIM12 for one hour followed by saline or 1 μg/ml LPS for 30 min and fixed for immunofluorescence to examine p65 translocation; DAPI (blue), isolectin (green), p65 (red). **E-F.** BV-2 cells were treated with 30 μM SB216763 (SB21) to inhibit GSK3β for 1 hour, followed by 1 μg/ml LPS and co-treatment with 10 μM C-DIM12 for 24 hours. NOS2 and TNFa mRNA was assessed for fold change expression, data are expressed as mean ± SEM; * $p < 0.05$, ** $p < 0.01$, *** $p < 0.001$, **** $p < 0.0001$.

FIGURE 23
C-DIM12 ENHANCES NURR1 TRANSREPRESSION

FIGURE 23
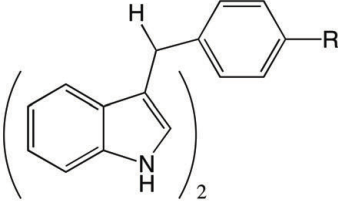C-DIM12 ENHANCES NURR1 TRANSREPRESSION

Figure 23. C-DIM12 enhances Nurr1 recruitment to NOS2 promoter, decreases p65 binding, and stabilizes corepressors. BV-2 cells were treated with 10 µM C-DIM12 for one hour followed by 1 µg/ml LPS over a 24-hour time-point and assessed at the NOS2 promoter using chromatin immunoprecipitation (ChIP). **A.** The amount of p65 bound to the NOS2 promoter was measured in LPS or LPS + C-DIM treatments. **B.** The level of Nurr1 bound to the NOS2 promoter with or without C-DIM12 over 24 hour timecourse with LPS. **C-D.** ChIP assessment of nuclear corepressor NCoR2 and corepressor complex CoREST bound to the NOS2 promoter. **E-F.** Total NCoR2 and HDAC3 protein from 24 hour timecourse treatment with saline or LPS + 10 µM C-DIM12. **G.** Hypothesized mechanism by which C-DIM12 promotes Nurr1-dependent transrepression of p65 at the NOS2 promoter in BV-2 microglia. Data are expressed as percent input ± SEM over control IgG; * $p < 0.05$, ** $p < 0.01$, *** $p < 0.001$, **** $p < 0.0001$.

TABLE 6
C-DIM SCREENING

Table 6. Suppression of LPS-induced inflammatory gene expression by C-DIM compounds.

		Nos2 mRNA (Fold-Induction)		Il1β mRNA (Fold-Induction)	
		Saline	**LPS**	**Saline**	**LPS**
		1± 0.2	240.5 ± 24.4*	1.0 ± 0.2	175.7 ±16.5*
		LPS +		**LPS +**	
C-DIM	*R*-Group	**C-DIM (1 uM)**	**C-DIM (10 uM)**	**C-DIM (1 uM)**	**C-DIM (10 uM)**
1	-CF$_3$	160.6 ± 13.1	**50.8 ± 8.7†**	167.6 ± 18.2*	**34.1 ± 3.1†**
2	-Br	175.5 ± 34.9	73.1 ± 23.1	129.4 ± 43.0	**40.6 ± 3.7†**
3	-F	133.8 ± 8.6	**3.3 ± 1.5†**	156.7 ± 10.6*	**7.1 ± 1.8†**
4	-*tert*-Butyl	107.8 ± 20.5	84.8 ± 8.0	125.3 ± 8.0	93.9 ± 10.2
5	-OCH$_3$	141.4 ± 24.0	**14.7 ± 4.7†**	142.6 ± 6.1*	**15.4 ± 2.3†**
6	-N(CH$_3$)$_2$	224.2 ± 68.0*	99.5 ± 21.7	164.9 ± 30.0*	65.1 ± 9.1
7	-H	184.9 ± 36.1*	**12.4 ± 4.4†**	142.9 ± 44.5*	**12.6 ± 2.3†**
8	-OH	189.3 ± 61.8*	**0.7 ± 0.4†**	136.2 ± 48.3*	**9.3 ± 1.4†**
9	-Phenyl	136.2 ± 47.7	180.9 ± 34.5*	137.4 ± 47.4*	127.2 ± 5.8
10	-CN	96.0 ± 21.6	**34.5 ± 5.8†**	140.1 ± 7.5*	**23.8 ± 1.8†**
11	-CH$_3$	140.0 ± 5.5	**32.0 ± 6.8†**	152.2 ± 15.7*	**36.4 ± 3.5†**
12	-Cl	180.4 ± 26.2	**60.6 ± 17.5†**	186.9 ± 27.6*	**45.9 ± 8.9†**
13	-COOCH$_3$	255.5 ± 78.8*	**90.9 ± 7.8†**	185.2 ± 11.5*	**44.0 ± 15.2†**
14	-I	242.9 ± 83.9*	**122.7 ± 33.5†**	161.4 ± 43.6*	72.4 ± 15.0

*Different from Control group (*p*<0.05)
†Different from LPS group (*p*<0.05)

Primary murine mixed glial cultures were treated with saline or 1 μg/ml LPS and 1 μM or 10 μM doses of one of 14 C-DIM analogs. Structural differences displayed as '*R*-Group' and significant suppression of NOS2 and IL-1β mRNA levels from LPS control are indicated in bold. Data are expressed as mean ± SD, mRNA fold induction over LPS (β-actin internal control).

CHAPTER 6

DISCUSSION

Parkinson's disease is a severe, degenerative movement disorder affecting millions worldwide, with substantial implications in an aging population (Hirsch and Hunot, 2009a). While symptomatic treatments exist to alleviate motor deficits, dyskinesias and the reduction in benefit over time to dopamine mimetics such as L-DOPA limit their usefulness. A great challenge exists to find small molecule therapies aimed at reducing the inflammatory component of PD, in which the glia in the ventral midbrain continuously release components neurotoxic to dopamine neurons. The studies presented here, were designed to provide better efficacy in evaluating the loss of dopamine neurons from the SN in mouse models of PD, and to elucidate the mechanism by which novel anti-inflammatory C-DIM compounds provide neuroprotective benefit.

The development of a stereological method for counting immunofluorescent neurons in the SN of animals treated with MPTP was an important tool necessary for the robust analysis of future neuroprotection models. Typical methods of stereology utilize immunohistochemistry, where a low-contrasting background can lead to difficulty of precise neuron detection (West and Gundersen, 1990). The secondary amplification of fluorophore-containing secondary antibodies helps to identify TH-positive neurons against a black background, while still maintaining the 3D model-based accuracy of stereology that encompasses the SN. The sensitivity of this assay to small changes in dopamine neuron number after low-grade MPTP exposure indicated that our developed method of stereology was useful in detection of early stage disease progression.

In attempt to streamline the clinical translation of novel *para*-phenyl substituted

118

diindolylmethanes, we measured the pharmacokinetics of four C-DIMs differing in one structural substitution. Results comparing areas under the curve (AUC) from each compound in plasma and brain conferred the pharmacokinetics of each C-DIM was altered by the phenyl-substituted position on C-DIM5, C-DIM7, C-DIM8, and C-DIM12. We observed an interesting reduction in C-DIM8 after oral dosing of the compound, which we determined was the result of a rapid, direct conjugation of glucuronide to the phenyl-hydroxyl group. Despite structure-dependent differences in metabolism, all four C-DIMs examined had acceptable pharmacokinetic and metabolism profiles, confirming that they both enter the brain and are orally bioavailable. This is a critical factor because intravenous dosing of drugs in neurodegenerative disease has many barriers. One example of this is the antioxidant glutathione, which is given intravenously to prevent its metabolism. While early clinical trials have shown mild efficacy using this therapy, administration requires an intravenous line in elderly patients that could potentially have both short and long-term risks (Hauser et al., 2009). The neuroprotection conveyed by the C-DIM compounds in pilot studies using an MPTPp mouse model of neurodegeneration shows that these compounds are both efficacious and reach the brain when delivered orally.

To further understand the mechanisms by which the C-DIM compounds prevented progressive dopamine neuron loss, we recapitulated an MPTPp lesion in the SN, where adult mice were administered C-DIMs via daily oral gavage 7 days after the onset of neuron loss. We observed that C-DIM compounds attenuated dopamine neuron loss, measured using stereology, by inhibiting glial activation in the SN and the ST. Using a transgenic NF-κB-EGFP reporter mouse, we targeted intrinsic expression of inflammatory gene regulator NF-κB to coincide with worsening of both dopamine neuron loss and astrocyte and microglial activation. Both the reduction of global NF-κB expression and the specific measurement of NF-κB-regulated

cytokines in the SN were suppressed by C-DIMs. Of note, C-DIM5 did not appear to suppress cytokine production as significantly as C-DIM12, despite dopamine neuroprotection and gliosis reduction. C-DIM5 is reported to be an activator of nuclear receptor NR4A1 (Nur77/TR3) in human pancreatic cancer cell lines, which leads to the enhanced expression of apoptotic proteins such as retinoids, p21, TRAIL and Fas (Lee et al., 2011).While the mechanism of C-DIM5 in glial cells has yet to be established, it is possible that the action of C-DIM5 on Nur77 could be altering inflammatory signaling differently than in C-DIM8 or C-DIM12 treated animals. The role that Nur77 plays in glial inflammation in the CNS has yet to be elucidated, however mechanistic studies of C-DIM5 in primary mouse astrocytes are currently being investigated by our lab.

The recent discovery that NR4A family member Nurr1 (NR4A2) suppresses NF-κB-regulated gene expression in glia (Saijo et al., 2009b) led us to wonder if C-DIM12 may be pharmacologically inducing this pathway. C-DIM12 is activates Nurr1 expression in bladder cancer cells, increasing the activation of caspases, C-PARP, and TRAIL, and also inhibits bladder cancer growth *in vivo*. We observed that C-DIM12 reduced the expression of LPS-induced NF-κB-regulated cytokines in BV-2 microglia in a Nurr1-dependent manner, losing its effect when Nurr1 was knocked down using dsRNAi. Additionally, Nurr1 recruitment to the NOS2 promoter in microglia treated with LPS was increased by C-DIM12. The transrepressive mechanism by which Nurr1 tethers nuclear corepressors (CoREST) to NF-κB-p65 elements bound to NOS2 is also modulated by C-DIM12, where stabilization of CoREST removes p65 from the promoter. Site-directed mutagenesis to binding areas of Nurr1 in microglia would confirm specific activation or co-activation by C-DIM12, however these experiments were out of the scope of this study.

FINAL CONCLUSIONS

A major shift in the way neurodegenerative disease is studied, modeled, and treated has led to new and exciting targets for which potential therapies can be designed. These studies highlight the efficacy of novel therapeutic C-DIM compounds, striving to use the most sensitive methods of pathological analysis and preclinical pharmacokinetic data in order promote clinical translation. The mechanism by which C-DIM5, C-DIM8, and C-DIM12 convey neuroprotection was investigated and has revealed a suppression of NF-κB-induced glial inflammation. Finally, the specific action of C-DIM12 was discovered to act on nuclear receptor Nurr1 transrepression of NF-κB on the NOS2 inflammatory promoter in microglia. Together, these data indicate a novel way to suppress glial inflammation in a mouse model of PD, and provide insight into a new therapeutic agent targeted at the intricate process driving dopamine neuron loss.

LITERATURE CITED

Alladi, P.A., Mahadevan, A., Vijayalakshmi, K., Muthane, U., Shankar, S.K., and Raju, T.R. (2010). Ageing enhances alpha-synuclein, ubiquitin and endoplasmic reticular stress protein expression in the nigral neurons of Asian Indians. Neurochem. Int. *57*, 530–539.

Antosz, H., and Osiak, M. (2013). NOD1 and NOD2 receptors: integral members of the innate and adaptive immunity system. Acta Biochim. Pol. *60*, 351–360.

Baiguera, C., Alghisi, M., Pinna, A., Bellucci, A., De Luca, M.A., Frau, L., Morelli, M., Ingrassia, R., Benarese, M., Porrini, V., et al. (2012). Late-onset Parkinsonism in NFκB/c-Rel-deficient mice. Brain *135*, 2750–2765.

Baquet, Z.C., Williams, D., Brody, J., and Smeyne, R.J. (2009). A comparison of model-based (2D) and design-based (3D) stereological methods for estimating cell number in the substantia nigra pars compacta (SNpc) of the C57BL/6J mouse. Neuroscience *161*, 1082–1090.

Bensinger, S.J., and (null) (2009). A Nurr1 pathway for neuroprotection. Cell *137*, 3.

Bianchi, R., Giambanco, I., and Donato, R. (2010). S100B/RAGE-dependent activation of microglia via NF-κB and AP-1: Co-regulation of COX-2 expression by S100B, IL-1β and TNF-α. Neurobiology of Aging *31*, 665–677.

Brambilla, R., Bracchi-Ricard, V., Hu, W.-H., Frydel, B., Bramwell, A., Karmally, S., Green, E.J., and Bethea, J.R. (2005). Inhibition of astroglial nuclear factor kappaB reduces inflammation and improves functional recovery after spinal cord injury. J. Exp. Med. *202*, 145–156.

Brown, G.C., and Neher, J.J. (2010). Inflammatory Neurodegeneration and Mechanisms of Microglial Killing of Neurons. Mol Neurobiol *41*, 242–247.

Burke, R.E., and O'Malley, K. (2013). Axon degeneration in Parkinson's disease. Experimental Neurology *246*, 72–83.

Cannon, J.R., and Greenamyre, J.T. (2009). NeuN is not a reliable marker of dopamine neurons in rat substantia nigra. Neurosci. Lett. *464*, 14–17.

Cannon, J.R., Tapias, V., Na, H.M., Honick, A.S., Drolet, R.E., and Greenamyre, J.T. (2009). A highly reproducible rotenone model of Parkinson's disease. Neurobiology of Disease *34*, 279–290.

Cao, S., Theodore, S., and Standaert, D.G. (2010). Fcγ receptors are required for NF-κB signaling, microglial activation and dopaminergic neurodegeneration in an AAV-synuclein mouse model of Parkinson's disease. Mol Neurodegener *5*, 42.

Carbone, D.L., Popichak, K.A., Moreno, J.A., Safe, S., and Tjalkens, R.B. (2008). Suppression of 1-Methyl-4-phenyl-1,2,3,6-tetrahydropyridine-Induced Nitric-Oxide Synthase 2 Expression in

Astrocytes by a Novel Diindolylmethane Analog Protects Striatal Neurons against Apoptosis. Molecular Pharmacology *75*, 35–43.

Carta, A.R., Frau, L., Pisanu, A., Wardas, J., Spiga, S., and Carboni, E. (2011). Rosiglitazone decreases peroxisome proliferator receptor-gamma levels in microglia and inhibits TNF-alpha production: new evidences on neuroprotection in a progressive Parkinson's disease model. Neuroscience *194*, 250–261.

Cho, B.P., Sugama, S., Shin, D.H., DeGiorgio, L.A., Kim, S.S., Kim, Y.S., Lim, S.Y., Park, K.C., Volpe, B.T., Cho, S., et al. (2003). Microglial phagocytosis of dopamine neurons at early phases of apoptosis. Cell Mol Neurobiol *23*, 551–560.

Cleren, C., Yang, L., Lorenzo, B., Calingasan, N.Y., Schomer, A., Sireci, A., Wille, E.J., and Beal, M.F. (2008). Therapeutic effects of coenzyme Q10 (CoQ10) and reduced CoQ10 in the MPTP model of Parkinsonism. Journal of Neurochemistry *104*, 1613–1621.

Collingwood, T.N., Urnov, F.D., and Wolffe, A.P. (1999). Nuclear receptors: coactivators, corepressors and chromatin remodeling in the control of transcription. J Mol Endocrinol *23*, 255–275.

Correa, F., Ljunggren, E., Mallard, C., Nilsson, M., Weber, S.G., and Sandberg, M. (2011). The Nrf2-inducible antioxidant defense in astrocytes can be both up- and down-regulated by activated microglia:Involvement of p38 MAPK. Glia *59*, 785–799.

Crowe, S.L., Tsukerman, S., Gale, K., Jorgensen, T.J., and Kondratyev, A.D. (2011). Phosphorylation of histone H2A.X as an early marker of neuronal endangerment following seizures in the adult rat brain. J. Neurosci. *31*, 7648–7656.

Damier, P., Hirsch, E.C., Agid, Y., and Graybiel, A.M. (1999). The substantia nigra of the human brain. II. Patterns of loss of dopamine-containing neurons in Parkinson's disease. Brain *122 (Pt 8)*, 1437–1448.

De Miranda, B.R., Miller, J.A., Hansen, R.J., Lunghofer, P.J., Safe, S., Gustafson, D.L., Colagiovanni, D., and Tjalkens, R.B. (2013). Neuroprotective efficacy and pharmacokinetic behavior of novel anti-inflammatory para-phenyl substituted diindolylmethanes in a mouse model of Parkinson's disease. Journal of Pharmacology and Experimental Therapeutics *345*, 125–138.

Dehmer, T., Heneka, M.T., Sastre, M., Dichgans, J., and Schulz, J.B. (2003). Protection by pioglitazone in the MPTP model of Parkinson's disease correlates with IκBα induction and block of NFκB and iNOS activation. Journal of Neurochemistry *88*, 494–501.

Emborg, M.E. (2004). Evaluation of animal models of Parkinson's disease for neuroprotective strategies. J. Neurosci. Methods *139*, 121–143.

Fearnley, J.M., and Lees, A.J. (1991). Ageing and Parkinson's disease: substantia nigra regional selectivity. Brain *114 (Pt 5)*, 2283–2301.

Ferris, C.F., Marella, M., Smerkers, B., Barchet, T.M., Gershman, B., Matsuno-Yagi, A., and Yagi, T. (2013). A phenotypic model recapitulating the neuropathology of Parkinson's disease. Brain Behav *3*, 351–366.

Gao, H.-M., and Hong, J.-S. (2008). Why neurodegenerative diseases are progressive: uncontrolled inflammation drives disease progression. Trends in Immunology *29*, 357–365.

García-Yagüe, Á.J., Rada, P., Rojo, A.I., Lastres-Becker, I., and Cuadrado, A. (2013). Nuclear import and export signals control the subcellular localization of Nurr1 protein in response to oxidative stress. Journal of Biological Chemistry *288*, 5506–5517.

Ghisletti, S., Huang, W., Jepsen, K., Benner, C., Hardiman, G., Rosenfeld, M.G., and Glass, C.K. (2009). Cooperative NCoR/SMRT interactions establish a corepressor-based strategy for integration of inflammatory and anti-inflammatory signaling pathways. Genes & Development *23*, 681–693.

Ghosh, S., May, M.J., and Kopp, E.B. (1998). NF-kappa B and Rel proteins: evolutionarily conserved mediators of immune responses. Annu. Rev. Immunol. *16*, 225–260.

Gilmore, T.D. (2006). Introduction to NF-kappaB: players, pathways, perspectives. Oncogene *25*, 6680–6684.

Glass, C.K., Saijo, K., Winner, B., Marchetto, M.C., and Gage, F.H. (2010). Mechanisms Underlying Inflammation in Neurodegeneration. Cell *140*, 918–934.

Hartmann, A., Hunot, S., and Hirsch, E.C. (2003). Inflammation and dopaminergic neuronal loss in Parkinson's disease: a complex matter. Experimental Neurology *184*, 561–564.

Hauser, D.N., and Cookson, M.R. (2011). Astrocytes in Parkinson's disease and DJ-1. Journal of Neurochemistry *117*, 357–358.

Hauser, R.A., Cantillon, M., Pourcher, E., Micheli, F., Mok, V., Onofrj, M., Huyck, S., and Wolski, K. (2011). Preladenant in patients with Parkinson's disease and motor fluctuations: a phase 2, double-blind, randomised trial. Lancet Neurol *10*, 221–229.

Hauser, R.A., Lyons, K.E., McClain, T., Carter, S., and Perlmutter, D. (2009). Randomized, double-blind, pilot evaluation of intravenous glutathione in Parkinson's disease. Mov. Disord. *24*, 979–983.

He, B.P., Wen, W., and Strong, M.J. (2002). Activated microglia (BV-2) facilitation of TNF-alpha-mediated motor neuron death in vitro. J. Neuroimmunol. *128*, 31–38.

Hirsch, E.C., and Hunot, S. (2009). Neuroinflammation in Parkinson's disease: a target for neuroprotection? Lancet Neurol *8*, 382–397.

Huang, W., and Glass, C.K. (2010). Nuclear receptors and inflammation control: molecular mechanisms and pathophysiological relevance. Arterioscler. Thromb. Vasc. Biol. *30*, 1542–1549.

Hunot, S., Brugg, B., Ricard, D., Michel, P.P., Muriel, M.P., Ruberg, M., Faucheux, B.A., Agid, Y., and Hirsch, E.C. (1997). Nuclear translocation of NF-kappaB is increased in dopaminergic neurons of patients with parkinson disease. Proc. Natl. Acad. Sci. U.S.a. *94*, 7531–7536.

Inamoto, T., Papineni, S., Chintharlapalli, S., Cho, S.D., Safe, S., and Kamat, A.M. (2008). 1,1-Bis(3'-indolyl)-1-(p-chlorophenyl)methane activates the orphan nuclear receptor Nurr1 and inhibits bladder cancer growth. Molecular Cancer Therapeutics *7*, 3825–3833.

Jackson-Lewis, V., and Przedborski, S. (2007). Protocol for the MPTP mouse model of Parkinson's disease. Nat Protoc *2*, 141–151.

Jenner, P. (2009). Functional models of Parkinson's disease: A valuable tool in the development of novel therapies. Ann Neurol. *64*, S16–S29.

Kacimi, R., Giffard, R.G., and Yenari, M.A. (2011). Endotoxin-activated microglia injure brain derived endothelial cells via NF-κB, JAK-STAT and JNK stress kinase pathways. J Inflamm (Lond) *8*, 7.

Kadkhodaei, B., Ito, T., Joodmardi, E., Mattsson, B., Rouillard, C., Carta, M., Muramatsu, S.-I., Sumi-Ichinose, C., Nomura, T., Metzger, D., et al. (2009). Nurr1 Is Required for Maintenance of Maturing and Adult Midbrain Dopamine Neurons. J. Neurosci. *29*, 15923–15932.

Kahle, P.J., Waak, J., and Gasser, T. (2009). DJ-1 and prevention of oxidative stress in Parkinson's disease and other age-related disorders. Free Radical Biology and Medicine *47*, 1354–1361.

Kaltschmidt, B., Ndiaye, D., Korte, M., Pothion, S., Arbibe, L., Prüllage, M., Pfeiffer, J., Lindecke, A., Staiger, V., Israël, A., et al. (2006). NF-kappaB regulates spatial memory formation and synaptic plasticity through protein kinase A/CREB signaling. Mol. Cell. Biol. *26*, 2936–2946.

Kung, J., and Henry, R.R. (2012). Thiazolidinedione safety. Expert Opin Drug Saf *11*, 565–579.

Lambertsen, K.L., Clausen, B.H., Babcock, A.A., Gregersen, R., Fenger, C., Nielsen, H.H., Haugaard, L.S., Wirenfeldt, M., Nielsen, M., Dagnaes-Hansen, F., et al. (2009). Microglia protect neurons against ischemia by synthesis of tumor necrosis factor. J. Neurosci. *29*, 1319–1330.

Lee, S.O., Abdelrahim, M., Yoon, K., Chintharlapalli, S., Papineni, S., Kim, K., Wang, H., and Safe, S. (2010). Inactivation of the Orphan Nuclear Receptor TR3/Nur77 Inhibits Pancreatic Cancer Cell and Tumor Growth. Cancer Research *70*, 6824–6836.

Lee, S.-O., Li, X., Khan, S., and Safe, S. (2011). Targeting NR4A1 (TR3) in cancer cells and tumors. Expert Opin. Ther. Targets *15*, 195–206.

Lee, Y.-S., Song, Y.S., Giffard, R.G., and Chan, P.H. (2005). Biphasic role of nuclear factor-κ B on cell survival and COX-2 expression in SOD1 Tg astrocytes after oxygen glucose deprivation. J Cereb Blood Flow Metab *26*, 1076–1088.

Lei, P., Abdelrahim, M., Cho, S.D., Liu, S., Chintharlapalli, S., and Safe, S. (2008). 1,1-Bis(3'-indolyl)-1-(p-substituted phenyl)methanes inhibit colon cancer cell and tumor growth through activation of c-jun N-terminal kinase. Carcinogenesis *29*, 1139–1147.

Li, X., Lee, S.-O., and Safe, S. (2012). Structure-dependent activation of NR4A2 (Nurr1) by 1,1-bis(3'-indolyl)-1-(aromatic)methane analogs in pancreatic cancer cells. Biochem. Pharmacol. *83*, 1445–1455.

Liepelt-Scarfone, I., Gauss, K., Maetzler, W., Müller, K., Bormann, C., Fruhmann Berger, M., Timmers, M., Streffer, J., and Berg, D. (2013). Evaluation of progression markers in the premotor phase of Parkinson's disease: the progression markers in the premotor phase study. Neuroepidemiology *41*, 174–182.

Liu, X. (2006). Manganese-Induced Neurotoxicity: The Role of Astroglial-Derived Nitric Oxide in Striatal Interneuron Degeneration. Toxicological Sciences *91*, 521–531.

Magness, S.T., Jijon, H., Van Houten Fisher, N., Sharpless, N.E., Brenner, D.A., and Jobin, C. (2004). In vivo pattern of lipopolysaccharide and anti-CD3-induced NF-kappa B activation using a novel gene-targeted enhanced GFP reporter gene mouse. J. Immunol. *173*, 1561–1570.

Maguire-Zeiss, K.A., and Federoff, H.J. (2010). Future directions for immune modulation in neurodegenerative disorders: focus on Parkinson's disease. J Neural Transm *117*, 1019–1025.

Matthews, R.T., Yang, L., Browne, S., Baik, M., and Beal, M.F. (1998). Coenzyme Q10 administration increases brain mitochondrial concentrations and exerts neuroprotective effects. Proc. Natl. Acad. Sci. U.S.a. *95*, 8892–8897.

Maxwell, M.A., and Muscat, G.E.O. (2006). The NR4A subgroup: immediate early response genes with pleiotropic physiological roles. Nucl Recept Signal *4*, e002.

McGeer, P.L., Itagaki, S., Boyes, B.E., and McGeer, E.G. (1988). Reactive microglia are positive for HLA-DR in the substantia nigra of Parkinson"s and Alzheimer"s disease brains. Neurology *38*, 1285–1291.

McGeer, P.L., and McGeer, E.G. (2011). History of innate immunity in neurodegenerative disorders. Front Pharmacol *2*, 77.

Meredith, G.E., Totterdell, S., Potashkin, J.A., and Surmeier, D.J. (2008). Modeling PD pathogenesis in mice: Advantages of a chronic MPTP protocol. Parkinsonism & Related Disorders *14*, S112–S115.

Miller, J.A., Trout, B.R., Sullivan, K.A., Bialecki, R.A., Roberts, R.A., and Tjalkens, R.B. (2011). Low-dose 1-methyl-4-phenyl-1,2,3,6-tetrahydropyridine causes inflammatory activation of astrocytes in nuclear factor-κB reporter mice prior to loss of dopaminergic neurons. J. Neurosci. Res. *89*, 406–417.

Mohan, H.M., Aherne, C.M., Rogers, A.C., Baird, A.W., C Winter, Des, and Murphy, E.P. (2012). Molecular Pathways: The Role of NR4A Orphan Nuclear Receptors in Cancer. Clin.

Cancer Res. *18*, 3223–3228.

Napoli, I., Kierdorf, K., and Neumann, H. (2009). Microglial precursors derived from mouse embryonic stem cells. Glia *57*, 1660–1671.

Niatsetskaya, Z.V., Sosunov, S.A., Matsiukevich, D., Utkina-Sosunova, I.V., Ratner, V.I., Starkov, A.A., and Ten, V.S. (2012). The oxygen free radicals originating from mitochondrial complex I contribute to oxidative brain injury following hypoxia-ischemia in neonatal mice. J. Neurosci. *32*, 3235–3244.

Nolan, Y.M., Sullivan, A.M., and Toulouse, A. (2013). Parkinson's disease in the nuclear age of neuroinflammation. Trends Mol Med *19*, 187–196.

Petroske, E., Meredith, G.E., Callen, S., Totterdell, S., and Lau, Y.S. (2001). Mouse model of Parkinsonism: a comparison between subacute MPTP and chronic MPTP/probenecid treatment. Nsc *106*, 589–601.

Phillipson, O.T. (2014). Management of the aging risk factor for Parkinson's disease. Neurobiology of Aging *35*, 847–857.

Polazzi, E., and Monti, B. (2010). Microglia and neuroprotection: from in vitro studies to therapeutic applications. Prog. Neurobiol. *92*, 293–315.

Przedborski, S., Jackson-Lewis, V., Djaldetti, R., Liberatore, G., Vila, M., Vukosavic, S., and Almer, G. (2000). The parkinsonian toxin MPTP: action and mechanism. Restor. Neurol. Neurosci. *16*, 135–142.

Qin, C., Morrow, D., Stewart, J., Spencer, K., Porter, W., Smith, R., Phillips, T., Abdelrahim, M., Samudio, I., and Safe, S. (2004). A new class of peroxisome proliferator-activated receptor gamma (PPARgamma) agonists that inhibit growth of breast cancer cells: 1,1-Bis(3'-indolyl)-1-(p-substituted phenyl)methanes. Molecular Cancer Therapeutics *3*, 247–260.

Rossi, D., and Volterra, A. (2009). Astrocytic dysfunction: Insights on the role in neurodegeneration. Brain Research Bulletin *80*, 224–232.

Saijo, K., Crotti, A., and Glass, C.K. (2013). Regulation of microglia activation and deactivation by nuclear receptors. Glia *61*, 104–111.

Saijo, K., Winner, B., Carson, C.T., Collier, J.G., Boyer, L., Rosenfeld, M.G., Gage, F.H., and Glass, C.K. (2009a). A Nurr1/CoREST Pathway in Microglia and Astrocytes Protects Dopaminergic Neurons from Inflammation-Induced Death. Cell *137*, 47–59.

Saijo, K., Winner, B., Carson, C.T., Collier, J.G., Boyer, L., Rosenfeld, M.G., Gage, F.H., and Glass, C.K. (2009b). A Nurr1/CoREST Pathway in Microglia and Astrocytes Protects Dopaminergic Neurons from Inflammation-Induced Death. Cell *137*, 47–59.

Saucedo-Cardenas, O., Quintana-Hau, J.D., Le, W.D., Smidt, M.P., Cox, J.J., De Mayo, F., Burbach, J.P., and Conneely, O.M. (1998). Nurr1 is essential for the induction of the

dopaminergic phenotype and the survival of ventral mesencephalic late dopaminergic precursor neurons. Proc. Natl. Acad. Sci. U.S.a. *95*, 4013–4018.

Schintu, N., Frau, L., Ibba, M., Caboni, P., Garau, A., Carboni, E., and Carta, A.R. (2009). PPAR-gamma-mediated neuroprotection in a chronic mouse model of Parkinson's disease. Eur. J. Neurosci. *29*, 954–963.

Shults, C.W., Flint Beal, M., Song, D., and Fontaine, D. (2004). Pilot trial of high dosages of coenzyme Q10 in patients with Parkinson's disease. Experimental Neurology *188*, 491–494.

Tansey, M.G., and Goldberg, M.S. (2010). Neuroinflammation in Parkinson's disease: Its role in neuronal death and implications for therapeutic intervention. Neurobiology of Disease *37*, 510–518.

Thompson, W.L., and Van Eldik, L.J. (2009). Inflammatory cytokines stimulate the chemokines CCL2/MCP-1 and CCL7/MCP-7 through NFκB and MAPK dependent pathways in rat astrocytes. Brain Research *1287*, 47–57.

Tjalkens, R.B., Liu, X., Mohl, B., Wright, T., Moreno, J.A., Carbone, D.L., and Safe, S. (2008). The peroxisome proliferator-activated receptor-γ agonist 1,1-bis(3′-indolyl)-1-(p-trifluoromethylphenyl)methane suppresses manganese-induced production of nitric oxide in astrocytes and inhibits apoptosis in cocultured PC12 cells. J. Neurosci. Res. *86*, 618–629.

Tripanichkul, W., and Jaroensuppaperch, E.-O. (2013). Ameliorating effects of curcumin on 6-OHDA-induced dopaminergic denervation, glial response, and SOD1 reduction in the striatum of hemiparkinsonian mice. Eur Rev Med Pharmacol Sci *17*, 1360–1368.

van Loo, G., De Lorenzi, R., Schmidt, H., Huth, M., Mildner, A., Schmidt-Supprian, M., Lassmann, H., Prinz, M.R., and Pasparakis, M. (2006). Inhibition of transcription factor NF-kappaB in the central nervous system ameliorates autoimmune encephalomyelitis in mice. Nat. Immunol. *7*, 954–961.

West, M.J., and Gundersen, H.J. (1990). Unbiased stereological estimation of the number of neurons in the human hippocampus. J. Comp. Neurol. *296*, 1–22.

Yoon, K., Lee, S.-O., Cho, S.D., Kim, K., Khan, S., and Safe, S. (2011). Activation of nuclear TR3 (NR4A1) by a diindolylmethane analog induces apoptosis and proapoptotic genes in pancreatic cancer cells and tumors. Carcinogenesis *32*, 836–842.

Zhang, L., Le, W., Xie, W., and Dani, J.A. (2012). Age-related changes in dopamine signaling in Nurr1 deficient mice as a model of Parkinson's disease. Neurobiology of Aging *33*, 1001.e7–.e16.

Zhao, Y., and Bruemmer, D. (2010). NR4A orphan nuclear receptors: transcriptional regulators of gene expression in metabolism and vascular biology. Arterioscler. Thromb. Vasc. Biol. *30*, 1535–1541.